UNIVERSITÄTSKLINIKUM HAMBURG-EPPENDORF

Institut für Biochemie und Molekulare Zellbiologie

Prof. Dr. Dr. Andreas H. Guse

Organelle ion channel control of directional mesenchymal cell migration

Dissertation

zur Erlangung des Doktorgrades PhD

an der Medizinischen Fakultät der Universität Hamburg.

vorgelegt von:

Marie Adler

aus Stade, Deutschland

Hamburg 2026

(wird von der Medizinischen Fakultät ausgefüllt)

Angenommen von der
Medizinischen Fakultät der Universität Hamburg am: 20.03.2026

Veröffentlicht mit Genehmigung der
Medizinischen Fakultät der Universität Hamburg.

Prüfungsausschuss, der/die Vorsitzende: Prof. Dr. Pablo J. Sáez

Prüfungsausschuss, zweite/r Gutachter/in: Prof. Dr. Maike Frye

The present work was performed at the Institute of Biochemistry and Molecular Cell Biology in the Cell Communication and Migration Laboratory at the University Medical Center Hamburg-Eppendorf (UKE) under the supervision of Prof. Dr. Pablo J. Sáez from April 2023 to January 2026. The work was co-supervised by Prof. Dr. Maike Frye at the Institute of Clinical Chemistry and Laboratory Medicine (UKE) and Prof. Dr. Thomas Oertner at the Institute of Synaptic Neuroscience (Center for Molecular Neurobiology Hamburg, ZMNH, UKE).

Für meine Mama und
für meinen Papa …

Table of Contents

Publications, manuscripts, internships and presentations at national and international conferences

Publications

Karen Lahme, Wiebke Sachs, Sarah Froembling, Desiree Loreth, Vincent Böttcher-Dierks, Katrin Neumann, Frederik-Michael Hann, Nick Arkan, Michael Brehler, Julia Reichelt, Antonia Sgries, Kristin Surmann, Simone Gaffling, **Marie R. Adler**, Pablo J. Sáez, Uta Wedekind, Alina Lampert, Elena Tasika, Paul Saftig, Christian Conze, Roland Thünauer, Sinah Skuza, Karen Neitzel, Stephanie Zieliniski, Johannes Brand, Stefan Bonn, Stephan Michalis, Uwe Völker, Marina Zimmermann, Thorsten Wiech, Tobias N. Meyer, Lars Fester, Catherine Meyer-Schwesinger **(2025)**. *Autoantibody-triggered podocyte membrane drives autoimmune kidney disease.* **Accepted in Cell, January 2026.**
DOI: https://doi.org/10.1016/j.cell.2025.11.010

Aude Sagnimorte, **Marie R. Adler**, Gaspard de Tournemire, Pablo J. Sáez, David Gonzalez-Rodriguez, Claire A. Dessalles, Avin Babataheri **(2025)**. *1D confinement mimicking microvessel geometry controls pericyte shape and motility.*
DOI: https://doi.org/10.1101/2023.12.20.572195

Manuscripts in preparation

Subhajit Dutta, **Marie R. Adler**, Nir S. Gov, Pablo J. Sáez. *Decision-making during cell migration.*

Marie R. Adler, Johan M. Kux, Svitlana M. Palii, Javier Boix-Campos, Pablo J. Sáez. *Mitochondrial dysfunction associated with ER stress reduces cell migration.*

Internship at the Krishnan Laboratory at the University of Chicago

Research internship from June 19th to July 31st, 2023, at the Krishnan Laboratory at the Department of Chemistry, University of Chicago, Illinois. Supported by a Boehringer Ingelheim Fonds (BIF) travel grant under the framework of a Human Frontier Science Program (HFSP) project (RGP0032/2022). The aim of the internship was to learn how to perform chemical imaging by measuring pH in different organelles (mitochondria, lysosomes).

Oral presentations at national conferences

Marie R. Adler, Javier Boix-Campos, Johan M. Kux, Pablo J. Sáez **(2023)**. *ER stress disruption of mitochondrial dynamics during cell migration.* Kick-off meeting *Voltare* project HFSP (RGP0032/2022), September 13-15, 2023, Hamburg, Germany.

Poster presentations at national and international conferences (attendant underlined)

Johan M. Kux, **Marie R. Adler**, Tamara López-López, Pablo J. Sáez **(2023)**. *Differential regulation of organelle dynamics and crosstalk during cell migration.* Imaging cell dynamics, May 14-17, 2023, Lisbon, Portugal.

Marie R. Adler, Tamara López-López, Johan M. Kux, Javier Boix-Campos, Pablo J. Sáez **(2023)**. *ER stress disrupts actin and organelle dynamics during cell migration.* 4th Endoplasmic Reticulum International Symposium, October 4-6, 2023, Paris, France.

Marie R. Adler, Javier Boix-Campos, Johan M. Kux, Pablo J. Sáez **(2024)**. *ER stress disrupts cytoskeleton and organelle dynamics during cell migration.* 90th Harden: European Cytoskeletal Forum: BSCB-Biochemical Society 2024 Cell Migration meeting, April 15-18, 2024, Birmingham, United Kingdom.

Marie R. Adler, Javier Boix-Campos, Johan M. Kux, Pablo J. Sáez **(2025)**. *ER stress disrupts membrane and mitochondria dynamics during cell migration.* EMBO Workshop – From molecules to organisms: An integrative view of cell biology, March 16-21, 2025, Radstadt, Austria.

Svitlana M. Palii, **Marie R. Adler**, José Luis Cortés-Muñoz, Arturo Sánchez, María Teresa Alonso, Pablo J. Sáez **(2025)**. *Endoplasmic reticulum Ca^{2+} and intercellular communication control of cell migration.* German Society for Biochemistry and Molecular Biology, Cellular Organelles, November 13-14, 2025, Düsseldorf, Germany.

EMBO | EMBL Symposium: Seeing is believing: imaging the molecular processes of life, October 8-11, 2025, Heidelberg, Germany. **Virtual participation.**

Abbreviations

ADP	adenosine diphosphate
AKAP450	A-kinase-anchoring protein 450
AMPK	AMP (adenosine monophosphate)-activated protein kinase
Arp	actin-related protein
ATF	activating transcription factor (ATF4 and ATF6)
ATP	adenosine triphosphate
BiP	immunoglobulin protein
°C	Celsius degree
CAMSAP2	calmodulin-regulated spectrin-associated protein 2
Cdc42	cell division control protein 42 homolog
CHOP	pro-apoptotic C/EBP homologous protein
CHX	calcium hydrogen exchanger
CLASPs	CLIP-associated proteins
Climp63	cytoskeleton-linking membrane protein 63
CLIP	cytoplasmic linker proteins
CoQ	coenzyme Q
1D, 2D, 3D	one-dimensional, two-dimensional, three-dimensional
DMSO	dimethyl sulfoxide
DPBS	Dulbecco's phosphate-buffered saline
Drp1	dynamin-related protein 1
EB1	end-binding protein 1
EC	endothelial cell
ECM	extracellular matrix
eIF2α	α-subunit of eukaryotic translation-initiation factor 2α
EM	electron microscopy
ER	endoplasmic reticulum
ERAD	ER-associated degradation
ETC	electron transport chain
FA	focal adhesion
$FADH_2$	flavin adenine dinucleotide, dyhydrogenated
FAK	focal adhesion kinase
FCCP	carbonyl cyanide-p-trifluoromethoxyphenyl-hydrazone
GaMTs	Golgi-associated microtubules
GTP	guanosine triphosphate
h	hour

HEPES	2-[4-(2-Hydroxyethyl)piperazin-1-yl]ethane-1-sulfonic acid
HUVEC	human umbilical vein endothelial cell
IMM	inner mitochondrial membrane
IMS	intermembrane space
IP_3Rs	inositol triphosphate receptors
IRE1α	inositol 1,4,5-triphosphate receptor
KHX	potassium hydrogen exchanger
LAMP	lysosome-associated membrane proteins
LINC	linker of nucleoskeleton and cytoskeleton
MAMs	mitochondria-associated membranes
MAP4K4	mitogen-activated protein kinase kinase kinase kinase 4
MCS	membrane contact site
MCU	mitochondrial calcium uniporter
MERCs	mitochondria-ER contacts
Mfn	Mitofusin, fusion proteins
mg	milligramm
min	minute
mL	milliliter
MLCK	myosin light chain kinase
mM	millimolar
MTs	microtubules
MTOC	microtubule-organizing center
mV	millivolt
NADH	nicotinamide adenine dinucleotide, hydrogenated
NHX	sodium hydrogen exchanger
NO	nitric oxide
OMM	outer mitochondrial membrane
OPA1	optic atrophy 1
OXPHOS	oxidative phosphorylation
PDMS	polydimethylsiloxane
PERK	RNA-dependent protein kinase (PKR)-like ER kinase
PFA	paraformaldehyde
PHEM	PIPES, HEPES, EGTA, magnesium sulfate ($MgSO_4$)
PIPES	Piperazine-N,N'-bis(2-hydroxypropanesulphonic acid)
pLL-PEG	poly(L-lysine) poly (ethylene glycol)
PLPP	photoactivatable reagent
P/S	penicillin-streptomycin

Rac1	Ras-related C3 botulinum toxin substrate 1
Rho	Ras homologue
Rhod123	rhodamine 123
RI	refractive index
RLC	regulatory light chain
ROCK	Rho-associated protein kinase
ROS	reactive oxygen species
RRBP1	ribosome-binding protein 1
RT	room temperature
RyR	ryanodine receptors
s	seconds
SERCA	sarcoplasmic/endoplasmic reticulum Ca^{2+}-ATPase
SOCE	store-operated calcium entry
S1P/S2P	protease site-1, protease site-2
SPARK	FAK-separation of phases-based activity reporter of kinases
STIM1	stromal interaction molecular 1
SUN	Sad1, Unc Homology
TAC	tip attachment complex
TAN	transmembrane actin-associated nuclear
TEM	transmission electron microscopy
TGN	*trans*-Golgi network
TI(M)M	translocase of inner (mitochondrial) membrane
TMRE	tetramethylrhodamine ethyl ester
TMRM	tetramethylrhodamine methyl
TN	tunicamycin
TO(M)M	translocase of outer (mitochondrial) membrane
TRPC	transient receptor potential channel
TRPML1	transient receptor potential channel, mucolipin subfamily 1
TRPV	transient receptor potential vanilloid
µL	microliter
µM	micromolar
UPR	unfolded protein response
VEGF	vascular endothelial growth factor
VDAC	voltage-dependent anion channel
WASP	Wiskott-Aldrich Syndrome Protein
WAVE	WASP-family verprolin-homologous protein
XBP1	X-box-binding protein 1

Abstract

Endothelial cells (ECs) play a critical role in the maintenance of vascular function. They line blood and lymphatic vessels, forming a selectively permeable barrier essential for the exchange of nutrients, immune cells and waste products. In pathologies such as obesity and other metabolic disorders, circulating signals negatively affect vascular function and directly alter EC states, triggering cellular stress responses. These stress responses are particularly evident in obese individuals during pregnancy, where maternal stress can be transferred to the fetus through the umbilical cord in a process called fetal programming. In the offspring, this cellular stress contributes to insulin resistance and endothelial dysfunction. Although the mechanisms underlying endothelial dysfunction remain poorly understood, previous research has identified a disproportionate activation of the endoplasmic reticulum (ER) stress response, characterized by a dysregulated unfolded protein response (UPR).

Because EC migration is critical for angiogenesis and vessel sprouting, this thesis investigates how ER stress affects EC behaviour during migration and identifies which UPR pathways drive these effects. Human umbilical vein endothelial cells (HUVECs) were treated with tunicamycin (TN), which *in vitro* mimics maternal obesity-induced ER stress. Using live-cell imaging, confocal microscopy, holotomography, ultrastructural electron microscopy, and advanced image analysis, the impact of TN-induced ER stress on EC migration was assessed during collective mesenchymal cell migration.

ER stress induction led to reduced migration speed and directionality in both collective and single-cell migration on two-dimensional and one-dimensional substrates. This impaired migration correlated with cytoskeletal distortion: F-actin fibers and microtubules became misaligned relative to the migratory axis. The misalignment of F-actin also altered membrane dynamics. Although TN-induced ER stress increased membrane ruffling, these dynamics were non-productive for motility. Consistent with these cytoskeletal changes, organelle morphology and polarity were disrupted. Both the ER and mitochondria exhibited structural alterations and misalignments to the migratory axis.

Pharmacological inhibition of the UPR identified RNA-dependent protein kinase (PKR)-like ER kinase (PERK) as the primary signalling branch regulating HUVEC migration. PERK inhibition prevented the ER stress-induced reduction in migration speed and directionality. Structurally, PERK inhibition also preserved cytoskeletal alignment and restored organelle organization to patterns similar to control conditions. Given the strong association between ER and mitochondria, confirmed through analysis of mitochondria-ER contacts (MERCs), the effects of ER stress on mitochondrial dynamics and function were further examined.

Live-cell imaging revealed that mitochondria moved into protrusions that ultimately determined migration direction. Because mitochondrial function depends on mitochondrial membrane potential ($\Delta\Psi$), changes in $\Delta\Psi$ were monitored during directional migration and after ER stress induction. Directionally migrating HUVECs exhibited more frequent depolarization events in mitochondria positioned towards the cell front. ER stress prolonged the duration of these depolarization events, an effect that was prevented by PERK inhibition. Since $\Delta\Psi$ relies on balanced ion transport, several ion channels were tested for their involvement in directional migration. While the inhibition of transient receptor potential channel 6 (TRPC6) or voltage-dependent anion channel 1 (VDAC1) did not prevent the ER stress-induced reduction in migration speed and directionality, VDAC1 was revealed as a key regulator of directional migration during collective mesenchymal migration under resting conditions.

These findings suggest the involvement of a cryptic protein that regulates directional migration through PERK signalling and mitochondrial membrane potential. Overall, this thesis demonstrates a central role for PERK signalling in directional mesenchymal cell migration. PERK-dependent ER stress reduces migration speed and directionality, disrupts cytoskeletal and organelle organization, alters membrane dynamics, and modifies mitochondrial membrane potential behaviour. These results position PERK as a promising candidate for further investigation in the context of endothelial dysfunction.

Zusammenfassung

Endothelzellen (ECs) spielen eine entscheidende Rolle bei der Aufrechterhaltung der Gefäßfunktion. Sie kleiden Blut- und Lymphgefäße aus und bilden eine selektiv durchlässige Barriere, die für den Austausch von Nährstoffen, Immunzellen und Abfallprodukten unerlässlich ist. Bei Erkrankungen wie Adipositas und anderen Stoffwechselstörungen beeinträchtigen zirkulierende Signale die Gefäßfunktion und verändern den Zustand von ECs, wodurch zelluläre Stressreaktionen ausgelöst werden. Diese Stressreaktionen sind besonders deutlich bei adipösen Personen während der Schwangerschaft zu beobachten, wo mütterlicher Stress über die Nabelschnur in einem als fetale Programmierung bezeichneten Prozess auf den Fötus übertragen werden kann. Bei den Nachkommen trägt dieser zelluläre Stress zu Insulinresistenz und endothelialer Dysfunktion bei. Obwohl die Mechanismen, die der endothelialen Dysfunktion zugrunde liegen, noch weitgehend unverstanden sind, haben frühere Forschungen eine unverhältnismäßige Aktivierung der Stressreaktion des endoplasmatischen Retikulums (ER) identifiziert, die durch eine dysregulierte Unfolded Protein Response (UPR) gekennzeichnet ist.

Da die EC-Migration für die Angiogenese und Gefäßsprossung entscheidend ist, untersucht diese Dissertation, wie ER-Stress das Verhalten von ECs während der Migration beeinflusst, und identifiziert, welche UPR-Signalwege diese Effekte steuern. Menschliche Nabelschnurvenenendothelzellen (HUVECs) wurden mit Tunicamycin (TN) behandelt, das *in vitro* den durch mütterliche Adipositas induzierten ER-Stress nachahmt. Mithilfe von Live-Cell-Imaging, Konfokalmikroskopie, Holotomographie, ultrastruktureller Elektronenmikroskopie und fortschrittlicher Bildanalyse wurde der Einfluss von TN-induziertem ER-Stress auf die EC-Migration während der kollektiven mesenchymalen Zellmigration untersucht.

Die Induktion von ER-Stress führte zu einer verringerten Migrationsgeschwindigkeit und -richtung, sowohl bei der kollektiven als auch bei der Einzelzellmigration auf zweidimensionalen und eindimensionalen Substraten. Diese beeinträchtigte Migration korrelierte mit einer Neuausrichtung des Zytoskeletts: F-Aktin Fasern und Mikrotubuli wurden relativ zur Migrationsachse fehlausgerichtet. Diese Fehlausrichtung von F-Aktin veränderte auch die Dynamik der Plasmamembran. Obwohl der TN-induzierte ER-Stress die Membranwellenbildung verstärkte, war diese Dynamik für die Motilität unproduktiv. In Übereinstimmung mit diesen Veränderungen des Zytoskeletts waren auch die Morphologie and Polarität der Zellorganellen gestört. Sowohl das ER als auch die Mitochondrien wiesen strukturelle Veränderungen und Fehlausrichtungen zur Migrationsachse auf.

Die pharmakologische Hemmung der UPR identifizierte die RNA-abhängige Proteinkinase (PKR)-ähnliche ER-kinase (PERK) als den primären Signalweg, der die HUVEC-Migration reguliert. Die PERK-Hemmung verhinderte die durch ER-Stress induzierte Verringerung der Migrationsgeschwindigkeit und -richtung. Strukturell bewahrte die PERK-Hemmung auch die Ausrichtung des Zytoskeletts und stellte die Organisation der Zellorganellen wieder her, die den Kontrollbedingungen ähnelten. Angesichts der starken Verbindung zwischen ER und Mitochondrien, die durch die Analyse der Mitochondrien-ER-Kontakte (MERCs) bestätigt wurde, wurden die Auswirkungen von ER-Stress auf die Dynamik und Funktion der Mitochondrien weiter untersucht.

Live-Cell-Imaging zeigte, dass sich Mitochondrien in Ausstülpungen der Plasmamembran bewegten, die letztlich die Migrationsrichtung bestimmten. Da die Mitochondrienfunktion vom Mitochondrienmembranpotenzial ($\Delta\Psi$) abhängt, wurden Veränderungen des $\Delta\Psi$ während der gerichteten Migration und nach Induktion von ER-Stress überwacht. Gerichtet migrierende HUVECs zeigten häufigere Depolarisationsereignisse in Mitochondrien, die zur Zellfront hin positioniert waren. ER-Stress verlängerte die Dauer dieser Depolarisationsereignisse; ein Effekt, der durch PERK-Hemmung verhindert wurde. Da $\Delta\Psi$ auf einem ausgeglichenen Ionentransport beruht, wurden mehrere Ionenkanäle auf ihre Beteiligung an der gerichteten Migration getestet. Während die Hemmung des Transient Receptor Potential Channel 6 (TRPC6) oder des Voltage-Dependent Anion Channel 1 (VDAC1) die durch ER-Stress induzierte Verringerung der Migrationsgeschwindigkeit und -richtung nicht verhinderte, erwies sich VDAC1 als ein wichtiger Regulator der gerichteten Migration unter Ruhebedingungen.

Diese Ergebnisse deuten auf die Beteiligung eines kryptischen Proteins hin, das die gerichtete Migration über PERK-Signale und das mitochondriale Membranpotenzial reguliert. Insgesamt zeigt diese Dissertation die zentrale Rolle der PERK-Signalübertragung bei der gerichteten Migration mesenchymaler Zellen. PERK-abhängiger ER-Stress verringert die Migrationsgeschwindigkeit und -richtung, stört die Organisation des Zytoskeletts und der Zellorganellen, verändert die Membrandynamik und modifiziert das Verhalten des mitochondrialen Membranpotenzials. Diese Ergebnisse positionieren PERK als vielversprechenden Kandidaten für weitere Untersuchungen im Zusammenhang mit endothelialer Dysfunktion.

Introduction

1. Cell migration

Cell migration plays a pivotal role in development during gastrulation, angiogenesis, organ formation, as well as other fundamental processes like the immune response and wound healing. Aberrant cell migration results in pathological conditions like cancer metastasis, cancer invasion, autoimmune diseases and chronic inflammation (Jerka et al. 2024; Doyle et al. 2013). Cells have the ability to migrate individually during single cell migration or in cell networks during collective cell migration. Single cell migration describes the movement of individual cells, which occurs for example during leukocyte migration in the context of the immune response (Trepat, Chen, and Jacobson 2012). Collective cell migration describes the coordinated movement of groups of cells connected by cell-cell junctions that is predominantly used during wound healing and tissue regeneration (Haeger et al. 2015; Trepat, Chen, and Jacobson 2012). However, these definitions are currently under re-evaluation in order to include a broader definition of collective cell migration where cells migrate together in ”loosely or closely associated groups” and cell-cell junctions are transient and constantly remodeled (Theveneau and Mayor 2011). During collective migration, two distinct cellular populations are identified: “leader” cells in the first layers of the moving group, and “follower” cells in the layers behind. Leader cells show a distinct intracellular distribution, establish a front-to-rear axis and guide the follower cells through the tissue. Leader cells also generate traction and – if needed – actively remodel the extracellular matrix (ECM) by displaying proteolytic activity (Khalil and Friedl 2010; Haeger et al. 2015). Further, leader cells are responsible for sensing the microenvironment and dictating the speed and direction of movement (Qin et al. 2021). They become leader cells upon external cues from the ECM, soluble factors or neighbouring cells (Mayor and Etienne-Manneville 2016). Follower cells comprise the majority of the moving group and become specialized during the migration process. These cells show no distinct intracellular polarity and experience symmetric adherent junctions to their neighbouring cells while leader cells display asymmetric junctions (Qin et al. 2021).

Whether migrating individually or collectively, motile cells exhibit different modes of migration ranging from mesenchymal migration, or crawling movement, to amoeboid and lobopodial migration. Depending on their microenvironment, in particular the spatial confinement, cells adapt their migratory mode with a high plasticity (Seetharaman and Etienne-Manneville 2020). Strong nuclear confinement and low adhesion properties are shown during amoeboid migration. When cells face a complex microenvironment, particularly during migration through the ECM, the nucleus as the largest and stiffest organelle is used to measure the degree of spatial confinement (Lomakin et al. 2020). Amoeboid migration is described by a more rounded cell morphology and low adhesive interactions between the cell and its environment,

as well as extreme cell body deformations (Yamada and Sixt 2019), which resembles the movement of an amoeba hence its name (**Fig. 1A**). During amoeboid movement, cells squeeze their body through the ECM by finding the path of least resistance, making it a faster locomotion with a cell speed of ~10 μm/min. In comparison, mesenchymal cell migration is characterized by proteolytic activity that changes the surrounding matrix to generate a path for the cell to migrate through. Mesenchymal migration is characterized by strong adhesions through stress-fiber linked focal adhesions (FAs), making the locomotion slower with speeds <1 μm/min (**Fig. 1B**). Lobopodial migration is described as a hybrid of amoeboid and mesenchymal motion. While cells show strong adherence to the surrounding matrix, they move by generating asymmetric intracellular pressure for bleb-like protrusions. To determine the migratory mode of a cell, three parameters are evaluated: (1) cellular adhesion to the substrate, (2) forward actin protrusion, and (3) actomyosin contractility (Yamada and Sixt 2019; Seetharaman and Etienne-Manneville 2020; Bear and Haugh 2014).

As mentioned above, cell migration requires a particular intracellular organization, named cell polarization (Vaidžiulyte, Coppey, and Schauer 2019). Indeed, cellular polarization is characterized by an asymmetric distribution of cellular components and differential cytoskeletal dynamics at the front and rear of the cell. Moreover, as a consequence of different cytoskeletal organization, polarized cells show a distinct distribution of their organelles (Vaidžiulyt, Macé, and Battistella 2022). During amoeboid migration, the nucleus is mostly positioned at the anterior part of the cell with the microtubule-organizing center (MTOC) behind (**Fig. 1A**). This allows the nucleus to act as a mechanical gauge and signal which path is sufficient for continuous migration, with the MTOC being regarded as the spatially associated directional selector (Renkawitz et al. 2019). Cells undergoing mesenchymal migration show a well defined polarity axis with a protruding front and a retracting back. The nucleus is mostly positioned posterior with the MTOC localized in front of it (**Fig. 1B**). During mesenchymal migration, distinct cycles are repeated that are summarized in five steps: (1) establishment of front-to-rear polarity axis, (2) leading edge extension, (3) formation of new adhesions, (4) cell body retraction, and (5) removal of old adhesions and rear retraction (Seetharaman and Etienne-Manneville 2020; Yamada and Sixt 2019). These cycles happen simultaneously, rather than in sequential steps, with the cytoskeleton providing the major driving forces (SenGupta, Parent, and Bear 2021). Because the cytoskeleton is one of the most complicated structures in cells and is distinctly organized and regulated during migration, its components will be described in more detail in the following sections (**Fig. 1**).

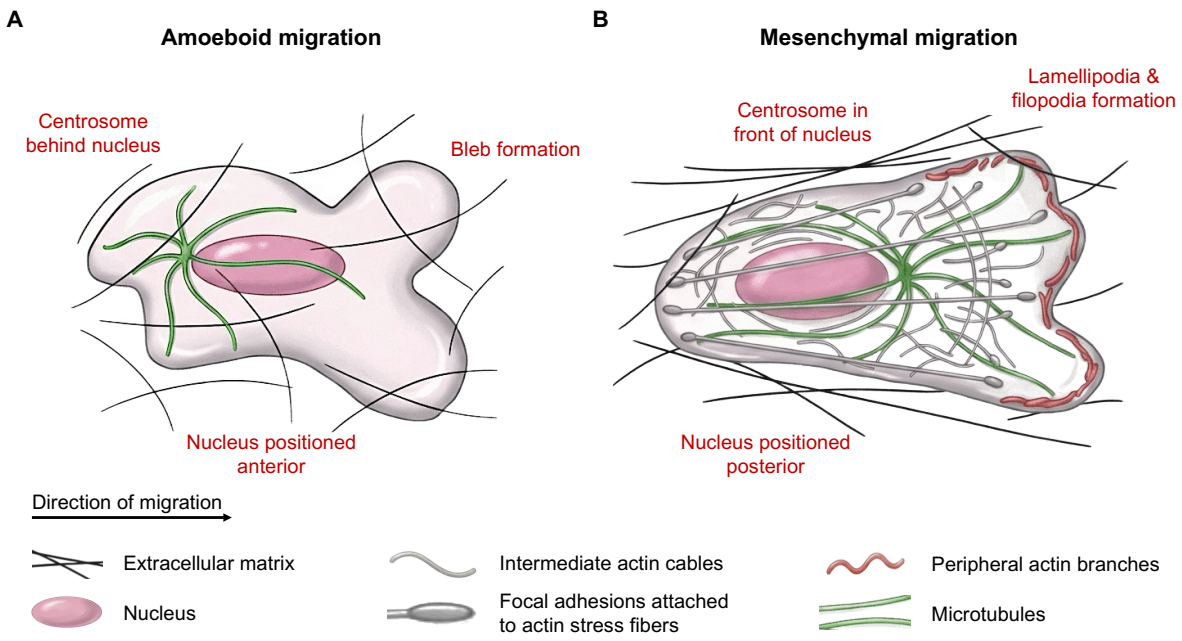

Figure 1: Cytoskeletal organization during amoeboid and mesenchymal migration.

(A) Cytoskeletal organization during amoeboid migration. Amoeboid cells display a rounded cell shape, low adhesive activity and they sqeeze through the extracellular matrix (ECM) by showing extensive deformations. Amoeboid migration is characterized by cell protrusions filling existing gaps without changing the composition of the ECM. The nucleus is positioned towards the front of the cell (anterior), with the centrosome behind it. This way the nucleus is used to determine the path of least resistence.
(B) Cytoskeletal organization during mesenchymal migration. Mesenchymal cells align along the lines of the ECM fibers and display proteolytic activety at the cell front to actively generate a path for migration. Mesenchymal migration is characterized by lamellipodia and filopodia formation at the cell front. The cell is attached to the ECM through focal adhesions that connect the ECM to intracellular actin fibers. The cell front is structurally made of peripheral actin branches. The nucleus is positioned towards the cell rear (posterior), with the centrosome in front of it. Microtubules extend throughout the cytoplasm into the cell periphery.
Image generated based on figures from Yamada & Sixt (2019), Hohmann & Dehghani (2019), Seetharaman & Etienne-Manneville (2020). Figure created with illustrae.com.

1.1. Actin cytoskeleton: Generating protrusive forces

The cytoskeleton comprises actin microfilaments, microtubules and intermediate filaments that work together in a coordinated manner to generate efficient migration (Seetharaman and Etienne-Manneville 2020) (**Fig. 1**). As mentioned, one major part of the cytoskeleton is actin which occurs in two different states inside the cell: monomeric, globular G-actin and filamentous F-actin. The actin cytoskeleton describes a network of polarized filaments. These filaments are composed of G-actin which polymerizes to asymmetric helical structures, termed F-actin, that have a typical length of 6-7 µm *in vitro* (Hohmann and Dehghani 2019). Actin filaments itself are polar, with a fast polymerizing barbed (+) end and slower polymerizing pointed (-) end. The formation of a trimer or tetramer is the most critical step in actin nucleation. One of the most prominent actin nucleators is the actin-related protein (Arp) 2/3 complex. This complex mimics actin monomers and together with two actin monomers and a pre-existing

filament gives rise to large networks of branched actin filaments (Schaks, Giannone, and Rottner 2019). Arp2/3 complex is further involved in forming peripheral branched actin networks that are usually formed at the cell front. For dense peripheral dendritic networks, capping proteins are needed to prevent continuous elongation of the (+)-end (Hohmann and Dehghani 2019). Depending on the actin organization, membrane protrusions at the leading edge can be divided into filopodia (finger-like structure, containing parallel actin bundles), lamellipodia (flat sheets, containing branched microfilaments), and pseudopodia (containing 3D actin networks) (Becchetti and Arcangeli 2010). Filopodia have a diameter of 0.1-0.2 µm and their fast-growing actin filament is oriented with the (+)-end towards the cell tip. These membrane extensions allow microenvironmental exploration, coexist with lamellipodia and are variable in their number, but in contrast to lamellipodia, they cannot drive cell motility on their own. Actin polymerization for filopodia protrusion is Arp2/3-independent and depends on signalling via formins (especially mDia2) and the actin bundling protein fascin. Using a fibroblast line, it was shown almost twenty years ago that filopodia, during cytoskeleton turnover, are recycled back to contribute to stress fiber bundles in the lamella region behind the lamellipodium (Nemethova, Auinger, and Small 2008).

The concept of the lamellipodium started fifty years ago with the identification of ~0.2 µm thick protrusions extending parallel to the substrate . When these protrusions curled upwards, the term membrane “ruffles” was used (Small et al. 2002). Lamellipodia kinetics are characterized by fast actin polymerization behind the leading edge, followed by filament depolarization a few micrometers back which creates a 2-4 µm-wide actin treadmilling array. Addition of monomers at the (+)-ends provides protrusion force and drives the retrograde flow of ~1 µm/min. As previously mentioned, the most important factor for lamellipodia generation is the Arp2/3-complex which is controlled by nucleation factors, e.g. Wiskott-Aldrich Syndrome Protein (WASP) and the Scar/WASP-family verprolin-homologous protein (WAVE) complex in a mechanism dependent on the small guanosine triphosphate(GTP)-ases of the Ras homologue (Rho) family, in particular Ras-related C3 botulinum toxin substrate 1 (Rac1) and cell division control protein 42 homolog (Cdc42) (Hohmann and Dehghani 2019; Tang and Gerlach 2017).

The lamella is a distinct structure comprising an area of 3-15 µm from the leading edge of a motile cell. Non-muscle myosin II (in this thesis referred to as “myosin”)-dependent retrograde flow of ~0.3 µm/min defines F-actin kinetics of the lamella. The so-called “convergence zone” describes an area where the retrograde flow of the lamella meets the myosin II-dependent anterograde flow of the cell body (Gupton et al. 2005). Additionally, myosin II is mainly responsible for the retraction of the cell rear and transmitting forces to the surrounding ECM via adhesion structures. It gets activated by the phosphory-lation of the regulatory light chain (RLC) or activation of myosin light chain kinases (MLCK). Prior to myosin II’s activation, RLC is activated by Rho-associated protein kinase (ROCK) and MLCK by Ca^{2+}. Myosin II is also

associated with stress fibers which are bundles of 10-30 anti-parallel actin filaments that are cross-linked by α-actinin, and linked to focal adhesions (Hohmann and Dehghani 2019). These stress fibers are a characteristic present only in mesenchymal migrating cells and are classified based on two distinct actin assembly mechanisms: Dorsal stress fibers and transverse arcs which are oriented perpendicular to each other, and ventral stress fibers. These dorsal stress fibers elongate from adhesions at the leading edge with their (+)-end pointing towards the cell front (Hotulainen and Lappalainen 2006; Vallenius 2013). Ventral stress fibers are found on the ventral cell surface underneath the nucleus and terminate at adhesions at the front and rear parts of the cell. Molecular differences between the stress fiber subtypes include different associations to myosin II isoform. While myosin IIA is found at both transverse arcs and ventral stress fibers, myosin IIB is mostly found on ventral stress fibers around the posterior parts of the cell. Dorsal stress fibers lack myosin II (Vallenius 2013).
To summarize, the dramatic changes during cellular polarization for movement are mostly generated by the F-actin cytoskeleton which is coupled to the ECM via FAs. GTPase activity of Rac and Cdc42 regulates actin-based protrusions that adhere to the substrate via small adhesions. Rho activity promotes the assembly of contractile actomyosin structures that push the cell forward through traction generation and disassembly of adhesions at the rear part of the cell (Gardel et al. 2010).

1.2. Focal adhesions: Generating traction

Focal adhesions were first described in 1978 (Heath and Dunn 1978) and are essential for the mechanical as well as chemical interaction of the cell with the ECM (Rosen and Dallon 2022). FAs are essential for force generation during cell migration. The typical lifecycle of FAs is described as follows: Nascent, integrin-mediated FAs (small, usual diameter of <250 nm) form at the leading edge of the cell and are either rapidly turned over or connect the intracellular actin cytoskeleton to the surrounding substrate/ECM. Forces generated through actomyosin-contractility allow a small subset of FAs to mature and grow, therefore providing traction forces that eventually push the cell forward. To be able to push forward, however, FAs have to be released and disassembled under the cell body (Stehbens and Wittmann 2014).
FAs are multi-protein structures consisting of clusters of transmembrane integrins that link to intracellular actin filaments. This linkage occurs through adaptor proteins like paxillin, talin and vinculin which connect to ECM proteins like fibronectin (De Pascalis and Etienne-Manneville 2017). The FA structure consists of three layers that are regulated in a temporal and functional way. The bottom integrin signalling layer forms first, with integrins binding to the ECM to establish clusters. Next, a middle force transduction layer follows, and the top layer consists of the actin-regulatory layer (Matrullo, Filomeni, and Rizza 2025). One of the main adaptor

and scaffolding proteins is paxillin which directly binds to integrins and recruits focal adhesion kinase 1 (FAK1). FAK1 as a non-receptor tyrosine kinase plays a major role during FA signalling by phosphorylating itself and other target proteins. Talin as a larger adaptor protein binds to integrins as well, and extends through the whole FA interacting with vinculin and actin. Talin is important during mechanosensing by transducing mechanical forces into biochemical signals. The interaction with vinculin actives it, but unlike paxillin and talin, vinculin does not bind to integrins and its main role is linking the FAs to actin filaments (Kumari et al. 2024; Matrullo, Filomeni, and Rizza 2025).

Using a phase separation-based FAK activity reporter, called FAK-separation of phases-based activity reporter of kinases (SPARK), it was recently proposed that the forces generated by actin and actomyosin contraction are stronger in the leading edge of a migrating cell (X. Li et al. 2023). This force is transmitted from the actin cytoskeleton to FAKs, suggesting a stronger FAK tension in the leading edge. Polarized FAK activity enhances actin polymerization via Rho-family GTPases suggesting that polarized tension and FAK activity may direct cell migration through actin polymerization and contractility at the leading edge (X. Li et al. 2023). FAKs importance is demonstrated when its absence leads to critically impaired cell migration as FAs are static and not turned over (Le Coq et al. 2022). To summarize FA dynamics during mesenchymal cell migration: Nascent adhesions form at the lamellipodia at the leading edge of migrating cells, a subset undergoes maturation into focal complexes at the lamellipodia-lamella interface which further mature into FAs under increased contractile forces generated through acto-myosin contractility by actin stress fibers. FA disassembly occurs at the rear part of the cell to allow forward movement of the cell body (Kumari et al. 2024).

Importantly, FAs do not only interact with the actin cytoskeleton, but also with microtubules. This interaction was shown at the cell periphery and led to microtubule polymerization stability (Akhmanova, Stehbens, and Yap 2009).

1.3. Microtubules: Establishing cell polarity

Microtubules make up another major part of the cytoskeleton and are much wider (diameter of 25 nm) and stiffer than actin or intermediate filaments. As hollow filaments usually consisting of 13 protofilaments, microtubules are composed of α-tubulin and β-tubulin heterodimers. These heterodimers assemble in a head-to-tail fashion giving microtubules an intrinsic polarity with two different ends: a plus end exposing β-tubulin and a minus end exposing α-tubulin (Garcin and Straube 2019). In most cells, the minus end is embedded in the centrosome, the main MTOC in animal cells (J. Zhang and Wang 2017), while the plus end grows through the intracellular space and often reaches the cell edges. This results in the microtubule network itself being polarized from the center – where the MTOC is located – towards the periphery

(Kaverina and Straube 2011; Wehrle-Haller and Imhof 2003). Microtubule growth is very dynamic, especially at the cell front, with continuous phases of catastrophe events (switching from growth to shrinkage) and rescue events (switching from shrinkage to growth). Growth describes the phase of polymerisation while shrinkage constitutes depolymerisation. To explain this dynamic, the GTP cap model is used: If GTP tubulin is present at the growing end, it contacts α-tubulin and creates a place where GTP hydrolysis occurs. Presence of “older”, not hydrolyzed GTP at the plus end stabilizes growth phases by acting as a GTP cap. Loss of the GTP cap results in catastrophe events where microtubule shrinkage occurs. These events mostly happen at the more dynamic plus end, as the minus ends lay connected inside the MTOC (Garcin and Straube 2019; Kaverina and Straube 2011).

The position of the MTOC is a prominent cell characteristic. While epithelial cells contain non-centrosomal MTOCs at apical membrane regions, mesenchymal cells display dominant centrosomal MTOCs close to the nucleus and Golgi apparatus (Thapa et al. 2023). This centrosomal organization has long been deemed important in defining the polarity of a cell during directional migration, in particular its localization relative to the nucleus. However, different microenvironmental conditions and cell types display dynamic centrosomal location changes, e.g. switching substrate geometry from two-dimensional (2D) to three-dimensional (3D) increased the probability of centrosome positioning behind the nucleus towards the cell rear in NIH3T3 fibroblasts (J. Zhang and Wang 2017).

In general, microtubules provide structure and act as trafficking platforms for the transport of vesicles and organelles inside the cell. Due to their own structure and polarity, they provide tracks for molecular motors of the kinesin superfamily, in particular kinesin and dynein, that enable the transport of molecules and organelles through every part of the cell. Kinesin motor proteins are responsible for transport towards the plus end (anterograde), while dynein moves towards the minus end (retrograde). Among the cargo transported are signaling molecules, like small GTPases (Rac and Cdc42), as well as membrane components and small intermediate filaments (Hohmann and Dehghani 2019). Polarized transport of vesicles containing integrins to the cell front promotes protrusion and FA assembly, while transport of dynamin and specific kinases (like mitogen-activated protein kinase kinase kinase kinase 4, MAP4K4) to the cell rear helps with FA disassembly at the back (Tang and Gerlach 2017). To summarize, microtubules play an important role during directional migration, as the MTOC will re-orient towards the direction of migration in 2D microenvironments. The polarized organization of microtubules from the center to the periphery helps with establishing polarized trafficking to the cell front and cell rear, while simultaneously providing structure for intracellular organization (Wehrle-Haller and Imhof 2003).

1.4. Role of ion channels in cell migration

Alongside an asymmetric distribution of cytoskeletal components, migrating cells show polarization of subcellular membrane proteins like chemokine receptors, transport proteins and ion channels. Local concentration gradients of different ions control the cell migration machinery, for example uneven distribution of intracellular Ca^{2+} and H^{+} concentration leads to spatially confined regulation of cell migration machinery components like the cytoskeleton. Independent of the ions involved, or the features of the ion gradient, uneven ion concentrations require uneven spatial distributions or a local difference in the regulation of the corresponding ion transporters and channels (Stock et al. 2013). As the role of ion channels during cell migration is vast and has been discussed in great detail in the following reviews (Schwab et al. 2012; Stock et al. 2013; Xu, Martinoia, and Szabo 2015), this sections aims to summarize only a few relevant ion channels and their location during cell migration (**Fig. 2**). In short, transient receptor potential channels (TRPCs, especially TRPC1 and TRPC6) are mechanosensitive ion channels that are mainly found on the plasma membrane, inducing local Ca^{2+} influxes that could steer cell migration through their influence on the actin cytoskeleton (Canales Coutiño and Mayor 2021; Canales et al. 2019). The expression of TRPCs is ubiquitous, but there are some tissue-specific channels, such as TRPC6, which is highly expressed in endothelial cells (ECs) (Schwab et al. 2012). Piezo channels are activated through mechanical changes making them an attractive target to study during mechanotransduction processes (Canales Coutiño and Mayor 2021). Transient receptor potential vanilloid (TRPV) channels also control localized Ca^{2+} influxes. High expression of TRPV4 is linked to increased cell migration of ECs, likely through its direct interaction with actin fibers and the promotion of Rac1 activity (Canales Coutiño and Mayor 2021; Canales et al. 2019). In mitochondria, the mitochondrial Ca^{2+} uniporter (MCU) is an inner membrane Ca^{2+} uptake channel that regulates adenosine triphosphate (ATP) production through oxidative phosphorylation (OXPHOS) tuning and reactive oxygen species (ROS) production (Xu, Martinoia, and Szabo 2015). Voltage-dependent anion channel (VDAC) on the outer membrane of mitochondria facilitates the rapid exchange of Ca^{2+}, ATP and other metabolites which supports high local energy production at the leading edge (Xu, Martinoia, and Szabo 2015; Feng and Kornmann 2018). ER Ca^{2+} changes are important for independent ER signalling and in ER-plasma membrane junctions. Inositol triphosphate receptors (IP_3Rs) are Ca^{2+} release channels responsible for local and global Ca^{2+} changes that drive actomyosin contractility and rear retraction in polarized cells. Ryanodine receptors (RyR) also release Ca^{2+} which amplifies Ca^{2+} signalling and contributes to contractility (Xu, Martinoia, and Szabo 2015; Huang et al. 2025). Stromal Interaction Molecular 1 (STIM1) and Orai1 act together in ER-plasma membrane junction to regulate the store-operated calcium entry (SOCE). STIM1 in

the ER membrane senses Ca^{2+} concentration senses. Upon Ca^{2+} decrease in the ER, STIM1 gets activated and diffuses to the cortical ER in ER-plasma membrane junction. There, STIM1 traps and clusters Orai1 in the plasma membrane to open its pore through which Ca^{2+} from the extracellular milieu reenters the cytoplasm to either refill the ER stores or act as an intracellular second messenger (Kodakandla, Akimzhanov, and Boehning 2023; Qiu and Lewis 2019).

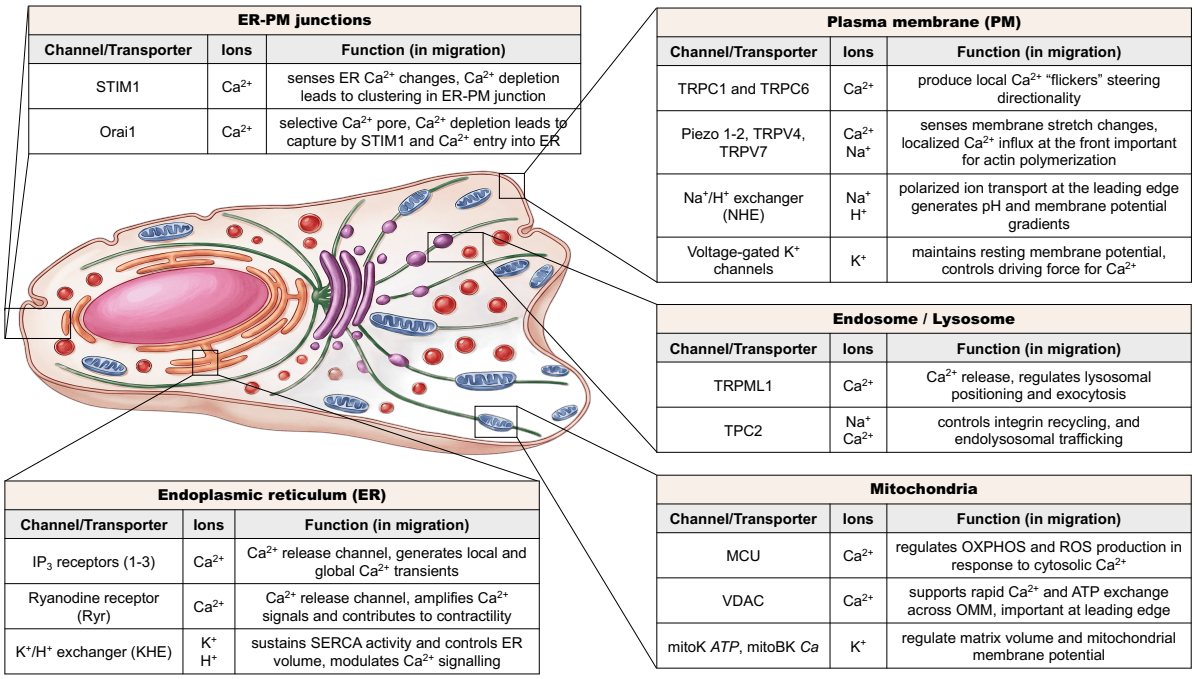

ER-PM junctions

Channel/Transporter	Ions	Function (in migration)
STIM1	Ca^{2+}	senses ER Ca^{2+} changes, Ca^{2+} depletion leads to clustering in ER-PM junction
Orai1	Ca^{2+}	selective Ca^{2+} pore, Ca^{2+} depletion leads to capture by STIM1 and Ca^{2+} entry into ER

Plasma membrane (PM)

Channel/Transporter	Ions	Function (in migration)
TRPC1 and TRPC6	Ca^{2+}	produce local Ca^{2+} "flickers" steering directionality
Piezo 1-2, TRPV4, TRPV7	Ca^{2+} Na^{+}	senses membrane stretch changes, localized Ca^{2+} influx at the front important for actin polymerization
Na^{+}/H^{+} exchanger (NHE)	Na^{+} H^{+}	polarized ion transport at the leading edge generates pH and membrane potential gradients
Voltage-gated K^{+} channels	K^{+}	maintains resting membrane potential, controls driving force for Ca^{2+}

Endosome / Lysosome

Channel/Transporter	Ions	Function (in migration)
TRPML1	Ca^{2+}	Ca^{2+} release, regulates lysosomal positioning and exocytosis
TPC2	Na^{+} Ca^{2+}	controls integrin recycling, and endolysosomal trafficking

Endoplasmic reticulum (ER)

Channel/Transporter	Ions	Function (in migration)
IP_3 receptors (1-3)	Ca^{2+}	Ca^{2+} release channel, generates local and global Ca^{2+} transients
Ryanodine receptor (Ryr)	Ca^{2+}	Ca^{2+} release channel, amplifies Ca^{2+} signals and contributes to contractility
K^{+}/H^{+} exchanger (KHE)	K^{+} H^{+}	sustains SERCA activity and controls ER volume, modulates Ca^{2+} signalling

Mitochondria

Channel/Transporter	Ions	Function (in migration)
MCU	Ca^{2+}	regulates OXPHOS and ROS production in response to cytosolic Ca^{2+}
VDAC	Ca^{2+}	supports rapid Ca^{2+} and ATP exchange across OMM, important at leading edge
mitoK *ATP*, mitoBK *Ca*	K^{+}	regulate matrix volume and mitochondrial membrane potential

Figure 2: Important ion channels during cell migration and their cellular location.

Different cellular compartments express distinct ion channels and transporters that act in cell signalling pathways. One of the most studied ions is calcium (Ca^{2+}) and every organelle discussed – endosomes, lysosomes, mitochondria and ER – displays clear transport mechanisms for Ca^{2+} entry and release. Every channel/transporter mentioned in this overview is described in either one or multiple of the following reviews: Schwab et al. (2012), Stock et al. (2013), Xu et al. (2015). Image of polarized cell created with illustrae.com.

1.5. Methods to study cell migration

There are multiple techniques available to study single and collective cell migration. Major findings on cell translocation and cell directionality have been made using flat, 2D culture substrate surfaces (Wu et al. 2025). However, it's been known for decades from other morphodynamics processes like cell division, that the 3D environment modulates cell behaviour (Yamada and Sixt 2019). The 3D environment, mainly composed of the ECM, provides physical and chemical cues to influence cell behaviours. To name a few examples, spatial cues like confinement and tissue topography steer the direction of migration by physically restricting some area for cell movement. Mechanical cues like tissue stiffness control speed and directionality of migrating cells (Stehbens, Scarpa, and White 2024).

Changing the environment from 2D to 3D or vice versa has effects on various cell components. Looking at FAs, cells on 2D surfaces form adhesions on only one surface while in 3D environments they are found in every direction. The structure of FAs also differs in 3D as cells typically do not form large FAs that are connected to actin stress fibers. Further, cells often lack thick contractile actomyosin stress fibers in 3D indicating complex cytoskeletal changes when changing the dimension cell migration takes place in (Saraswathibhatla, Indana, and Chaudhuri 2023).

When talking about the dimensions in which cell migration can take place, one-dimensional (1D) migration assays need to be mentioned. These 1D assays significantly simplify problems of cell shape as protrusions are generally restricted to two ends of a cell. Single cell migration is studied on 1D micropatterned lines and allows for high-throughput analysis of a larger amount of trajectories that can be considered as models for cell motion on fibers in the 3D ECM (Heyn, Rädler, and Falcke 2024). Comparing the different dimensions, 2D migration assays have the advantage of simplifying the physical microenvironment migration takes place in. This makes it easier to quantify, compare and model molecular mechanisms that influence cell migration. It further offers the opportunity to perform high throughput and advance imaging quality which is harder to achieve in complex 3D environments (Pawluchin and Galic 2022; Kramer et al. 2013).

2. Endothelial cells and vascular function

Endothelial cells (ECs), first described in 1865, originate from mesodermal cells that differentiate into hemangioblasts (His 1865; Lamalice, Le Boeuf, and Huot 2007). These cells form primitive blood islands as the first vascular structures during development. From those blood islands, the peripheral hemangioblasts differentiate into angioblasts, which are the precursors of mature ECs. During a process called vasculogenesis, ECs migrate and fuse blood islands, remodelling them into the first tubular structures that give rise to the vascular plexus which further develops into larger vessels. Mature ECs form the vascular endothelium, the coating of the interior walls of arteries, capillaries, veins and lymphatic vessels (this thesis will focus exclusively on blood ECs) (Lamalice, Le Boeuf, and Huot 2007; Marziano, Genet, and Hirschi 2021). They anchor to the basal lamina, and both ECs and basal lamina form the vascular intima, also called tunica intima, with an estimated surface area of 3000-6000 m^2 of the human body. The number of ECs in the human body varies from 1 to 6 $x10^{13}$ cells, but their morphology is generally 10-30 µm wide and slightly elongated with 30-50 µm in length. Moreover, ECs are thin and they exhibit a heterogenous thickness ranging from 0.1-10 µm in height (Lamalice, Le Boeuf, and Huot 2007; Krüger-Genge et al. 2019). The tunica intima is the main inner layer of the arterial vessel wall, followed by the tunica media and the tunica

adventitia as the outer layer. The cells that form part of the tunica media include smooth muscle cells, while the tunica adventitia includes connective tissue and fibroblasts (Y. Wang et al. 2025).

Under physiological conditions, the vascular microenvironment is essential for vascular homeostasis, a state of stable internal environment of all life activity (cells, tissues, organs and whole organisms), as well as vascular structure and function (Y. Wang et al. 2025).

Under pathological conditions, endothelial dysfunction is defined by alterations impacting the vasoprotective homeostatic function, in particular reduced nitric oxide (NO) production and reduced sensitivity to vasodilators or changes in blood pressure. This state leads to proinflammatory, prothrombotic conditions and a less compliant vessel wall. The proinflammatory conditions often appear under worsened ROS production suggesting a correlation between oxidative stress, inflammation and endothelial dysfunction (X. Wang and He 2024). Endothelial dysfunction plays a central role in a plethora of diseases, ranging from cardiovascular diseases to atherosclerosis, diabetes mellitus, insulin resistance, chronic kidney failure and tumor growth (Rajendran et al. 2013). Interestingly, several studies suggest that a disproportionate activation of the unfolded protein response (UPR) following endoplasmic reticulum (ER) stress contributes to endothelial dysfunction (Cimellaro et al. 2016). Further, a dysregulated UPR upon ER stress is observed in many diseases ranging from metabolic disorders and obesity to Parkinson's, Alzheimer's and cardiovascular diseases (Koksal, Verne, and Zhou 2021).

2.1. Maternal obesity associates with endoplasmic reticulum stress

As mentioned before, ER stress is linked to different diseases, one of them being obesity. Moreover, these disease conditions are associated with vascular dysfunctions, such as endothelial dysfunction or distorted angiogenesis (Sáez et al. 2014). Angiogenesis is the process in which new blood vessels are generated from pre-existing vasculature. During angiogenesis, ECs break through a basement membrane and migrate towards an angiogenic stimulus, usually vascular endothelial growth factor (VEGF). For ECs forming blood vessels VEGF-A is the pro-angiogenic factor, for lymphatic vasculature its predominantly VEGF-C (Shin, Huggenberger, and Detmar 2008; Shibuya 2011). Behind the migratory front, EC proliferation takes place to generate enough cells for new vessel formation (Auerbach et al. 2003). Different subtypes of endothelial cells are responsible for exerting the different stages of angiogenesis. Tip cells are migratory cells initiating vessel sprouting, elongation and anastomosis. Cellular components important for proliferation and growth are synthesized by stalk cells, while phalanx cells are non-proliferating and rest inside the newly built vessel structure (Luo et al. 2023). ER stress disrupts two mechanisms required for angiogenesis,

VEGF signalling and endothelial migration. However, the molecular mechanisms regulating endothelial migration upon ER stress induction remain unknown. In the context of maternal obesity, the pathological environment may not only affect the mother, but also the fetal tissue (Sáez et al. 2014) (**Fig. 3A**). Through a process called fetal programming, the fetus senses, receives and responds to the intrauterine environment which can lead to structural and functional changes in cells, tissues and organ systems (Lindsay et al. 2019). During pre-pregnancy maternal obesity, the ER stress response leads to insulin resistance in human umbilical vein endothelial cells (HUVECs) and the risk of ER-stress induced endothelial dysfunction can be transferred to the offspring. Several of the proteins involved in ER stress signalling and insulin resistance, in particular Rho and Akt, also play important roles in the cytoskeletal crosstalk during migration, suggesting that this response is impaired or distorted during ER stress conditions (Villalobos-Labra et al. 2018).

To study ER stress *in vitro*, tunicamycin (TN) is used as a trigger of the UPR. TN inhibits N-glycosylation resulting in accumulation of misfolded, unglycosylated proteins that have been shown to initiate all three branches of the UPR (Sáez et al. 2014; Abdullahi et al. 2017) (**Fig. 3B**). Compared to other ER stress inducers like thapsigargin, TN works as a rapid inducer and better recapitulates the metabolic alterations associated with ER stress (Abdullahi et al. 2017). HUVECs obtained after term pregnancy from women with a normal weight during pregnancy, showed the UPR protein activating transcription factor 6 (ATF6) mainly in perinuclear areas. HUVECs isolated from maternal obesity pregnancies, showed nuclear ATF6 localization, a phenotype that could be mimicked with TN-treatment in unstressed cells (Villalobos-Labra et al. 2018). As ER stress happens inside the ER and alters several structural proteins, ER morphology and function will be described in more detail in the following sections.

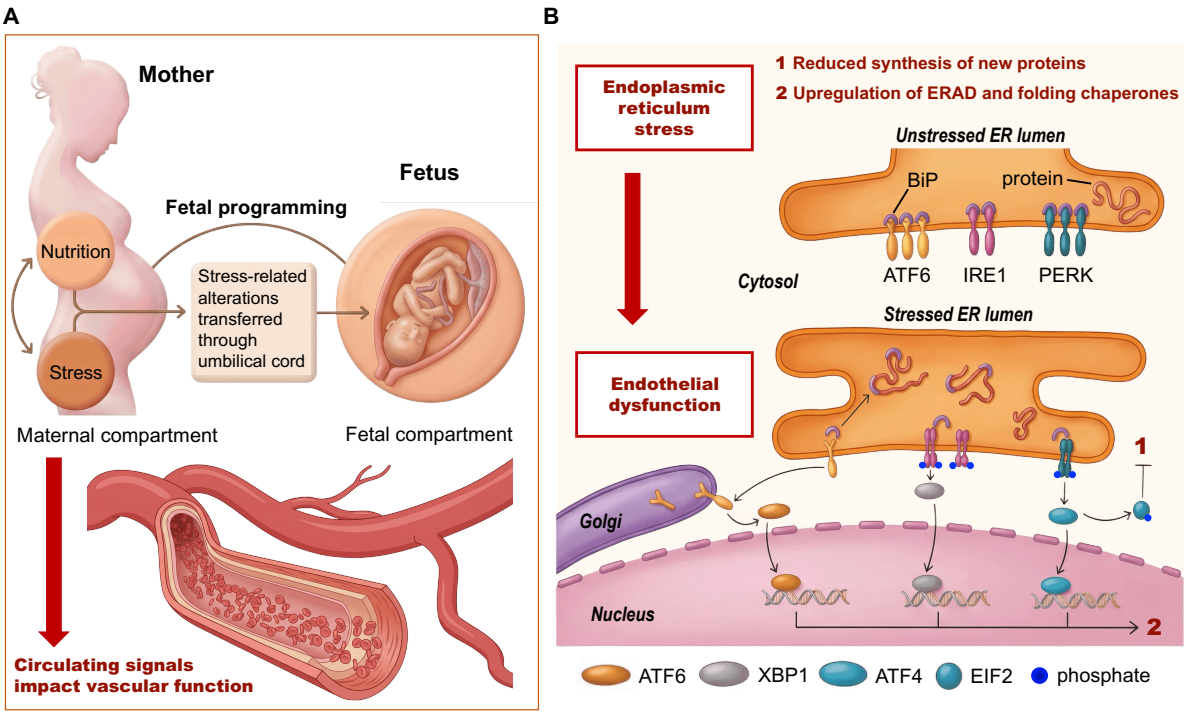

Figure 3: Maternal obesity induced fetal programming impacts vascular function.

(A) During maternal obese pregnancy, cellular stress can be transferred through the umbilical cord in a process called fetal programming. In the offspring, this cellular stress can lead to insulin resistance and endothelial dysfunction, as circulating signals impact vascular function.
(B) Circulating signals during obesity and metabolic disorders affect the cellular state and trigger a stress response. During ER stress, where unfolded or misfolded proteins accumulate, the unfolded protein response (UPR) gets activated which aims to (1) reduce the synthesis of new proteins, and (2) upregulate the ERAD and folding chaperones to restore ER homeostasis. ER stress conditions are linked to vascular dysfunction and could affect endothelial behaviour.
(A) adapted from Lindsay et al (2018). (B) adapted from Todd et al. (2008). Figure created with illustrae.com.

2.2. Endoplasmic reticulum morphology and function

The endoplasmic reticulum is among the largest organelles in eukaryotic cells, and plays key roles in protein and lipid synthesis, protein folding and trafficking, as well as Ca^{2+} storage and release. The ER has distinct structural domains, with the largest domain wrapping around the nucleus and forming a double membrane called the nuclear envelope (Schwarz and Blower 2016) . Connected to this domain is the peripheral ER that spans throughout the cell and is divided into the smooth ER and rough ER. Using super-resolution techniques, the peripheral ER is described as a network of ER “sheets” and ER tubules that are separated from the cytosol and other cellular compartments by the ER membrane. The ER membrane is a single lipid bilayer, responsible for governing the passage of molecules between the cytosol and ER lumen. Super-resolution techniques have further revealed that the previously described ER sheets are not continuous in nature, but riddled with spaces and composed of dense tubular matrices, termed ER matrices (Phillips and Voeltz 2016; Nixon-Abell et al. 2016). While the

flattened ER sheets display a lower membrane curvature, ER tubules are dynamic and present a high membrane curvature (Z. Chen et al. 2025). As morphology follows function, ER sheets are generally covered with ribosomes (therefore often termed rough ER), whereas ER tubules are branched and interconnected, spreading out through the cytosol and associating with significantly less ribosomes (therefore termed smooth ER). Synthesis, folding and post-translational modifications of secreted and membrane-bound proteins take place inside the ER sheet structures, Ca^{2+} storage and lipid synthesis happen inside the ER tubules (Oakes and Papa 2015; Di Conza and Ho 2020). The ER as a dynamic organelle is constantly moved and maintained in its reticular network by microtubule motor proteins. Through fluorescent labelling, it was revealed that the ER moves by sliding the ER tubules along microtubules from the center to the periphery. This ER tubule sliding is mainly facilitated by kinesin-1, but can also occur through the interaction of ER tubules with tip attachment complexes (TACs) at the (+)-ends of microtubules. End-binding protein 1 (EB1) at the growing (+)-end interacts with STIM1 on the ER membrane site generating TACs. Static ER-microtubule interactions are mediated by other proteins, such as cytoskeleton-linking membrane protein 63 (Climp63) (Bola and Allan 2009).

Protein folding into three-dimensional shapes happens inside the ER lumen with the help of chaperone complexes. Once properly folded, proteins will be trafficked from the ER and progress down the secretory pathway to their destined location (Oakes and Papa 2015; Malhotra and Kaufman 2011). If proteins do not reach the quality criteria (e.g. defects in the cytosolic domain or lesions in the luminal domain), they will be targeted to the ER associated degradation (ERAD) system (Meusser et al. 2005). If the protein folding demand outweighs the protein folding capacity of the ER, unfolded or improperly folded proteins accumulate inside the ER lumen, a condition termed ER stress that will be discussed in more detail below. The ER stress condition can also be triggered by alterations in Ca^{2+} homeostasis (Limia et al. 2019).

2.3. Endoplasmic reticulum stress and the Unfolded Protein Response

The ERs intraluminal environment is sensitive to disturbances like energy shortages, oxidative stress, depletion in Ca^{2+} concentration, gene mutations and elevated protein traffic. These alterations in ER homeostasis may lead to an accumulation of unfolded or misfolded proteins inside the ER lumen, a condition known as ER stress. Under homeostatic conditions, three transmembrane proteins, ATF6 (activating transcription factor 6), IRE1α (inositol-requiring 1α) and PERK (double stranded RNA-dependent protein kinase [PKR]-like ER kinase), reside inside the membrane of the ER and display three structural domains: the ER-luminal domain senses unfolded or improperly folded proteins, the transmembrane domain targets the sensor

proteins to the ER membrane, and the cytosolic domain transmits the signals to the downstream targets (K. Zhang and Kaufman 2008). In unstressed cells, the ER chaperone binding immunoglobulin protein (BiP, also called immunoglobulin-heavy-chain-binding protein, GRP78) is bound to the luminal domains of ATF6, IRE1α and PERK, rendering them inactive (Frakes and Dillin 2017). Once unfolded or misfolded proteins accumulate, BiP dissociates from the ER sensors (which activates them) and binds to the unfolded or misfolded proteins (Oslowski and Urano 2011). Unfolded proteins also directly bind the ER stress sensors IRE1α and PERK, resulting in their dimerization, oligomerization and finally their activation (Frakes and Dillin 2017). The most immediate response of the UPR is the homodimerization and *trans*-phosphorylation of PERK. PERK further phosphorylates the α-subunit of eukaryotic translation-initiation factor 2α (eIF2α). Phosphorylated eIF2α inhibits the assembly of the 80S ribosome which will inhibit protein synthesis, reducing ER workload. Despite decreased translation, certain transcripts will keep being translated, including the activating transcription factor 4 (ATF4). ATF4 regulates genes like the pro-apoptotic C/EBP homologous protein (CHOP). This pathway is activated to initiate apoptosis if protein homeostasis is not restored to protect the organism from detrimental effects. IRE1α activation is the most evolutionary conserved branch of the UPR. Once activated, the transmembrane kinase and endoribonuclease initiates the regulated splicing of a 26-base intron from mRNA encoding X-box-binding protein 1 (XBP1) which results in a frameshift generating spliced XBP1 isoforms. XBP1 shows potent activity as a transcription factor. It activates target genes like chaperones important for proper protein folding. If BiP releases the luminal domain of ATF6, it translocates to the Golgi where it will be cleaved by protease site-1 and site-2 (S1P and S2P) to release the NH_2-terminal domain. This ATF6 fragment is released into the cytosol from where it will translocate to the nucleus and initiate the transcription of XBP1 and other genes required in the ERAD (Read and Schröder 2021; Oslowski and Urano 2011; Jain 2013; K. Zhang and Kaufman 2008; Frakes and Dillin 2017; Todd, Lee, and Glimcher 2008). The UPR aims to (1) reduce the amount of newly synthesized proteins that need to be further processed by the ER, (2) increase the translocation and degradation of misfolded proteins inside the ER lumen, and (3) augment the protein folding capacity of the ER (Rao, Ellerby, and Bredesen 2004).

2.4. Endoplasmic reticulum – organelle contacts

Historically, membrane-bound organelles like the ER were viewed as separate compartments. However, this is not the case, as organelles directly interact through membrane contact sites (MCSs). These MCSs are regions where the membranes of organelles are tethered together without actually fusing. The ER is known to interact with mitochondria, lysosomes, endosomes, lipid droplets, peroxisomes, Golgi and the plasma membrane through MCSs

(Hong and Inagi 2025). Here, the focus will be kept on the interaction of ER and mitochondria, as well as ER and plasma membrane. Through electron micrographs and tomography, it was revealed that ribosomes are excluded in the MCSs interface. The distance between ER and mitochondria has been measured at 6-15 nm, and the ER will interact at multiple small positions with mitochondria. Interestingly, organelle trafficking does not impact MCSs, as ER and mitochondria tethering is maintained over long distances (Phillips and Voeltz 2016). The junctions formed between ER and mitochondria are called mitochondria-associated membranes (MAMs) or mitochondria-ER contacts (MERCs) (Stacchiotti et al. 2019). Next to the impact on cell migration, these contacts are essential for processes like autophagy, lipid and Ca^{2+} fluxes, apoptosis and mitochondrial division. Further, through these junctions, rapid exchanges of biological molecules are made possible which maintain cellular health (Paupe and Prudent 2018; Missiroli et al. 2018). Many proteins have been identified that are directly involved in the tethering of ER and mitochondria and their functional interaction. Fusion proteins like mitofusin 2 (Mfn2) is one of the proteins that directly link ER and mitochondria as it is present in both organelle membranes (Scorrano 2013). Another important protein that has been shown to reside in MAMs is PERK which interacts with Mfn2 and increases the contact surface between ER and mitochondria (Martucciello et al. 2020). A rather new function of MERCs was established after it was shown that ER tubules cross over and wrap around mitochondria leading to mitochondrial membrane constriction and a diameter reduction by almost 30%. This leads to mitochondrial fission independent of dynamin-related protein 1 (Drp1) (Vannuvel et al. 2013). This raises the question how ER stress-related changes in morphology affect mitochondrial dynamics.

The contact between ER and plasma membrane is important during mechanotransduction events. ER-plasma membrane contacts are known to regulate the activation of SOCE, autophagosome biogenesis, and lipid transfer. Using tendon cells, it was shown very recently that ER membrane tension increases adaptively after cyclic mechanical strain on the plasma membrane suggesting a key role of the ER in propagating mechanical signals from the plasma membrane to the cell interior (Z. Chen et al. 2025).

3. Mitochondria morphology and function

Mitochondria are cellular organelles that constitute for up to 40% of cytoplasmic volume in eukaryotic cells depending on their energy demand (A. Li et al. 2020). Originating from eubacteria, mitochondria have an outer membrane and an inner membrane system with distinct functions. The space between those two membranes, the intermembrane space (IMS), is roughly 20-30 nm wide and coordinates the exchange of proteins, lipids, and metal ions between the mitochondria matrix and the cytosol, among other functions. The IMS has the

largest variability of protein import mechanisms, as most nuclear-coded mitochondrial proteins have to be imported into the mitochondria from the cytosol space (Herrmann and Riemer 2010; Edwards, Eaglesfield, and Tokatlidis 2021). Within the IMS, cytochrome c is sequestered which directly activates caspases that are required for the predominant form of programmed cell death, apoptosis. Caspases cleave a plethora of hundred different proteins which in turn leads to rapid apoptosis. Visual characteristics of apoptosis include plasma membrane blebbing and nuclear condensation (Tait and Green 2012) (**Fig. 4A**).

The outer mitochondrial membrane (OMM) represents the boundary towards the cytoplasm and OMM proteins, like Drp1 and fusion proteins like mitofusins (Mfn1, Mfn2), play a part in the establishment of contact sites between mitochondria and other organelles as well as the communication between them (Xian and Liou 2021). The voltage-dependent anion channel (VDAC), another protein present on the OMM, is the major transit pore that transports metabolites and metal ions across the OMM. VDAC1 shows a preference for negatively charged substrates like glutamate and adenosine triphosphate (ATP), but is also able to transport positively charged metabolites like acetylcholine or dopamine (Daniilidis et al. 2025) (**Fig. 4A**).

The inner mitochondrial membrane (IMM) extensively folds into itself giving rise to structures called cristae. The IMM divides the IMS from the matrix and is divided into a smooth inner boundary membrane close to the OMM, and the cristae membrane that projects into the matrix and expands the IMM surface ~4- to 5-fold (**Fig. 4A**). The electron transport chain (ETC) and the ATP synthase are embedded inside those cristae and are important for energy generation in the form of ATP. Five complexes together with cytochrome c make up the ETC: Complex I = NADH:ubiquinone (coenzyme Q, CoQ) dehydrogenase; Complex II = succinate dehydrogenase or succinate-CoQ reductase; Complex III = cytochrome bc_1 complex or CoQ-cytochrome c reductase; Complex IV = cytochrome-c oxidase; Complex V = F_0F_1-ATPase/H^+ pump or F_0F_1-ATP synthase or F-ATPase (Tábara, Segawa, and Prudent 2025; Freeman, Grinstein, and Orlowski 2023). As mitochondria are termed the “powerhouse of the cell”, their function was often reduced to the synthesis of ATP through oxidative phosphorylation (OXPHOS). However, it is well known that mitochondria actively participate in cellular signalling through regulation of signalling molecules like Ca^{2+} and ROS. They also serve as physical platforms where protein-protein signalling occurs through direct contact with other organelles (Tait and Green 2012; Peng et al. 2023) (**Fig. 4B**).

Mitochondria are dynamic organelles with varying sizes, ranging from ~0.2-0.5 µm in width and ~0.5-10 µm in length. Often, they display a network-like distribution and are in constant movement (Walsh et al. 2017). Mitochondria shape is associated with their function, which differs between cell types and can shift drastically under metabolic stress conditions (Stacchiotti et al. 2019). These mitochondrial dynamics are the result of a constant change

between fusion and fission events that have to be kept in balance to allow cell survival and optimal cell function (Adebayo et al. 2021). Fusion events produce elongated or tubular, interconnected mitochondria, while fission events lead to small, spherical mitochondria through shortening processes (Galloway and Yoon 2013; Stacchiotti et al. 2019). Both fusion and fission are essential for mitochondrial redistribution and growth (van der Bliek, Shen, and Kawajiri 2013) and are regulated by different protein machineries that remodel the OMM and IMM (Scorrano 2013). Fusion events require fusion of the OMM and IMM and are mediated by Mfn1, Mfn2 and optic atrophy (OPA1). Mfn1 and Mfn2 are two dynamin-related GTPases that are anchored to the OMM mediate the fusion of the OMM to another OMM, while OPA1 is located on the IMM to facilitate its fusion with another IMM. Fusion events take place when maximal ATP production is needed, when mitochondria have to fully rely on OXPHOS, or when they have to cope with stress conditions. It was shown that fusion events are dependent on the mitochondrial membrane potential ($\Delta\Psi_m$): if $\Delta\Psi_m$ collapses, mitochondria are unable to form elongated mitochondria (Brocard, Rintoul, and Reynolds 2003). Fission of mitochondria is dependent on Drp1 which is mainly localized in the cytoplasm. Upon activation, Drp1 translocates to mitochondria where it forms helical structures that encircle and penetrate the mitochondria (Vannuvel et al. 2013; Da Silva et al. 2014). Fission events eliminate damaged mitochondria through a process termed mitophagy, the autophagy of mitochondria, and relocalizes mitochondria inside the cell (Vannuvel et al. 2013).

Mitochondria are transported along microtubules and accumulate at sites where high metabolic activity is required (McCarron et al. 2013). In addition to the transport of mitochondria, microtubules also anchor them in place. Movement along microtubules is bidirectional and depends on the activity of kinesin 1 (anterograde transport) and dynein (retrograde transport) that bind the OMM via the Miro-Milton complex. Mitochondrial associated to microtubules also plays a role during fusion and fission with mitochondrial length mimicking microtubule length (Chalmers et al. 2016). Cells with shorter microtubules undergo increased fission while longer microtubules protect from fission events (Rube and van der Bliek 2004; Mehta et al. 2019; Paupe and Prudent 2018). To summarize, mitochondria are dynamic organelles that adapt to the energy requirements of the cell. Because their main function of providing energy is mediated through the ECM and dependent on a chemical (ΔpH_m) and electrical gradient ($\Delta\Psi_m$), these two factors will be described in more detail in the following sections.

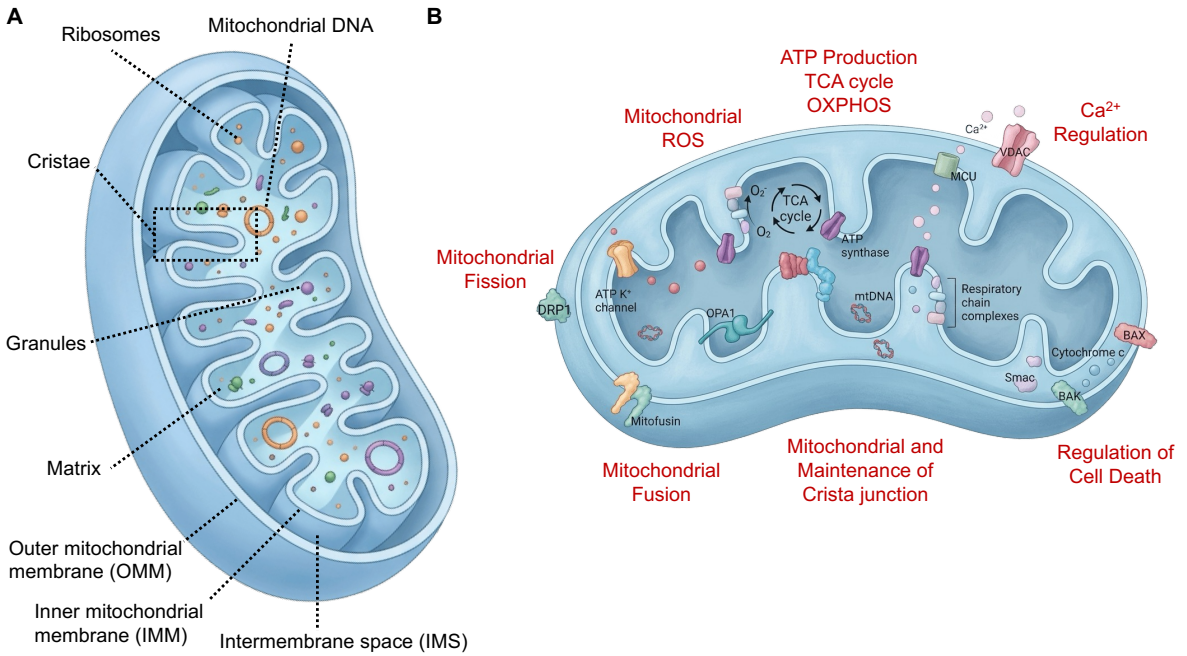

Figure 4: Mitochondria structure relates to mitochondria function.

(A) Mitochondria structure. Mitochondria are double-membrane organelles made up of an outer mitochondrial membrane (OMM), the intermembrane space (IMS), and the inner mitochondrial membrane (IMM) that folds into itself giving rise to cristae. The IMM separates the IMS from the mitochondria matrix which houses the mitochondrial DNA (mtDNA), ribosomes and granules.
(B) Mitochondria function. Mitochondria execute a variety of functions ranging from the regulation of cell death and calcium regulation to reactive oxygen species (ROS) and ATP production via oxidative phosphorylation (OXPHOS). Mitochondria function is associated to shape and the dynamics of mitochondrial shape are controlled by fusion and fission events and the maintenance of cristae junctions.
(B) adapted from Peng et al. (2023). Figure created with illustrae.com.

3.1. Mitochondrial pH

Organelles exhibit distinct pH values that are essential for the optimal rate and coordination of the biochemical reactions they supply to the cell machinery (Lee et al. 2025). These pH values differ between subcellular compartments giving rise to proton (H^+) gradients. While the pH of the cytoplasm has been studied extensively, less is known about the pH regulations of intracellular organelles like mitochondria (Freeman, Grinstein, and Orlowski 2023).

Mitochondrial functions depend on the ability of mitochondria to move H^+ across the IMM during OXPHOS. Complexes I, III, and IV of the ETC use the free energy of substrate oxidation to generate a H^+ gradient across the IMM. Complex V then uses the energy stored in the proton gradient to catalyze the conversion of adenosine diphosphate (ADP) to ATP within the matrix (Santo-Domingo and Demaurex 2012). Briefly summarized, complexes I and II receive nicotinamide adenine dinucleotide hydrogen (NADH) and flavin adenine dinucleotide, dihydrogenated form ($FADH_2$) from the citric acid cycle. Through a series of redox reactions, electrons are transferred sequentially through complexes I-IV that are coupled to the vectoral

export of protons from the matrix to the IMS. These redox reactions culminate in a reduction of oxygen into water and the generation of a H^+ gradient across the IMM (Freeman, Grinstein, and Orlowski 2023). Because the IMM displays a low permeability for ions, including H^+, transport of H^+ by the ETC complexes creates an electrochemical gradient, also termed the proton-motive force Δp. Δp is the sum of $\Delta\Psi_m$ (electrical gradient) and ΔpH_m (chemical gradient). While both gradients contribute equally to Δp, other mechanisms rely solely on either $\Delta\Psi_m$ or ΔpH_m. Prominent examples for $\Delta\Psi_m$ reliance are the Ca^{2+} uptake via the mitochondrial Ca^{2+} uniporter (MCU) or the import of mitochondrial resident proteins through the translocase of outer membrane (TOM) and translocase of inner membrane (TIM) complexes. In contrast, the Ca^{2+}-H^+ exchanger (CHX), the K^+-H^+ exchanger (KHX), and the Na^+-H^+ exchanger (NHX) rely solely on ΔpH_m. To measure the pH in mitochondria, the $\Delta\Psi_m$ needs to be recorded as well. Δp is predominantly comprised of $\Delta\Psi_m$ (70-80%). ΔpH_m contributes 20-30% to Δp. In isolated mitochondria, Δp was found to range between 180 to 220 mV with $\Delta\Psi_m$ ranging from 150 to 180 mV and ΔpH_m from 0.5 to 1.2 pH units, which results in pH of mitochondria from 8.2 to 7.5 (Santo-Domingo and Demaurex 2012).

3.2. Mitochondrial membrane potential (Ψ)

Mitochondria function is directly linked to $\Delta\Psi_m$, as intact mitochondria display a polarized state with a negative charge (~180 mV) across their inner membrane. A loss of $\Delta\Psi_m$ is accompanied by cytochrome c release, and observed during apoptotic cell death (Walsh et al. 2017; Crowley, Christensen, and Waterhouse 2016). The $\Delta\Psi_m$ serves as an intermediate energy form which is used by the ATP synthase to synthesize ATP. However, $\Delta\Psi_m$ is not only used in ATP synthesis, but has recently been described as a factor controlling mitochondria viability and participating in the elimination of unhealthy mitochondria (Zorova et al. 2018).

As described above, the generation and importance of $\Delta\Psi_m$ makes it an attractive property to study during cellular changes. Several fluorescent lipophilic cationic dyes, e.g. tetramethylrhodamine methyl (TMRM) and ethyl ester (TMRE) and Rhodamine 123 (Rhod123), are able to directly measure $\Delta\Psi_m$. These positively charged dyes accumulate inside mitochondria in inverse proportion as their net charge remains negative. During hyperpolarization events (interior more negative), more dye is accumulated resulting in increased fluorescence. In contrast, depolarization events (interior less negative) lead to less accumulation and therefore less fluorescence. In order to test mitochondrial function, p-trifluoromethoxy carbonyl cyanide phenyl hydrazone (FCCP) is used as positive control for depolarization events (Perry et al. 2011). Brief episodes of depolarization events are described as $\Delta\Psi_m$ flickering and may not lead to significant functional changes. Prolonged depolarization

events – however, the time threshold is highly variable and cell dependent – lead to a critical turning point where mitochondria function is irreversibly impaired (Zorova et al. 2018).

4. Role of other organelles in cell migration

To provide a complete and comprehensive overview of cell migration, it is essential to mention the role of other cellular organelles. As previously mentioned, migrating cells show a distinct subcellular positioning of their organelles that is associated to the cell type, the dimension migration takes place in (1D vs. 2D vs. 3D) as well as their activities. The interest in the role of organelles during migration has grown in recent years. Which organelle takes precedence over the other, however, remains unknown and is regularly debated when discussing directional cell migration (van Bergeijk, Hoogenraad, and Kapitein 2016). While the cytoskeletal components determine the cell shape and provide the scaffold for the internal organization of cellular compartments, other organelles like the nucleus, Golgi apparatus and lysosomes contribute to the cell migration machinery (Harris, Jreij, and Fletcher 2018) and will be discussed in the following sections.

4.1. Nucleus: Determining mode of migration

The nucleus in mammalian cells is composed of a nuclear envelope and a nuclear lamina just beneath it. Its main role resides in safeguarding the genetic information and controlling the transcriptional machinery translating it (Hertzog and Erdel 2023). Even though the nucleus lacks membrane-bound compartments, it is seen as spatially organized, especially at the level of chromosomes. These chromosomes are folded and positioned inside the nucleus in a cell-type specific way. Differentiated cells display globule-like structures that are positioned in distinct territories within the nuclear interior (Meldi and Brickner 2011). The positioning of the nucleus inside the cell differs depending on the biological processes taking place, e.g. during cell division or cell migration. Nuclear positioning is closely related to cell function: While leukocytes position their nucleus close to the leading edge during amoeboid migration, most other migrating cells, including cancer cells, show the nucleus positioned close to the cell rear, a morphology associated with mesenchymal cell migration. The reward positioning of the nucleus during mesenchymal migration is mediated by the actin cytoskeleton in fibroblasts, in particular an actin retrograde flow controlled by myosin and Cdc42 (Calero-Cuenca, Janota, and Gomes 2018). The linker of nucleoskeleton and cytoskeleton (LINC) physically links the nucleus to the cytoskeleton. LINC is a protein complex composed of KASH-domain proteins and Sad1, Unc Homology (SUN)-domain proteins, SUN1 and SUN2. In vertebrates, KASH-domain proteins are called nesprins and these proteins span the outer nuclear membrane

interacting with SUN-domain proteins on the inner nuclear membrane within the perinuclear space. Different nesprins further interact with cytoskeletal components, e.g. nesprin-1 and nesprin-2 interact with actin filaments, while both together with nesprin-4 interact with microtubules through dynein and kinesin (Navarro, Collins, and Folker 2016). In the early phases of polymerization and nucleus repositioning, nesprin-2 and SUN2 together with actin form transmembrane actin-associated nuclear (TAN) lines that are aligned parallel to transverse arcs and undergo retrograde flow to push the nucleus to the rear part of the cell behind the centrosome. These TAN lines are anchored by A-type laminins (laminin A) which allows force transmission of the actin cytoskeleton across the nuclear envelope to move the nucleus and properly position it before migration takes place (Calero-Cuenca, Janota, and Gomes 2018; Gant Luxton et al. 2011).

Actin filaments above the nucleus are important to orient the nucleus in the direction of migration. These filaments, termed the perinuclear actin cap, contain phosphorylated myosin II and α-actinin-1 and terminate at focal adhesions that contain vinculin. The actin cap connects to the nucleus via nesprin-2 and controls mechanotransduction (Davidson and Cadot 2021). To summarize the nuclear dynamics during cell migration: TAN lines are important in the early phases during cellular polarization to reposition the nucleus towards the cell rear behind the centrosome (Gant Luxton et al. 2011), while actin caps made up of apical parallel actin cables (Kim et al. 2017) align the nucleus with the migratory axis and play a role in the maintenance of directional persistence. These actin caps are terminated by their own focal adhesions and are, in contrast to ventral actin stress fibers underneath the nucleus, tightly connected to the apical surface of the nuclear envelope through LINC complexes (Chambliss et al. 2013).

4.2. Golgi apparatus: Determining direction of migration

The Golgi apparatus consists of flattened membrane sacs that are generally organized in polarized stacks. These membrane sacs are called cisternae and depending on the cell type, stacks contain from 3 up to 20 cisternae (Day, Staehelin, and Glick 2013). The stacks of cisternae are highly polarized and consist of a *cis*-face that receives cargos, polysaccharides, lipids and proteins, from the ER, and a *trans*-face sorting cargo for post-Golgi export to other organelles like endosomes, lysosomes and the plasma membrane (Millarte and Farhan 2012). The *trans*-face is mostly referred to as the *trans*-Golgi-network, TGN. In some organisms like plants and fungi, individual Golgi stacks are distributed through the cytoplasm independent to other stacks, while most vertebrate cells consist of fused Golgi stacks organized into compact ribbon structure that is positioned close to the MTOC (Makhoul, Gosavi, and Gleeson 2019). Considering its main roles in post-translational modifications, like glycosylation, lipidation and

proteolytic processing, and protein sorting, it is widely accepted that the Golgi is important in regulating directional cell migration. Most findings on Golgi positioning during directional migration were obtained using 2D scratch-wound assays, and ongoing research still needs to prove that those findings can be transferred to the physiological processes occurring *in vivo*. One of the earliest findings correlating Golgi positioning and persistence of directional migration showed that the repositioning of the Golgi network towards the leading edge was coupled to the centrosome, proving a functional relationship between the two (Millarte and Farhan 2012; Kupfer, Dennert, and Singer 1983; Cui et al. 2025). During cell migration, centrosome- and Golgi-derived microtubules maintain the Golgi structure in coordination with actin filaments. In addition, Golgi membrane components nucleate and stabilize microtubules at both the *cis*- and *trans*-face, which is why the Golgi itself is seen as a MTOC (Makhoul, Gosavi, and Gleeson 2019). These nucleations and stabilizations of Golgi microtubules are regulated by A-kinase-anchoring protein (AKAP450), CLIP-associated proteins (CLASPs) and calmodulin-regulated spectrin-associated protein 2 (CAMSAP2). Using stochastic optical reconstruction microscopy, it was recently shown that post-Golgi cargo trafficking was significantly faster on Golgi-associated microtubules (GaMTs). These GaMTs were more polarized towards the leading edge and displayed fewer inter-microtubule intersections. These fewer intersections lead to less pausing events and directional switches of cargos during post-Golgi trafficking (Hao et al. 2020). To summarize the importance of the Golgi network on cell migration, the Golgi's structure and positioning is relevant for the proper polarization of the cell during directional migration, while the Golgi-associated microtubules are relevant for the persistence of cell migration in one direction as they support the efficient anterograde trafficking of modified post-Golgi cargos towards the cell's leading edge (Millarte and Farhan 2012; Hao et al. 2020; Vaidžiulyte, Coppey, and Schauer 2019; Vaidžiulyt, Macé, and Battistella 2022).

4.3. Lysosomes: Maintaining persistence of migration

Another organelle relevant for the persistence of cell migration is the lysosomes, which have recently been shown to contribute to this response in different ways. Lysosomes, first described in 1955 (Novikoff, Beaufay, and De Duve 1956), are cytoplasmic organelles important for the degradation of various biomacromolecules. Consisting of a single membrane, a phospholipid bilayer with selective permeability, they display different morphologies ranging from spherical to elliptical. Their size ranges from 0.2 to 0.8 µm (Bi et al. 2025). To carry out one of their main functions, degradation, lysosomes have over 60 luminal hydrolases. Most of them require an acidic pH for optimal function which is why the luminal pH of the lysosomes lies between 4.5-5.0 and is maintained by a proton-pumping V-type ATPase inside the

lysosomal membrane. Next to other membrane proteins, the lysosomal membrane includes highly-glysosylated lysosome-associated membrane proteins (LAMPs) that prevent degradation of the membrane from lysosomal hydrolases. Lysosomes are very dynamic organelles and broadly distributed through the cytoplasm (Pu et al. 2016). While they display a more perinuclear distribution close to the MTOC in non-polarized cells, many still reach the periphery. Similar observations are made in polarized cells like neurons. To reach the cell periphery, lysosomes are transported along microtubule tracks in a bidirectional way. For anterograde transport (towards the microtubule plus-end), lysosomes are transported by kinesins, while dynein mediates retrograde transport (towards the microtubule minus-end). This bidirectional transport follows a stop-and-go fashion, suggesting that lysosomal transport is strongly regulated (Pu et al. 2016). As their positioning shows functional relevance, lysosomal dynamics were observed in different migratory modes. In epithelial monolayers migrating in a 2D microenvironment, lysosomes accumulated at the cell periphery at the leading edge during migration. This lysosomal accumulation was a distinct feature of leader cells, as follower cells did not show changes in lysosomal distribution. In addition, these leader cells showed a distinct front-to-rear asymmetry in lysosomal distribution. The function of these peripheral lysosomes was determined to be lamellipodia extension, as the main lamellipodia growth happened in zones enriched with lysosomes (Marwaha et al. 2025). In dendritic cells, lysosomes are located at the cell rear around an actin patch during migration. This rearward distribution of lysosomes and actin is important for myosin-II-mediated contraction, also named actomyosin contractility, pushing the cell forward. As lysosomes are important calcium storage organelles, Ca^{2+} release through transient receptor potential channel, mucolipin subfamily 1 (TRPML1) activates myosin II at the cell rear, leading to faster and directional migration (Bretou et al. 2017).

To summarize, the mode of migration that endothelial cells adapt during angiogenesis is mesenchymal migration which depends on cell symmetry breaking and the formation of adhesions to the ECM. Polarized ECs display a well-characterized distribution of the cytoskeletal components: actin fibers, microtubules and FA dynamics. This distribution is mirrored in organelle organization (**Fig. 5**) and intracellular signalling cascades. Angiogenesis is a process that is disturbed in different diseases associated with ER stress, which is why the effect of ER stress induction on endothelial cell migration will be investigated in this thesis.

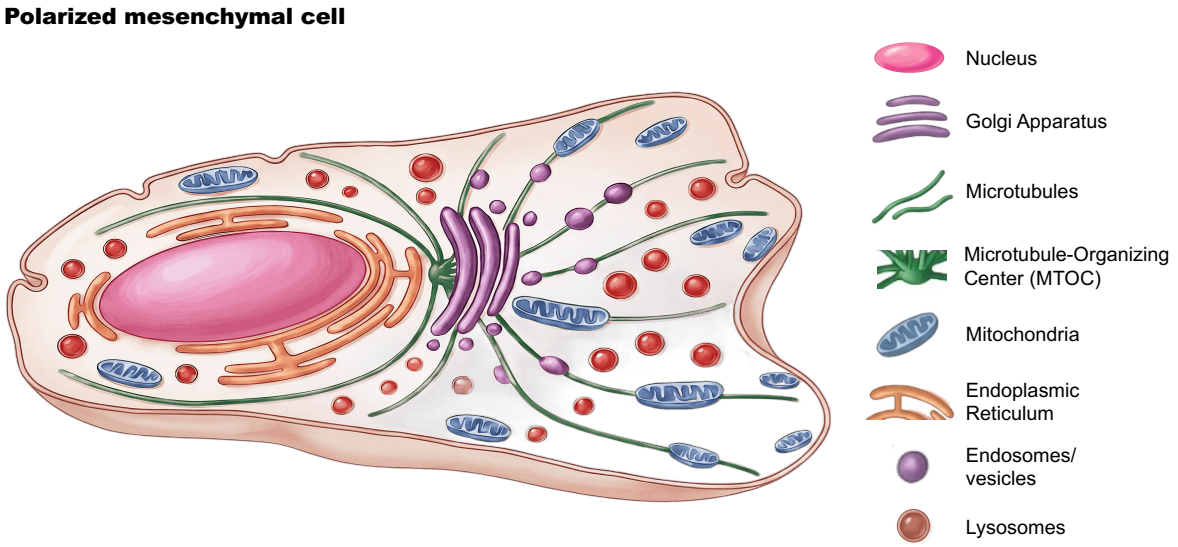

Figure 5: Organelle distribution in a polarized mesenchymal cell.

For proper cell migration to occur, a cell needs to break its intracellular symmetry and polarize. This polarization happens on the cytoskeletal level, but also on an organelle level with organelles showing a distinct distribution inside the cell. In a polarized mesenchymal cell, the nucleus is positioned close to the rear with the MTOC positioned in front of it. Microtubules span through every part of the cell, reaching the front. The ER is in direct contact with the nucleus through its nuclear envelope connection. Mitochondria vary in size and shape, displaying elongated networks through mitochondrial fusion, or smaller, fragmented pieces after mitochondrial fission. The Golgi is positioned close to the MTOC. Polarized trafficking of endosomes, vesicles and lysosomes takes place on microtubules.
Figure created with illustrae.com.

Study objective

The ER stress response is linked to different diseases that are associated with vascular dysfunctions like distorted angiogenesis (Cimellaro et al. 2016; Sáez et al. 2014; Villalobos-Labra et al. 2018). As endothelial cell migration is essential during angiogenesis (Auerbach et al. 2003; Luo et al. 2023), this thesis aims to study the ER stress response during endothelial cell migration and its effect on the intracellular organization of the cytoskeleton and organelles, in particular the ER and mitochondria as these two organelles form direct membrane contact sites that are maintained over long distances (Phillips and Voeltz 2016; Hong and Inagi 2025).

Hypothesis: ER stress induction and consequent UPR activation leads to alterations in the cytoskeletal organization and subsequent organelle function, distribution, and crosstalk, in particular of ER and mitochondria. The disruption of ER-mitochondria crosstalk results in mitochondria dysfunction, which in conjunction with the disruption of cytoskeletal dynamics results in impaired endothelial cell migration.

Study objectives:

I. Monitor the changes in collective and single endothelial cell migration after ER stress induction.
II. Determine the main branch of the UPR responsible for the observed changes in migration after TN-induced ER stress.
III. Evaluate the effect of TN-induced ER stress on the organization and distribution of the cytoskeleton and ER-mitochondria crosstalk.
IV. Assess the role of mitochondria during single and collective endothelial cell migration and the effect of TN-induced ER stress on mitochondria function.
V. Discover the possible role of relevant ion channels on the observed changes during directional migration and elucidate their role during TN-induced ER stress.

Material and Methods

1. Culture of Human Umbilical Vein Endothelial Cells

Primary human umbilical vein endothelial cells (HUVECs) from pooled donors were obtained from PromoCell (C-12202) or Lonza (CC-2519) containing ≥ 500,000 cells per cryotube, respectively.

For culturing pooled HUVECs obtained from PromoCell, Corning culture dishes with 60 or 100 millimeter (mm) diameter were coated with fibronectin from bovine plasma (1 microliter [µL]/1 milliliter [mL], final concentration: 1 microgram [µg]/1 mL) for 20 minutes (min) at 37°C and 5% CO_2. Dishes were washed with 1X DPBS and ready-to-use endothelial growth medium was added and pre-warmed at 37°C and 5% CO_2. HUVECs were used between passages 2 and 10. Passaging of HUVECs was done every 2 to 3 days around 90% confluency in new fibronectin-coated culture dishes with 100 mm diameter. To subculture HUVECs, old media was removed and cells were washed with 1X DPBS. Then, 3 mL of TrypLE Express (1X) were used to detach HUVECs at 37°C and 5% CO_2 for 3 min. Next, 3 mL of full media were added to trypsinated cells to inactive the enzymatic reaction of detachment, the suspension was transferred to a 15 mL falcon and centrifuged at 1,000 RPM (rounds per minute) for 5 min. After centrifugation, the supernatant was discarded and cells were resuspended in fresh full endothelial growth medium and seeded on fibronectin-coated culture dishes.

For culturing pooled HUVECs obtained from Lonza, media was added to T75 culture flasks with filter cap and pre-warmed at 37°C and 5% CO_2. HUVECs were used between passages 2 and 9. Passaging was done like described above, with the exception of T75 culture flasks not being coated with fibronectin. HUVECs obtained from Lonza used in experiments were plated on fibronectin-coated dishes, however.

1.1 Buffers and solutions

- Bovine Fibronectin from bovine plasma, liquid solution, Sigma-Aldrich, #F1141
- Dulbecco's Phosphate Buffered Saline (DPBS, Calcium-Chloride/Magnesium-Chloride-free): Gibco, ThermoFisher Scientific, #14190169
- Gibco™ TrypLE™ Express Enzyme (1X), phenol red, ThermoFisher Scientific, #12605028
- Endothelial Cell Growth Medium (ready-to-use, #C-22010): Endothelial Cell Basal Medium + Premixed SupplementMix, supplemented with 1% (v/v) penicillin-streptomycin (P/S) (final concentration: 100 U/mL), PromoCell GmbH, Heidelberg, Germany = full media

- EGM® Endothelial Cell Growth Medium BulletKit®: EBM® Basal Medium and EGM® Endothelial Cell Growth Medium SingleQuots® Supplements, supplemented with 1% (v/v) P/S (final concentration: 100 U/mL), Lonza Bioscience, Lonza Walkersville, Inc. = media

2. Wound Healing (WH)

To analyze spontaneous collective migration in a 2D microenvironment, 100,000 cells/mL of HUVECs were plated on fibronectin-coated (1 µg/mL) FluoroDishes with glass cover bottoms and a 35 mm diameter and incubated in full media for 2 d at 37°C and 5% CO_2. After cells reached ~90% confluency, inhibitors for ATF6, IRE1, PERK and mechanosensitive ion channels, especially TRPC6 antagonists, were added as pre-treatments to full media for 2 h at 37°C and 5% CO_2. After, a sterile 1000 µL micropipette tip was used to scratch the cell monolayer and mimic an *in vivo* wound. The tip was angled vertically and consistent medium pressure was applied to guarantee roughly the same scratch width, smooth edges and prevent detachment of the cell monolayer (**Fig. 6**). After the scratch, the cell monolayer was gently washed with full media to remove cell debris and any remaining floating cells, as previously described (Grada et al. 2017). Nuclei were stained with Hoechst 33342 trihydrochloride, trihydrate (80 nanomolar [nM], #H1399) for 20 min at 37°C and 5% CO_2 to allow tracking analysis of individual cells. Fresh full media was added to each dish with a final volume of 2 mL. Treatments were added directly into fresh full media before live-cell imaging, which was performed at 37°C and 5% CO_2.

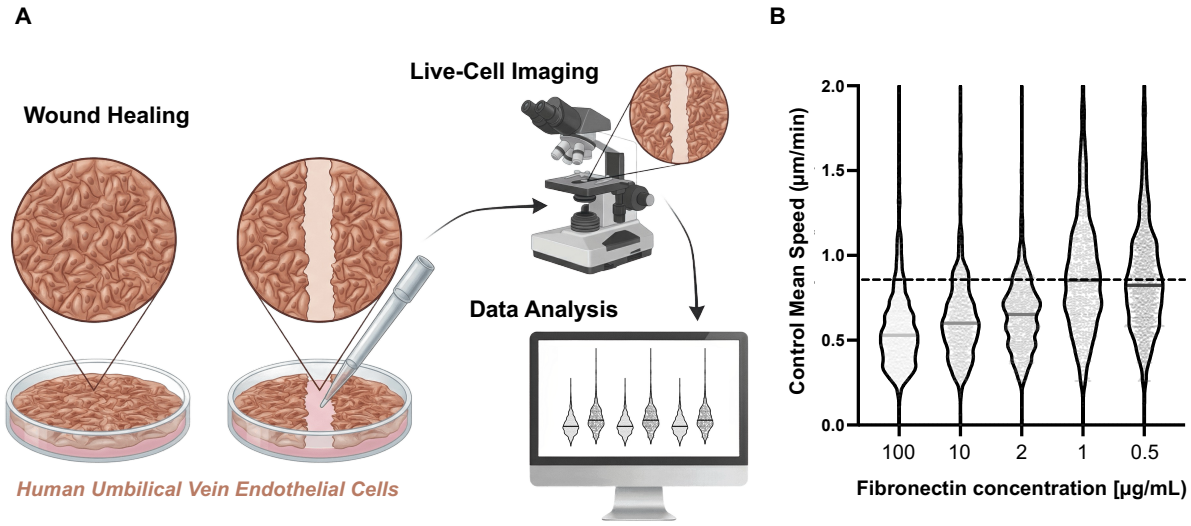

Figure 6: Wound Healing procedure and fibronectin concentration test.

(A) HUVECs at ~90% confluency were scratched using a 1000 µL micropipette tip. Live-cell imaging was performed under culture conditions for 16-24 h. Data analysis of nuclei tracking was done with Fiji (ImageJ). Figure created with BioRender and illustrae.com.
(B) Different fibronectin concentrations were tested to find the optimal concentration for collective mesenchymal migration. Cells showed the highest speed [in µm/min] with 1 µg/mL fibronectin concentration, indicated by the dotted line.

2.1. Treatments

Table 1: Treatments used in Human Umbilical Vein Endothelial Cells

Treatment	Concentration	Company
Ceapin A7, selective inhibitor of ATF6α	added as pre-treatment at 2.5 µM concentration	Tocris Bioscience #6955
AMG 18 hydrochloride, potent and selective IRE1α inhibitor	added as pre-treatment at 0.5 µM concentration	Tocris Bioscience #6166
AMG PERK 44, potent and selective PERK inhibitor	added as pre-treatment at 2.5 µM concentration	Tocris Bioscience #5517
FCCP, potent uncoupler of oxidative phosphorylation in mitochondria	added as treatment at 10 µM or 50 µM concentration	Tocris Bioscience #0453
Tunicamycin, inhibits N-linked glycosylation	added as treatment at 10 µM concentration	Sigma-Aldrich #654380
Azetidine, non-protein amino acid	added as treatment at 3 mM concentration	Sigma-Aldrich #A0760
GsMTx4, selectively inhibits mechanosensitive channels like Piezo or transient receptor potential cation channels (TRPC, 1 and 6)	added as pre-treatment at 200 nM concentration	Tocris Bioscience #4912
BI-749327, potent, highly selective TRPC6 antagonist	added as pre-treatment at 1, 5 or 10 µM concentration	MedChemExpress #HY-111925
VBIT-12, potent inhibitor of Voltage dependent anion-selective channel 1 (VDAC1)	added as pre-treatment at 10, 20 or 50 µM concentration	Selleckchem #S8936

3. Random migration

To analyze random free migration in a 2D microenvironment, 50,000 cells/mL of HUVECs were plated on fibronectin-coated (1 µg/mL) 35 mm FluoroDishes with glass cover bottoms. After seeding the cells, they were incubated for 24 h at 37°C and 5% CO_2. To ensure random free migration and avoid cellular interactions, the confluency was kept low (not higher than ~40%). PERK inhibition with AMG PERK 44 (2.5 µM) was performed at 37°C and 5% CO_2 for 2 h in full media.

Before starting live-cell imaging, cells were stained with Hoechst 33342 (80 nM) in full media for 20 min at 37°C and 5%. After, staining media was discarded and fresh full media was added to control dishes with a final volume of 2 mL for acquisition.

TN-treatment (10 µM) was added to full media before live-cell imaging to study random free migration under ER stress.

To visualize mitochondrial dynamics during live-cell imaging, cells were stained with 100 nM tetramethylrhodamin, ethyl ester (TMRE, #ab113852) for 20 min at 37°C and 5% CO_2 in full media. Afterwards, cells were washed twice with full media, then kept in fresh full media during acquisition.

4. Immunofluorescence (IF)

HUVECs were seeded on 15 mm, 16 mm, 18 mm or 20 mm fibronectin-coated glass coverslips inside a 12-well plate with a number of 50,000-75,000 cells/mL per coverslip and incubated at 37°C and 5% CO_2. After cells reached ~95% confluency, inhibitors for ATF6, IRE1 and PERK were added as pre-treatments to the media and incubated for 2 h at 37°C and 5% CO_2. After 2 h, the cell monolayer on the coverslips was scratched using a 200 µL micropipette tip for 15 mm and 16 mm coverslips, or a 1000 µL micropipette tip for 18 mm and 20 mm coverslips. After scratching, coverslips were transferred to a new 12-well plate to get rid of floating or dead cells. TN-treatment, also in combination with the previously mentioned inhibitors, was added, and cells were incubated for 6 h at 37°C and 5% CO_2. 6 h were chosen based on existing evidence that in several other cell types, ER stress was induced by treating cells with TN for a minimum of 5 h (Oslowski and Urano 2011). After 6 h, full media was discarded and cells were fixed with 4% paraformaldehyde (PFA) for 15 min at room temperature (RT). PFA was discarded and cells were washed 3x with 1X DPBS. Cells could be stored in 1X DPBS at 4 °C until the immunostaining procedure.

Antibody staining was performed on parafilm in a humid chamber. Cells were blocked in a blocking solution for 15 min at RT. Primary antibody staining solution was prepared in 1X saponin solution. The primary antibody staining procedure was done overnight at 4°C. On the second day, cells were washed 3x with 1X DPBS for 5 min each. Secondary antibody staining

was prepared in 1X saponin solution. Alexa Fluor™ 647 or Alexa Fluor™ 405 Phalloidin were added into 1X saponin solution and stained during the secondary antibody staining procedure, which was done on fresh parafilm for 1 h at RT in the dark. After, cells were washed 3x with 1X DPBS for 5 min each. 1X DAPI staining was done for 15 min at RT in the dark. Before the mounting procedure, cells were washed once more with 1X DPBS and mounted on microscopy slides using Fluoromount-G™. Immunofluorescent images were taken with a Zeiss Axio Examiner .Z1 with LSM 980 in Airyscan 2 mode with a 63x Plan-APOCHROMAT/1.4 numerical aperture oil objective. Images were processed using the Zeiss Zen blue edition software. Post-processing was done by choosing “Airyscan Processing”.

4.1. Buffers and solutions

- 4% paraformaldehyde (PFA) for fixation: prepared from 16% PFA solution (EM-grade, Electron Microscopy Sciences, #15710) with 1X DPBS
- Blocking solution: prepared in 1X DPBS with 2% bovine serum albumin (BSA, Sigma-Aldrich, #A2153) and 0.1 M glycine
- Saponin solution for permeabilization: 1X saponin solution was prepared from a 10X saponin solution stock containing 2% BSA, 0.5% saponin (Saponin – CAS 8047-15-2, Merck Millipore, #558255) in 1X DPBS
- Invitrogen™ Fluoromount-G™ Mounting Medium, ThermoFisher Scientific, #00-4958-02

4.2. Antibodies and stainings

Table 2: Antibodies and stainings used for immunofluorescence assay

Antibody / Staining	Origin	Target	Dilution	Company
Monoclonal *anti*-TOM20 [primary]	Mouse	Mitochondria	1:750	BD Transduction Laboratories #612278
Polyclonal *anti*-TOM20 [primary]	Rabbit	Mitochondria	1:750	Proteintech #11802-1-AP
Polyclonal *anti*-Nogo [primary]	Rabbit	Endoplasmic Reticulum	1:250	Novus Biologicals #NB100-56681SS

Monoclonal *anti*-alpha Tubulin [DM1A, primary]	Mouse	Microtubules	1:750	Abcam #ab7291
Polyclonal *anti*-Paxillin [primary]	Sheep	Focal Adhesions	1:250	Novus Biologicals #AF4259-SP
F(ab')-2 goat *anti*-mouse IgG Alexa Fluor™ 488 [secondary]	Goat	-	1:250	ThermoFisher Scientific #A11017
Donkey *anti*-rabbit IgG Alexa Fluor™ 546 [secondary]	Donkey	-	1:250	ThermoFisher Scientific #A10040
Donkey F(ab')2 *anti*-Sheep IgG [secondary]	Donkey	-	1:250	Biozol #JIM-713-166-147
Alexa Fluor™ Plus 405 Phalloidin	Phallotoxin	F-Actin	1:100	ThermoFisher Scientific #A30104
Alexa Fluor™ 647 Phalloidin	Phallotoxin	F-Actin	1:100	ThermoFisher Scientific #A22287

5. Transfection of Human Umbilical Vein Endothelial Cells

To visualize organelle dynamics and their interactions, HUVECs were transfected via electroporation. Electroporation uses high-voltage electric shocks to temporarily permeabilize the cell membrane to transfer DNA into cells (Potter and Heller 2018). For transfection of HUVECs, the Electroporation and Nucleofector® Technology from Lonza was applied. For primary cells like HUVECs, the P5 Primary Cell 4D-Nucleofector® X Kit L with the P5 Primary Cell Nucleofector® Solution and Supplement 3 was used. Transfection in cuvette vessels was done for ≥ 1,000,000 cells, well strip vessels were used for ≤ 1,000,000 cells.

Cultured HUVECs were detached and counted to determine the transfection vessel. The specific cell number chosen was centrifugated at 1,000 RPM for 5 min at RT and resuspended in either 20 µL of P5 kit for well strip vessels, or 100 µL P5 kit for the cuvette vessels. Chosen plasmids (Table 3) were added at the indicated concentrations and the sample was electroporated inside the 4D-Nucleofector® X Unit. For HUVECs, programme CA-167 on the 4D-Nucleofector® Core Unit was chosen.

After transfection, cells were transferred into pre-incubated full media culture dishes and incubated at 37°C and 5% CO_2 overnight. Transfected cells were imaged after 24 h or 48 h, depending on the transfection efficiency.

Table 3: Plasmids for transfection of Human Umbilical Vein Endothelial Cells

Plasmid	Concentration	Supplier
DsRed2-ER-5, endoplasmic reticulum	1 µg/mL	Addgene, plasmid #55836
EMTB-3XGFP, microtubules	1 µg/mL	Addgene, plasmid #26741
Mito GFP, mitochondria	1 µg/mL	Addgene, plasmid #44385

6. Measurement of mitochondrial membrane potential (ΔΨ)

To visualize and quantify membrane potential (ΔΨ) dynamics in mitochondria, cells were transiently transfected with MitoGFP plasmid, allowing for a stable staining of mitochondria independent of ΔΨ (for transfection protocol see **5.**) Transfected HUVECs were seeded in preparation for a WH. Once ~90% confluency was reached, the cell monolayer was scratched. To visualize changes in ΔΨ, the previously transfected cells were stained with 100 nM TMRE for 20 min at 37°C and 5% CO_2. TMRE is a positively charged dye that readily accumulates in healthy mitochondria which display a net negative charge of around ~180 mV. TMRE's red fluorescence can be captured with fluorescence microscopy making it possible to determine the ΔΨ of mitochondria inside a living cell (Crowley, Christensen, and Waterhouse 2016). TMRE staining was washed out twice with full media after 20 min. HUVECs transfected with MitoGFP and stained with TMRE were chosen and imaged in full media at 37°C and 5% CO_2 by capturing both the green fluorescence for the stable signal and the red fluorescence for the oscillating signal (**Fig. 7**).

To determine changes in ΔΨ under ER stress, cells were treated with 10 µM TN after the transfection and staining procedure. Pre-treatment with AMG PERK44 was performed for 2 h at 37°C and 5% CO_2 around 24 h after the transfection procedure. After 2 h of pre-treatment, cells were scratched and TMRE staining was done for 20 min at 37°C and 5% CO_2. Cells were washed twice with full media and treatment with PERK44 and TN was performed as previously described.

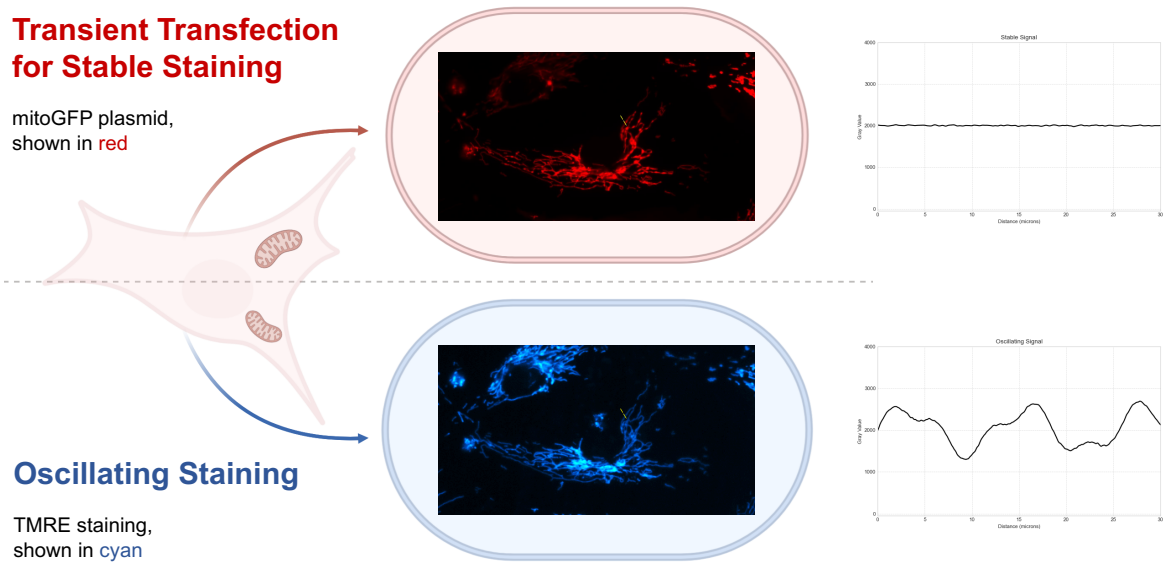

Figure 7: Qualitative measurement of mitochondrial membrane potential.

Cells were transiently transfected with the mitoGFP plasmid showing a stable signal, and stained with TMRE to quantify changes in $\Delta\Psi$. MitoGFP signal is shown in red, TMRE is shown in blue to better visualize depolarization events.
Mitochondrial membrane potential was analyzed as a ratio of TMRE dynamics over mitoGFP's stable fluorescence through 3D surface plots.

7. Micropatterning

To mimic frustrated cell migration and allow for cell shape control, protein micropatterning was used. 2D micropatterns of crossbow, ellipse and circle were created using the Inkscape® software. A circle with a 5 mm diameter was punched into a pre-made PDMS stencil and placed inside a 35 mm Fluorodish. The dish was plasma-cleaned for 5 min inside a Plasma Cleaner (#PDC-32G-2) to remove any contaminants from the surface of the Fluorodish bottom. After, the 5 mm circle was coated with 10 µL of pLL-PEG (1 mg/mL, SuSoS, Surface Technology) for 1 h at RT. pLL-PEG was washed off with MilliQ water.

The chosen pattern was uploaded to the Leonardo software (version 5.4) and the pattern was placed centrally inside the 5 mm circle. Then, 10 µL of PLPP photoreagent (Alvéole) was added inside the circle and degraded under UV illumination with a laser power of 600 mJ/mm^2 in the form of the desired pattern with a PRIMO photopatterning system (Alvéole) (Strale et al. 2016). PLPP was washed off with MilliQ water after the printing process. The pattern was coated with fibronectin (1 µg/mL) and fibrinogen 488 or 546 to stain the pattern (Invitrogen™, 1:10 concentration in fibronectin) for 20 min at 37°C and 5% CO_2. After, the circle was washed with 1X DPBS, the PDMS stencil was removed and 1 mL of full media was added to the dish. Then, 10 µL of cell suspension with 100 cells/µL was plated inside the circle (the area of the circle was highlighted on the underside of the dish bottom to allow for better orientation). HUVECs were incubated at 37°C and 5% CO_2 for 10-15 h to allow cell attachment inside the

micropattern (summarized in **Fig. 8**) . Upon visual inspection and once the cells were attached, the dishes were carefully washed once with full media to remove floating cells. During live-cell imaging, cells were imaged in full media under culture conditions.

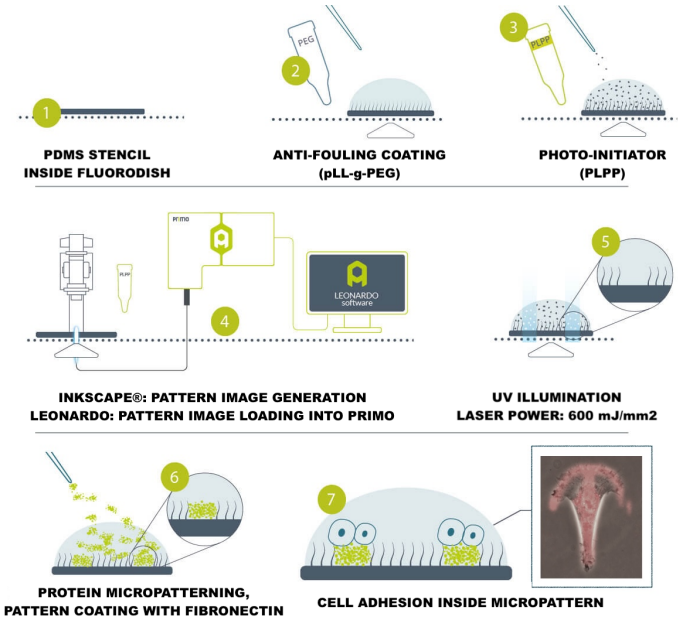

Figure 8: Key steps of micropatterning with the Alveole system.

PRIMO photopatterning uses an anti-fouling coating (here: pLL-g-PEG) that is degraded by applying a combination of a photo-initiator (here: PLPP) and UV illumination. The desired protein (here fibronectin) is added and will be adsorbed only inside the micropattern. Cells will adhere to this protein and take up the shape of the micropattern.
This overview was adapted from alveolelab.com "Key steps of protein micropatterning with PRIMO".

8. Angiogenesis Assay

Angiogenesis is the formation of new blood vessels and plays a part in both healthy development and numerous pathologies like metastasis and inflammation. Angiogenesis assays are used to test pro- and antiangiogenic agents. One of the most specific tests applied is testing endothelial cells for their ability to form 3D structures like tubes (Auerbach et al. 2003). To perform an angiogenesis assay with HUVECs, Matrigel® Basement Membrane Mix was used to generate a 3D microenvironment. The Matrigel® was thawed on ice at 4°C overnight. A 48-well plate as well as micropipette tips were pre-cooled overnight at 4°C. During the coating process of the 48-well plate, the plate was kept on ice and pre-cooled tips were used to transfer 75 µL of Matrigel® to each well. The plate was incubated at RT for 10 min, then transferred to the incubator at 37°C and 5% CO_2 for 30 min. HUVECs were cultured in EGM™-1 media, which is why VEGF at 100 µg/mL was added to media at the beginning of the experiment. The experimental angiogenesis inhibitor Suramin was chosen as a positive control. To the corresponding dishes, 125 µL of culture media containing the tested compounds at 2X concentration were added to each well and incubated at 37°C and 5% CO_2 for 30 min. The recommended cell seeding density of HUVECs for the performed assay is 65,000 to 80,000 cells/cm^2. As one well of a 48-well plate has an area of 0.6 cm^2, 50,000 cells/well were chosen for this assay. Therefore, 125 µL of cell suspension containing 400,000 cells/mL were plated into the prepared Matrigel® wells containing the media with compounds

at 2X concentration (adding the cell suspension at an equal amount will dilute the compounds to a 1X concentration). The 48-well plate was imaged in Phase contrast under culture conditions at 37°C and 5% CO_2 using a Leica Dmi8 inverted microscope. Tube formation was acquired by taking pictures every 20 min.

9. Proximity Ligation Assay (PLA)

The Proximity Ligation Assay (PLA) was used to detect organelle contacts at the level of protein-protein interactions (at distances <40 nm). Specific antibodies for the two proteins of interest were used with specific DNA primers covalently linked to those antibodies. If the antibodies are close enough to each other, the DNA primers hybridize to circular DNA which can be amplified and fluorescently labelled (Alam 2018).

Cells were prepared as described above in section (**4.**). Samples were incubated in a blocking solution for 15 min. Primary antibodies were prepared in 1X saponin solution. For detection of endo-plasmic reticulum-mitochondria contacts, mouse monoclonal *anti*-TOM20 and rabbit poly-clonal *anti*-NOGO were used as primary antibodies (see **Table 2.**). Incubation with the primary antibody solution was done for 1 hour at RT. For PLA, the Duolink® In Situ Kits from Sigma-Aldrich were used. The Duolink® In Situ PLA® Probe Anti-Mouse MINUS and the The Duolink® In Situ PLA® Probe Anti-Rabbit PLUS were diluted 1:5 in 1X Antibody Diluent. After washing off the primary antibody solution with 1X DPBS, the PLA probe solution (secondary antibody staining) was added to the sample and incubated for 1 h at 37°C in a pre-heated humid chamber. After, the secondary antibody solution was washed off with 1X DPBS and the hybridization and ligation step was performed. The Duolink® Ligation stock was diluted 1:5 in high purity water and mixed well. Ligase was added 1:40 to the ligation solution immediately before addition to the samples. Ligation was done for 30 min at 37°C in a pre-heated humid chamber. After, the ligation solution was washed off with 1X DPBS. For amplification and detection, the Duolink® Amplification stock was diluted 1:5 in high purity water and mixed well. The Polymerase was added 1:80 to the amplification solution immediately before addition to the samples. Amplification was done for 100 min at 37°C in a pre-heated humidity chamber in the dark. Before mounting the coverslips, cells were washed gently in 1X DPBS 3x and stained with DAPI for 15 min. Coverslips were mounted on microscope slides with Fluoromount-G™.

9.1. Reagents

- Duolink® In Situ Detection Reagents Orange, Sigma-Aldrich, #DUO92007
- Duolink® In Situ PLA® Probe Anti-Mouse MINUS, Sigma-Aldrich, #DUO92004
- Duolink® In Situ PLA® Probe Anti-Rabbit PLUS, Sigma-Aldrich, #DUO9200

10. Live-Cell Imaging

Live-Cell imaging was performed using a Leica Dmi8 M / C / A inverted microscope equipped with a 10x Plan Apo, a 20x Plan Apo and a 40x FLUOTAR objective. Images were recorded with an ORCA-Flash4.0 Digital camera using MetaMorph® versions 7.10.3.279, 7.10.5.476 software. For recording of wound healing assays, time-lapse microscopy with the 10x Plan Apo objective was applied. Pictures of HUVECs were taken with Phase contrast and stained nuclei were imaged under 405 nm illumination every 5 min over a duration of 14-24 hours.
HUVECs in micropatterns and during random free migration were imaged using the 40x FLUOTAR objective and pictures were taken every 3 s to monitor organelle dynamics, unless otherwise indicated. Random free migration was monitored by taking pictures every 5 min.
Every live-cell acquisition was performed under optimal culture conditions at 37°C and 5% CO_2 inside a humid chamber on the objective stage.

11. Holotomography

To visualize membrane dynamics and unlabelled organelles, holotomography was used, which combines holography and tomography. Holography describes a process where images are generated using variations in the phase-shift of light passing through a sample. Low-power light passing through a sample is altered depending on the properties of the internal structures in the sample. A detector encodes the light information as a phase-shift by comparing the object beam to a reference beam of light. To achieve a higher resolution, a rotating light-source is applied to illuminate the sample at an angle leading to a 200 nm resolution in x and y. Z-stack images are combined into a 3D holotomographic reconstruction, where the refractive index is depicted in a grayscale (Sandoz et al. 2019).
A WH assay in 35 mm FluoroDishes was prepared as described in section (**2.**). Cells were pre-treated, scratched and treated and incubated for 3-6 h to allow polarization of cells before image acquisition. Holotomographic images were acquired with the Nanolive 3D Cell Explorer-fluo, equipped with a 60x/0.8 numerical aperture objective (**Fig. 9**). Refractive index (RI) images were taken in max speed mode (every 2 s) for 3 min to visualize membrane dynamics and mitochondria movement for cells migrating directionally. All experiments were performed under optimal culture conditions at 37 °C and 5% CO_2 inside a humid chamber on the objective stage. Images were reconstructed using Fiji® (ImageJ).

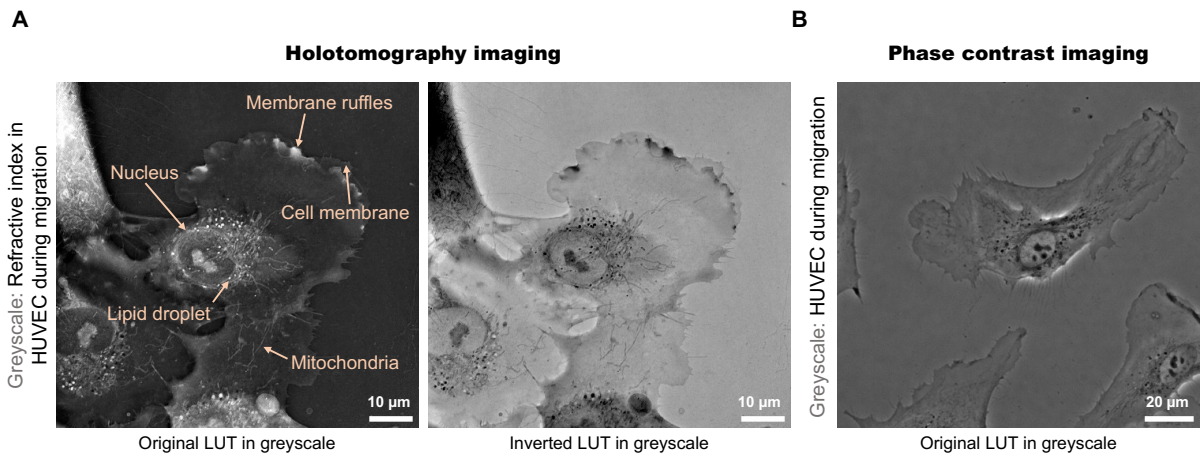

Figure 9: Comparison of Holotomography imaging to Phase contrast imaging.

(A) Holotomography utilizes the fact that cellular structures and organelles like mitochondria interact with light in different ways, which is interpreted in different refractive index (RI) values. The RI values are indicated in different brightness scales. A low RI corresponds to darker tones (e.g. cytoplasm and nucleus), while higher RIs are shown in brighter areas like lipid droplets. Scale bars: 10 µm.
(B) Phase contrast imaging also uses the different refractive indices of light shifting through a sample. Here, lipid droplets and mitochondria are indicated in darker areas as these structures are more dense, letting less light pass through. Scale bar: 20 µm.

12. Electron microscopy

HUVECs were seeded in fibronectin-coated 35 mm FluoroDishes in preparation for a WH assay as described above in section (**2.**). After cells reached ~95% confluency, AMG PERK 44 was added as a pre-treatment for 2 h, before cells were treated and scratched as described above in section (**2.**). HUVECs were incubated for 6 h at 37°C and 5% CO_2. After, cells were fixed in 2% formaldehyde and 2.5% glutaraldehyde in 0.1 M PHEM buffer (Karnovsky fixation). The fixative solution was added in an equal amount to the medium (1:1, half-strength fixative) for 15 min at RT. After, the half-strength fixative was replaced with full-strength fixate and cells were fixed for 2 h at RT. After fixation, cells were stored in 1% FA at 4°C before being processed further at the Klumperman Lab at the University Medical Center in Utrecht.

Cells were postfixed with 1% OsO_4/1.5% $K_3FE(III)(CN)_6$ [osmiumtetraoxide/potassium hexacyanoferrate (III)] in 0.065 M phosphate buffer. After post-fixation, cells were dehydrated in ethanol and embedded in Epon epoxy resin. Ultrathin sections of 60-70 nm were prepared by mounting the specimen on a holder inside an ultramicrotome for trimming. The sections were stained for contrast using uranyl acetate and lead citrate inside the EM AC20 “Automatic contrasting instrument for ultrathin sections” (Leica). After sample preparation, ultrathin sections were imaged in a Tecnai T20 Transmission Electron Microscope (FEI Company) using the serial EM software (Mastronarde 2005). Electron microscopy (EM) images were processed at a workstation computer and stitched together using the Etomo montage blending

software (IMOD 4.11) (Mastronarde and Held 2017). EM images were analysed using Fiji® (ImageJ) version 1.53t and 1.54p.

13. Data Analysis

13.1 Tracking of cell nuclei using Fiji® software

Before tracking cell nuclei during WH, the positions making up the field of view of the wound area were stitched together using the "Stitching" plugin (Preibisch, Saalfeld, and Tomancak 2009). Stitched pictures were compared and the condition where the wound area closes first was chosen for analysed duration time. A ROI of 850-1100 um (depending on the wound area) was drawn from the frame where both sides of the wound first touch. This ROI was transferred onto the other conditions. To analyze random migration, the left half of the drawn ROI was chosen, for directional migration the right half was chosen. Migrating cells were tracked using the TrackMate Batcher v.1.4.1. TrackMate settings were checked using TrackMate v7 (Ershov et al. 2022) and adapted individually for every experiment. The main settings used for tracking the migration of cell nuclei with TrackMate were the following:

- Detector: LoG Detector, target channel: nucleus, estimated object diameter: 15-20 micron
- Tracker: Nearest-neighbor tracker, maximal linking distance 15-20 micron (nucleus-dependent)

Quality filters were applied to exclude non-cellular particles and avoid "ghost" tracks. Once applied, the software generated data sets that allow reconstitution of cellular tracks over time for single cells as well as cells migrating collectively. The generated data sets also included the calculated mean speed of each cell analysed.

13.2 MotilityLab software

MotilityLab is used as an online community resource to study cell tracks utilizing quantitative and statistical analysis (Wortel et al. 2021). It was used to visualize the individual cell tracks for the analyzed conditions over the entire acquisition duration by generating a "Track display" graph.

13.3 Analysis of immunofluorescence pictures using Fiji® software

Organelle directionality was analyzed using the "Directionality" tool. The Directionality method chosen was "Fourier components", organelle directionality was displayed as a histogram starting at 0° and ending at 180°. The histogram was chosen as an index of the alignment of individual organelles with the migratory axis. Values close to 0° and 180° indicated a parallel

alignment to the migratory axis, while values around 90° stood for a perpendicular alignment to the migratory axis. Before Directionality analysis, cells were turned in the same direction, so every cell analyzed displayed a migratory phenotype towards the right.
Mitochondrial membrane potential was visualized with the “Surface Plot” plugin. TMRE signal and MitoGFP signal were analyzed independently at indicated timepoints and mitochondria populations were indicated in the generated plot profile with dashed boxes.

14. Statistics

GraphPad Prism 9 is an analysis and graphing solution software that was used to visualize the tracks obtained from image analysis using TrackMate®. Statistical analysis was performed using Prism 9 to show relevant statistical differences between different treatment conditions. Statistical values are presented in the corresponding figure legends. P values are represented as follows: *** P-value < 0.001, ** P-value < 0.01, * P-value < 0.05, and ns = not significant, P-value ≥ 0.05. Number of biological repeats is indicated as follows: N = number of independently performed experiments, n = number of analyzed cells per conditions.

15. Devices

- Corning® tissue-culture treated culture dishes, D x H = 100 mm x 20 mm, surface area: 55 cm^2, Sigma-Aldrich, #CLS430167
- Cell culture flask, T-75, standard surface, filter cap, surface area: 74.2 cm^2, Sarstedt, #83.3911.002
- FluoroDish, glass bottom, clear wall, 35 mm diameter, 10 mm well, World Precision Instruments, #FD3510-100
- Tissue culture plates, 12-well, surface area: 3.9 cm^2, Th.Geyer, #4672527
- Cell culture plate, 48-well, surface area: 85.6 mm^2, Eppendorf™, #0030723015
- Basic Plasma Cleaner, Harrick Plasma, #PDC-32G-2
- Zeiss Axio Examiner.Z1 with LSM 980 and Airyscan 2, Zeiss ZEN software 3.12, DFG code: INST 152/876-1 FUGG
- Nanolive, 3D Cell Explorer-fluo, STEVE FULL software v1.6.3496
- Leica DMi8 Inverted Microscope, MetaMorph (64-bit) software 7.10.5.476

Results

Impact of ER stress on mesenchymal cell migration

1. ER stress reduces single and collective mesenchymal cell migration

To study collective mesenchymal cell migration in a 2D microenvironment, a wound healing assay with HUVECs was performed. After scratching the cell monolayer, HUVECs were left untreated and imaged under culture conditions for a minimum of 15 h. Under control conditions, HUVECs exhibited coordinated collective cell migration and closed the wound completely after around 15 h. Analysis of cell migration in 2D revealed that cells under control conditions exhibited two distinct types of migratory behaviors corresponding to the leader-follower model, random and directional movement (**Fig. 10A, 10B**). Leader cells near the wounded area moved in a directional manner towards the right (or left) to close the area (**Fig. 10B**), whereas follower cells showcased random movement in multiple directions (**Fig. 10B**). In addition, image analysis of the cell trajectories revealed that HUVECs moving directionally showed an increase in speed compared to those moving randomly (**Fig. 10C**).

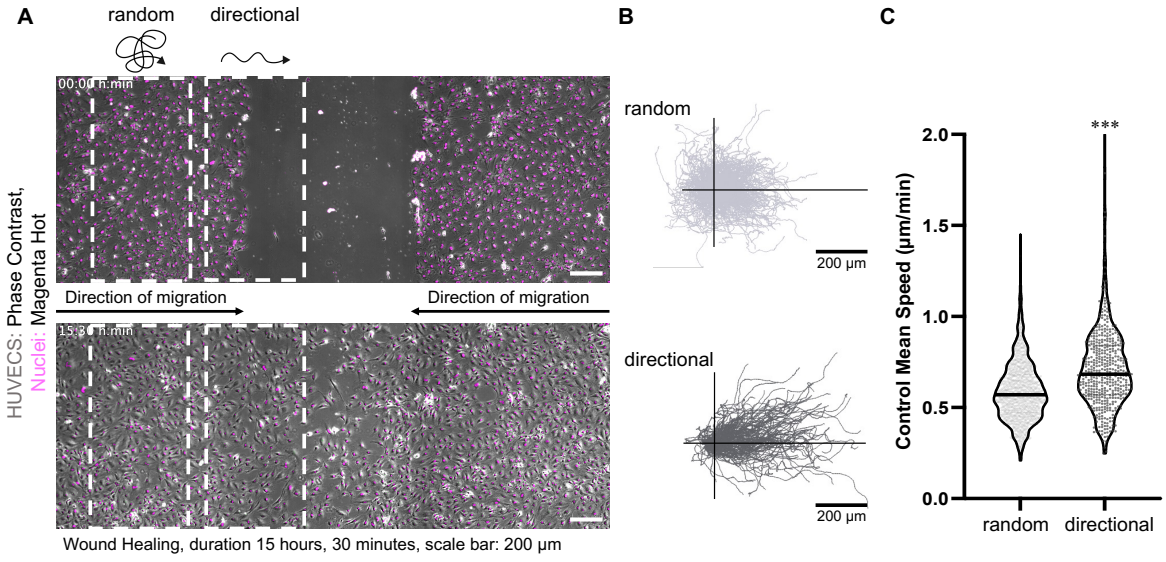

Figure 10: Collective migration of HUVECs conforms to the leader-follower model.

(A) Representative composite pictures of HUVECs undergoing random or directional migration at 0 h and 15 h 30 min. Phase contrast of HUVECs is shown in grey, the nucleus was stained with Hoechst (magenta). Dotted lines depict the area where cells move randomly (left) and directional (right). Scale bar: 200 µm.
(B) Track display of individual HUVECs moving randomly (light grey, top) and directionally (dark grey, bottom). Both plots show individual tracks of n > 500 cells for each population. Scale bar: 200 µm.
(C) Graph shows the instantaneous mean speed of HUVECs under control conditions in µm/min for random migration (light grey) and directional migration (dark grey) as truncated violin plots. The dark line indicates the median. ***P < 0.001, two-tailed Mann-Whitney test. n = 1605 cells of a representative experiment.

Disease-induced ER stress is mimicked *in vitro* by the pharmacological inhibition of chaperones and distortion of signalling pathways (Sáez et al. 2014; Villalobos-Labra et al. 2018, 2019). Therefore, different treatments that induce ER stress and activate the three branches of the UPR, such as TN and azetidine, were used to evaluate migratory changes of HUVECs. TN as an analogue of UDP-N-acetylglucosamine inhibits the first step of *N*-linked glycosylation which causes a buildup of misfolded or unfolded proteins that lead to ER stress (Adel and Abduljabar 2020). *L*-Azetidine-2-Carboxylic acid is a proline analogue that is incorporated incorrectly during protein synthesis leading to misfolded proteins and their aggregation (Roest et al. 2018).

Treatment with either 10 µM TN or 3 mM azetidine activated the three branches of the UPR (**Fig. 11A**). While control cells closed the wound after around 18 h of collective migration, cells under ER stress were unable to do the same in the same amount of time (**Fig. 11B**). Compared to control leader cells moving directionally, TN-treated cells displayed random movement in all directions and lost their capacity to move in a directional manner into the wounded area (**Fig. 11C**). Image analysis of speed revealed that cells treated with TN as well as azetidine showed a reduction in overall speed compared to control HUVECs (**Fig. 11D**). Moreover, TN-treated cells presented an impaired acceleration capacity (**Fig. 11E**).

Because TN and azetidine are dissolved in dimethyl sulfoxide (DMSO), collective migration under exposure to this vehicle was analyzed (**Supplementary Fig. 1**). While cells under DMSO showed an increase in speed, comparison between random and directional migration showed no significant decrease or increase in speed. Overall, cells increased their speed slightly, proving that the decrease in speed under ER stress is TN-dependent.

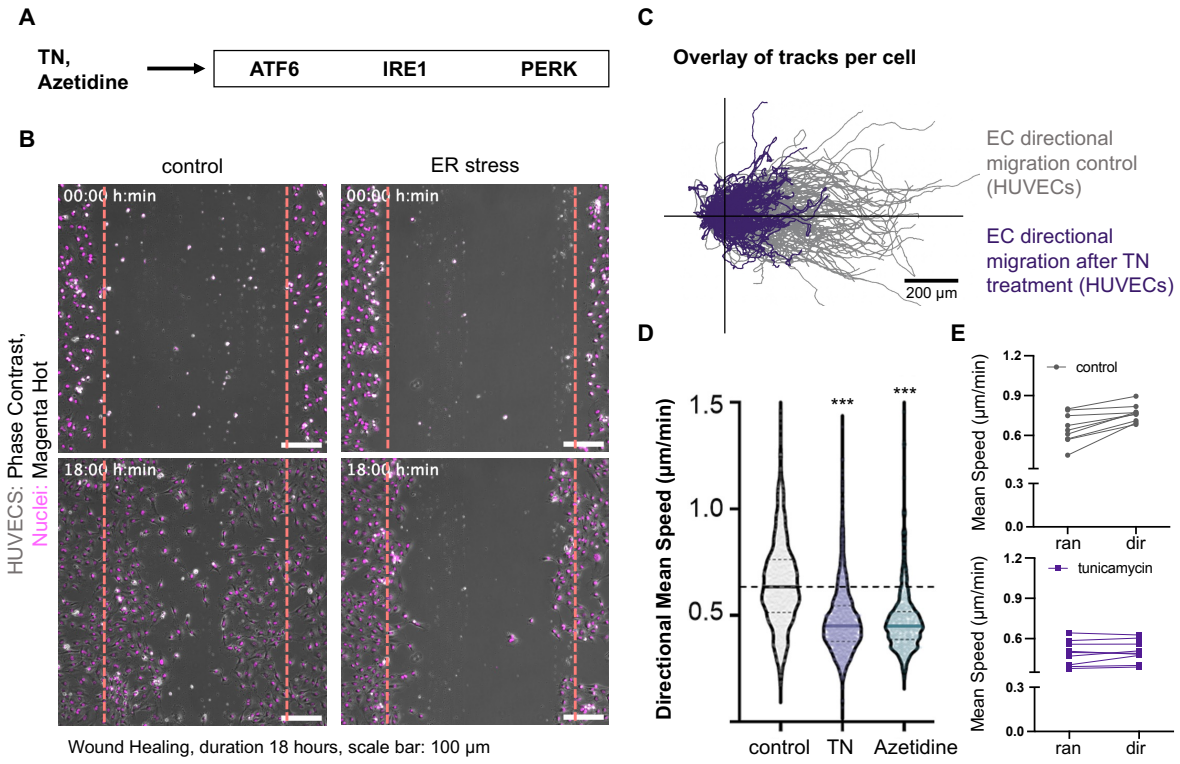

Figure 11: ER stress reduces collective mesenchymal cell migration.

(A) Scheme depicting that treatment with TN as well as azetidine activates the three UPR signalling branches, ATF6, IRE1 and PERK, through ER stress induction.
(B) Representative composite pictures of HUVECs under control conditions and ER stress conditions at 0 h and 18 h. Phase contrast of HUVECs is shown in grey, the nucleus was stained with Hoechst (magenta). Red dotted lines depict the scratched area representing the original wound. Scale bar: 100 µm.
(C) Track display of individual HUVECs moving directionally under control conditions (dark grey) and TN-treatment (purple). Both plots show individual tracks of n > 500 cells for each treatment. Scale bar: 200 µm.
(D) Graph shows the instantaneous mean speed of collectively migrating HUVECs in µm/min for control conditions (grey), TN-treatment (purple) and azetidine treatment (petrol) as truncated violin plots. The dark lines indicate the median of each condition, the dotted line corresponds to the median of the control. ***P < 0.001, Kruskal Wallis test. n > 1000 cells for each treatment.
(E) Analysis of the median of mean speed in µm/min for random and directional control HUVECs (grey) and random and directional TN-treated HUVECs (purple). control: N = 9, n = 16544 cells. TN-treatment: N = 9, n = 14584 cells.

The above-mentioned data shows that ER stress reduces cell migration, but whether this effect is cell-autonomous or not is yet unknown. Therefore, HUVECs were analyzed during single random migration in a 2D microenvironment. Image analysis of cell trajectories revealed that treatment with 10 µM TN reduced the speed of single random migration, indicating a cell-autonomous response to ER stress (**Fig. 12A**). Comparing individual cell tracks, control cells (**Fig. 12B**) as well as cells under ER stress (**Fig. 12C**) showed the same random movement during single cell migration with similar length of individual tracks.

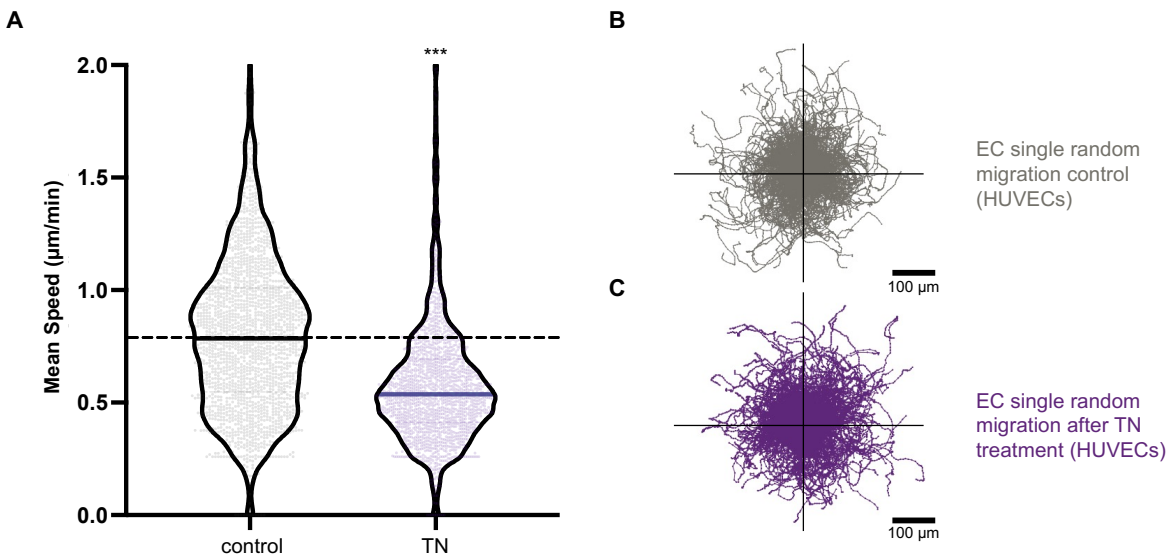

Figure 12: ER stress reduces single random mesenchymal cell migration.

(A) Graph shows the instantaneous mean speed of single migrating HUVECs in µm/min for control conditions (grey) and TN-treatment (purple) as truncated violin plots. The dark lines indicate the median of each condition, the dotted line corresponds to the median of the control. ***P < 0.001, Kruskal Wallis test. n > 500 cells for each treatment.
(B) Track display of individual HUVECs moving as single cells under control conditions (dark grey). The plot shows individual tracks of n > 500 cells. Scale bar: 100 µm.
(C) Track display of individual HUVECs moving as single cells after TN-treatment (purple). The plot shows individual tracks of n > 500 cells. Scale bar: 100 µm.

To corroborate that ER stress triggers a cell-autonomous response, HUVECs were plated on 1D micropatterned lines to increase (lateral) confinement without squeezing the cells. Their movement over 20 µm wide printed lines was analyzed and depicted with a kymograph describing the spatial position inside the line over time. Kymographs are a useful tool to visualize movements of a cell in a single picture by slicing through a time along the time-axis (*t*) (Heyn, Rädler, and Falcke 2024).

Two example cells, one for each condition – control and TN-treated –, were chosen and followed for a duration of 337 min. Their migration over 20 µm micropatterned fibronectin lines was analyzed by following their trajectories. 20 µm width were chosen based on the mean diameter of the nucleus HUVECs displayed during migration.

Control cells presented a stable and persistent migration towards the right over time, which is consequent with a well polarized cell (**Fig. 13A***, left panel*). In comparison, TN-treated cells displayed lower directional persistence over time and showed a marked biphasic motility with more sessile phases (**Fig. 13A***, right panel*). The kymographs depict this behaviour, showing stable migration towards the right over time under control conditions (**Fig. 13B***, left panel*). In contrast, the TN-treated cell showed no significant motion towards the right for roughly 60 min (from 139-200 min), staying stuck in one place before restarting the migration towards the right (**Fig. 13B**, *right panel*).

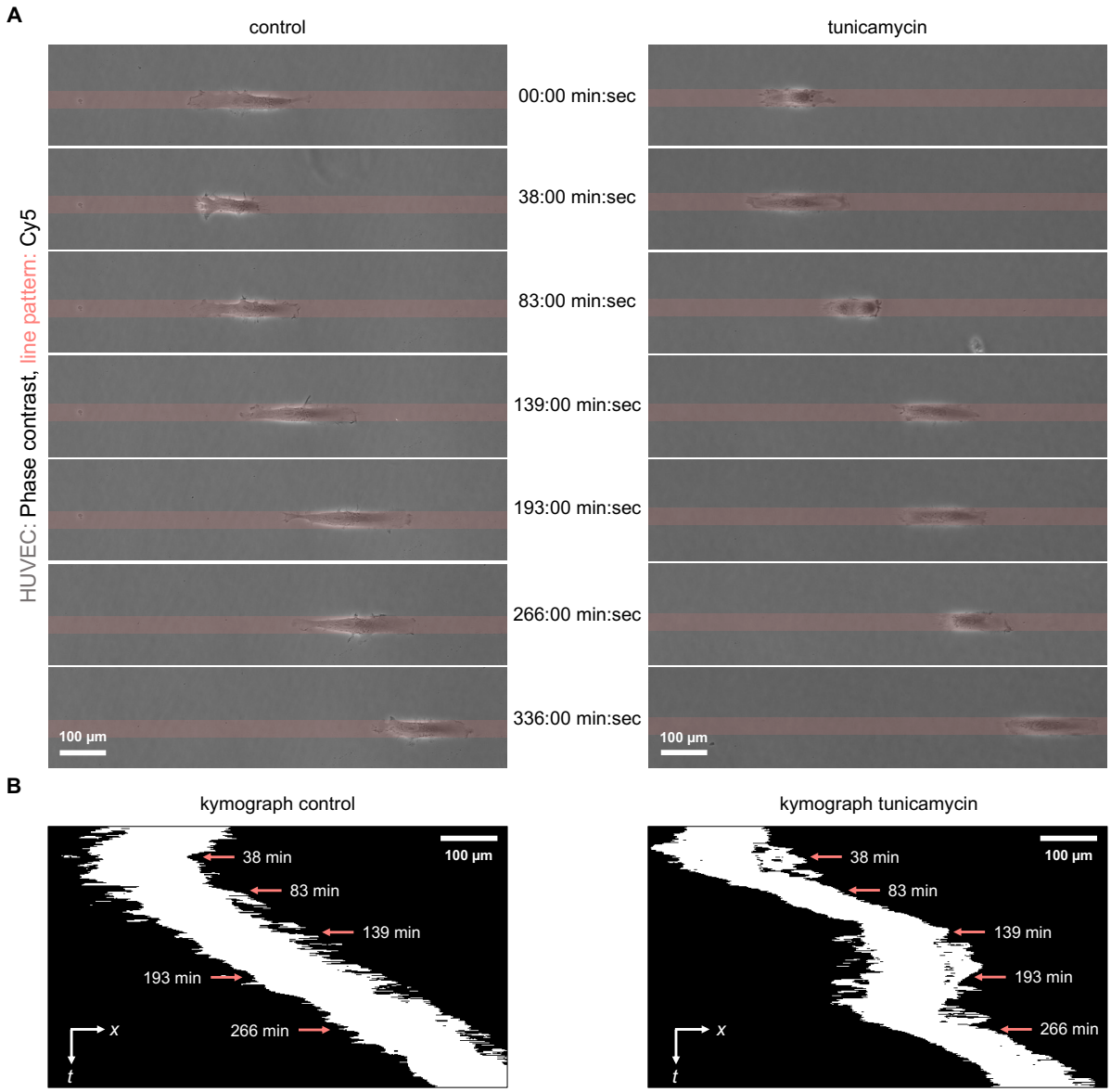

Figure 13: ER stress leads to less directional persistence on 1D micropatterned lines.

(A) Composite images of a representative control HUVEC (grey, left panel) and TN-treated HUVEC (grey, right panel) migrating inside a 1D micropatterned line of 20 µm width (light red) over a duration of 337 min. Scale bar: 100 µm.
(B) Kymograph of control HUVEC (left panel) and TN-treated HUVEC (right panel) with migration towards the right (*x*) depicted over time (*t*). Indicated are the timepoints chosen in (A). Scale bar: 100 µm.

2. PERK-inhibition restores collective mesenchymal cell migration

Treating HUVECs with either TN or azetidine activates the three branches of the UPR: ATF6, IRE1 and PERK (Sáez et al. 2014). To determine the contributions of the UPR branches to the observed reduction in speed during mesenchymal migration, specific inhibitors for each UPR branch were tested: Ceapin A7 selectively inhibits ATF6, AMG 18 hydrochloride inhibits IRE1α, and AMG PERK 44 inhibits PERK signalling (**Fig. 14A**). Cells under control conditions closed the wound area after around 18 h of collective migration while TN-treated cells were unable to do so. PERK inhibition increased wound closure and after around 18 h leader cells migrating at the front started to meet and close the wound (**Fig. 14B**). Image analysis of mean instantaneous speed revealed that only PERK inhibition with 2.5 µM of AMG PERK 44 was successful in preventing the reduction in the speed of migration after TN-treatment and display a speed similar to the one observed under control conditions. Inhibition of ATF6 or IRE1 showed a higher reduction in speed compared to TN-treatment. Using a mix of all three inhibitors was insufficient to prevent the decrease in the speed of migration after TN-treatment, indicating that only the PERK branch of the UPR is responsible for the observed reduction in speed under ER stress conditions (**Fig. 14C**), while suggesting differential roles for ATF6 and IRE1.

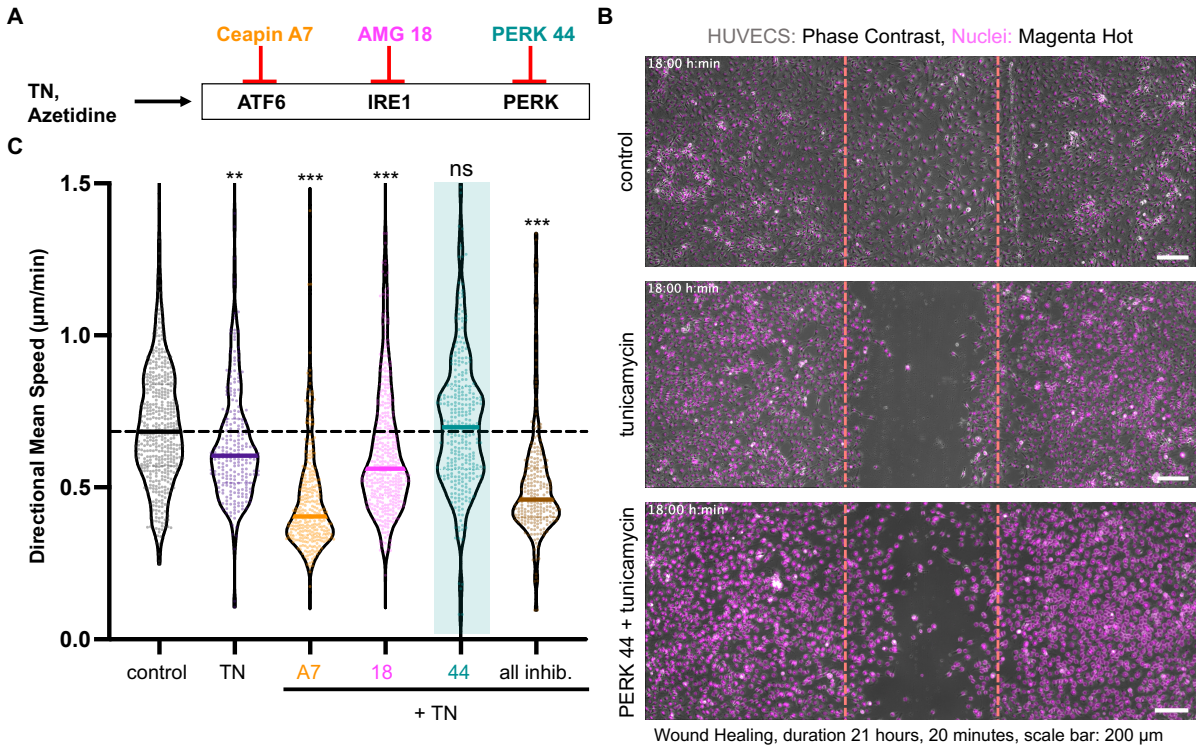

Figure 14: PERK inhibition restores collective mesenchymal migration after TN-treatment.

(A) Scheme depicting the specific inhibitors for each UPR branch used to illucidate which UPR protein is responsible for the observed changes in cell migration after ER stress induction.
(B) Representative composite pictures of HUVECs under control conditions (top panel), TN-treatment (middle panel) and PERK44 + TN treatment (bottom panel) 18 h after WH. Phase contrast of HUVECs is shown in grey, the nucleus was stained with Hoechst (magenta). Red dotted lines depict the scratched area representing the wound. Scale bar: 200 µm.
(C) Graph shows the instantaneous mean speed of HUVECs undergoing directional migration in µm/min for control conditions (grey), TN-treatment (purple), Ceapin A7 + TN-treatment (orange), AMG 18 + TN-treatment (pink), PERK44 + TN-treatment (petrol), and all 3 inhibitors combined + TN-treatment (brown) as truncated violin plots. The dark lines indicate the median of each condition, the dotted line corresponds to the median of the control. **P < 0.01, ***P < 0.001, ns = not significant, Kruskal Wallis test. n > 1000 cells each treatment.

3. PERK-inhibition restores alignment of cellular networks during collective migration

For migration, in particular directed cell migration, to take place, cell symmetry needs to be broken to develop a cell front and a cell rear that are aligned to a migratory axis which is continuously realigned to the direction of locomotion (Cramer 2010). This cellular polarization extends to the organelle level where organelles like the ER, Golgi and mitochondria show an asymmetric distribution and functional specialization downstream of the cytoskeleton. The cytoskeleton is often described as a cellular network with different protein filaments – actin, microtubules and intermediate filaments –, crosslinking to form a dynamic meshwork (Fletcher and Mullins 2010). Other organelles like the ER and mitochondria also form reticular networks. Mitochondrial connectivity is set by a balance of fusion and fission events. The morphology of

the ER is often referred to as a cellular network of ER sheets and tubules, extending throughout the cytoplasm (Giorgi et al. 2009).

As polarized cells show a distinct organization of their organelles and because ER stress is triggered by TN-treatment, ER morphology and alignment was analyzed. ER alignment was examined by calculating the directionality of ER tubules inside the front part of each cell migrating towards the right. Directionality of ER tubules was depicted from 0° to 180°: values of 0° or 180° meant complete alignment to the migratory axis, while values around 90° depicted a perpendicular/antiparallel alignment to the migratory axis. Overall, ER morphology did not show significant differences. All conditions presented perinuclear ER sheet-like structures and ER tubules spanning throughout the cell and reaching the tips of the cell (**Fig. 15A**). Control HUVECs showed a distribution of ER tubule direction that corresponds to an alignment with the migratory axis. Most tubules were oriented at around 0° or 180°, while the rest were distributed almost equally in every other direction. As ER tubules are a complex interconnected network, ER tubule directionality analysis should be consistent in representing this complexity, which is why every other possible orientation was found for some ER tubules (**Fig. 15B**, *top panel*). In comparison, TN-treated HUVECs showed ER tubule orientation with a peak around 80° reflecting a misalignment to the migratory axis (**Fig. 15B**, *middle panel*). PERK44 pre-treatment was sufficient to prevent the perpendicular alignment under ER stress conditions, showing most ER tubules with an orientation around 0° or 180° (**Fig. 15C**, *bottom panel*).

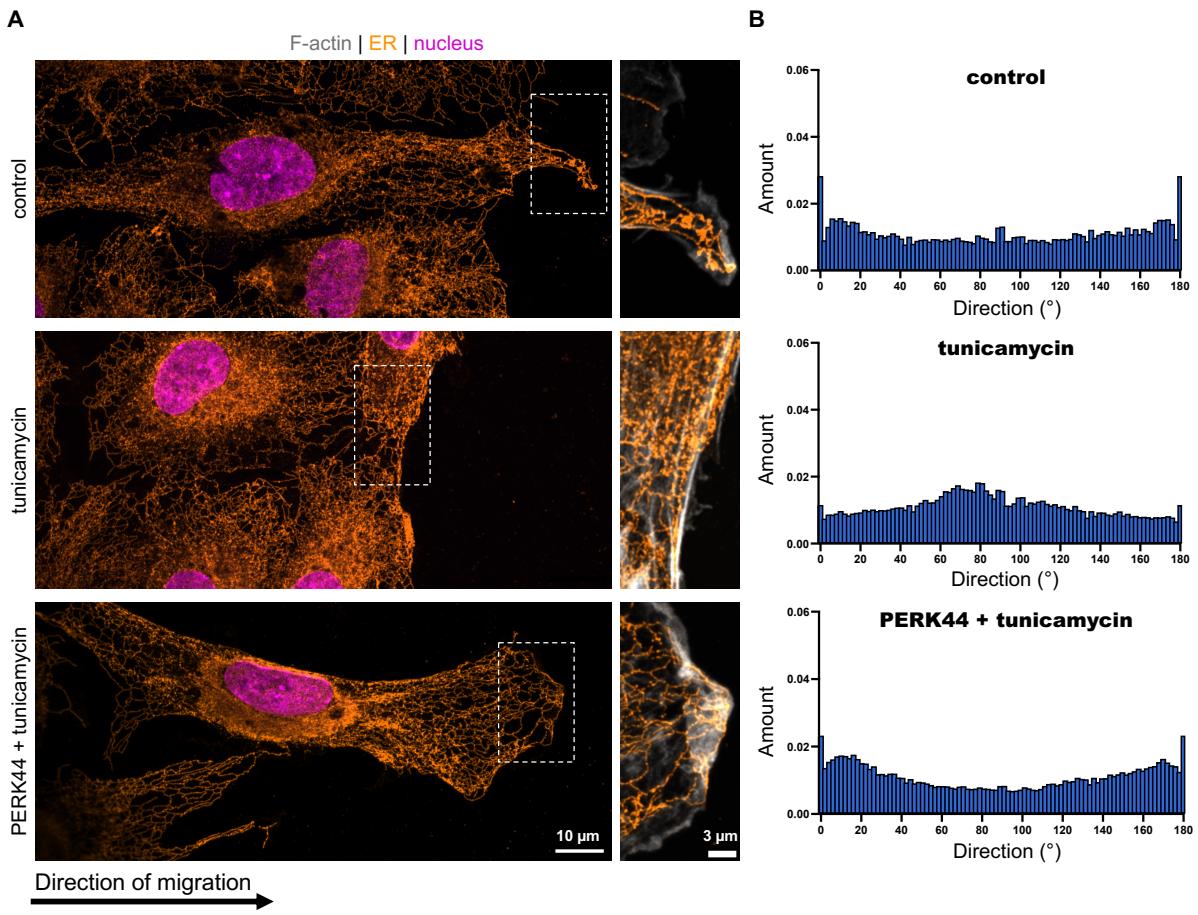

Figure 15: ER stress-induced ER tubule misalignment depends on PERK signalling.

(A) Representative confocal pictures of control cells (top panel), TN-treated cells (middle panel) and PERK44 + TN-treated cells (bottom panel) migrating towards the right. Cells were stained for F-actin (grey), ER (orange) and nucleus (pink). Scale bar: 10 µm, same for each image. Dashed boxes indicate area of the zoom-in pictures on the right of each large field of view, where F-actin is shown to depict the cell border. Scale bar of zoom: 3 µm, same for each image.
(B) Directionality analysis of ER tubules at the front of the cell. Graphs show the average directionality of 8 analyzed cells for control (top panel), TN-treatment (middle panel) and PERK44 + TN-treatment (bottom panel) each. 0° or 180° correspond to a total alignment with the migratory axis, while 90° correspond to a perpendicular alignment.
Of note: From this figure onwards, cells will always be depicted migrating towards the right, which will be indicated with a black arrow without the written caption.

Although it has been established recently that the shape of the ER is generated by evolutionary conserved membrane proteins that act independently of microtubules, it is a well known fact that the cytoskeleton, in particular the microtubules, is actively involved in distributing membrane-bound organelles like the ER (Tikhomirova et al. 2022). As ER tubules span throughout the whole cell and are found in the outermost tip of the cell front, a co-staining of microtubules in live and fixed control cells was performed. Live-cell imaging of transfected HUVECs revealed that ER tubules associate with microtubules at the cell front during migration (**Fig. 16A**). IF staining of fixed cells revealed that ER tubules reaching the outermost tip of the cell co-localize with microtubules (**Fig. 16B**).

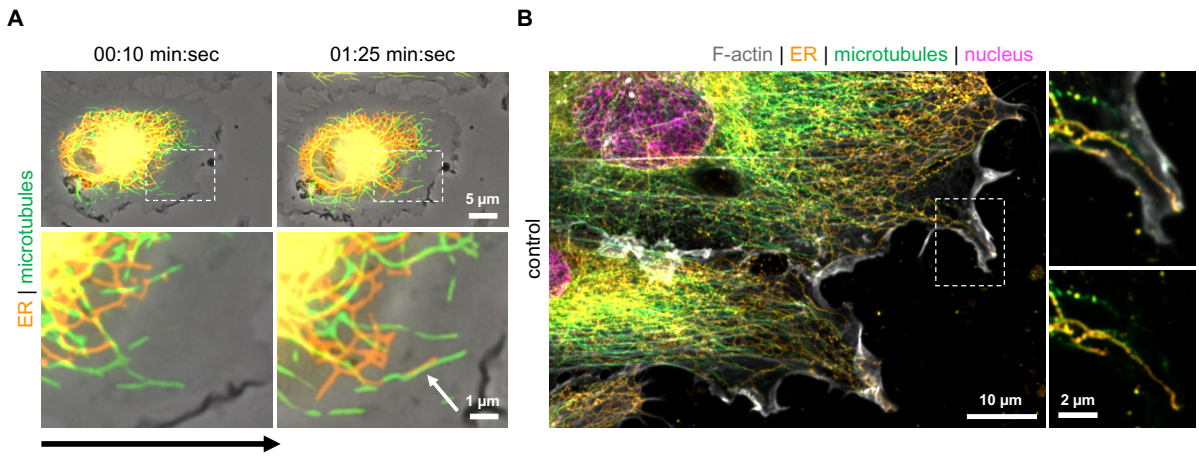

Figure 16: ER tubules associate with microtubules at the cell front during migration.

(A) Composite pictures of migrating HUVEC transfected with EMTB-3XGFP for microtubules (green) and DsRed2-ER-5 for ER (orange) at indicated timepoints. Dashed box indicates area of the zoom-in pictures below to highlight ER tubule and microtubule dynamics. Scale bar whole field of view: 5 µm for each image. Scale bar of zoom: 3 µm for each image. Credit to Svitlana Palii for performing the experiment.
(B) Representative confocal picture of control cells migrating towards the right. Cells were stained for F-actin (grey), ER (orange), microtubules (green) and nucleus (pink). Scale bar whole field of view: 10 µm, scale bar zoom: 2 µm for each image.
Black arrow indicates the direction of migration.

To determine whether microtubule distribution is similar to that observed for ER tubules, HUVECs were co-stained for ER and microtubules and directionality under the different conditions was analyzed.

Microtubules in control conditions showed a strong alignment to the migratory axis, extending throughout the cell into the leading edge (**Fig. 17A**, *top panel*). Directionality analysis showed most microtubules with a direction of 0° and 180° (**Fig. 17B**, *top panel*). TN-treatment showed a distortion of microtubule dynamics. While microtubules extended into the outermost parts of the cell (**Fig. 17A**, *middle panel*), their orientation was distributed around 80° proving a misalignment to the axis of migration (**Fig. 17B**, *middle panel*). PERK-inhibition was successful in preventing the misalignment, showing microtubules with a phenotype observed under control conditions (**Fig. 17A**, *bottom panel*). Their direction was determined at 0° and 180° showing their orientation aligned with the migratory axis (**Fig. 17B**, *bottom panel*).

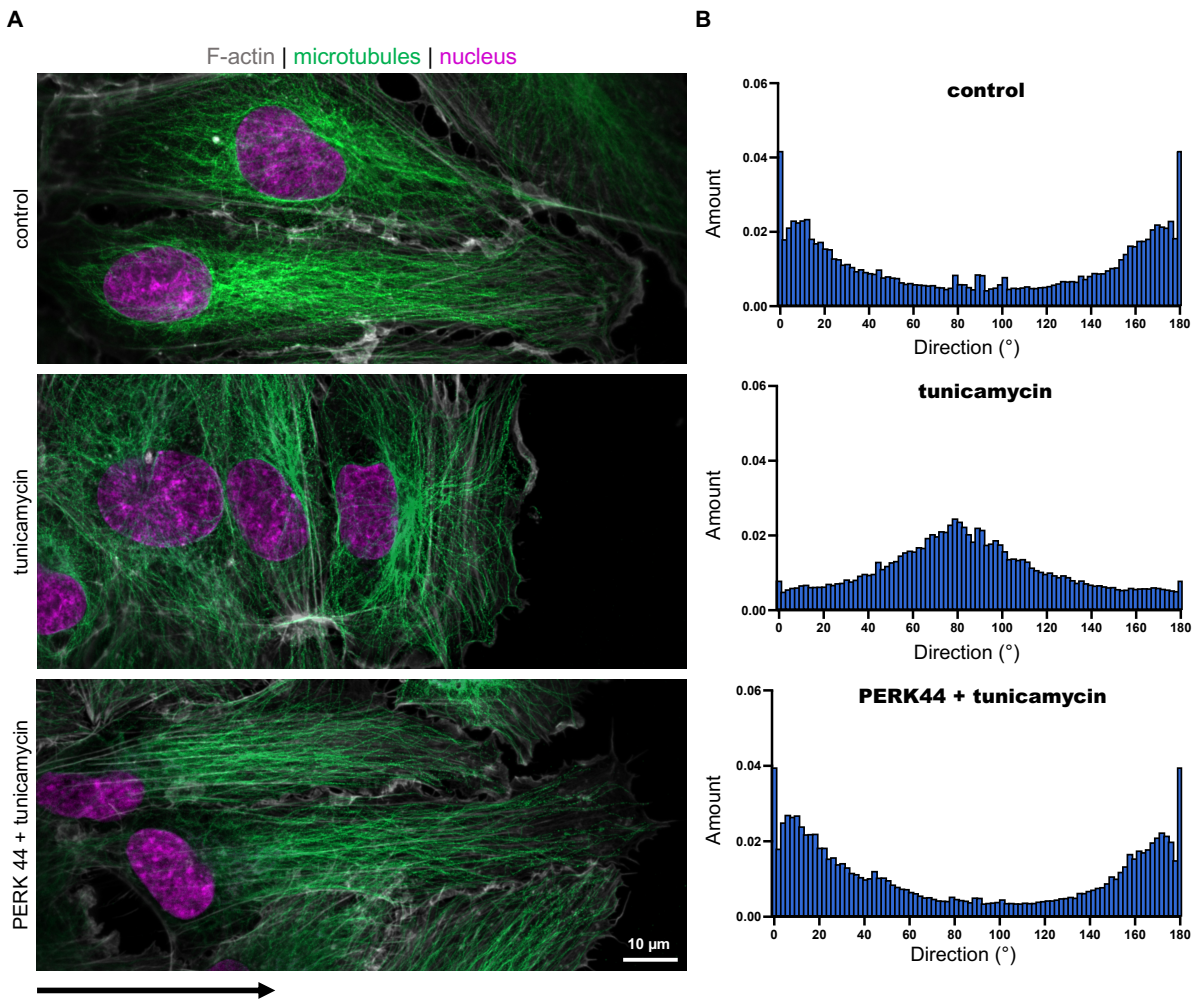

Figure 17: ER stress-induced microtubule misalignment depends on PERK signalling.

(A) Representative confocal pictures of control cells (top panel), TN-treated cells (middle panel) and PERK44 + TN-treated cells (bottom panel) migrating towards the right. Cells were stained for F-actin (grey), microtubules (green) and nucleus (pink). Scale bar: 10 µm, same for each image. Black arrow indicates the direction of migration.
(B) Directionality analysis of microtubules at the front of the cell. Graphs show the average directionality of 10 analyzed cells for control (top panel), TN-treatment (middle panel) and PERK44 + TN-treatment (bottom panel) each. 0° and 180° correspond to a total alignment with the migratory axis, while 90° correspond to a perpendicular alignment.

As shown before, TN-induced ER stress led to a decrease in directional migration and a lack of proper intracellular ER alignment. Because the actin cytoskeleton provides the major forces for migration through pushing and pulling dynamics (Wedlich 2005), and its localization is regulated by PERK signalling in other cellular models (Sánchez-Álvarez et al. 2021; van Vliet and Agostinis 2017), F-actin fiber orientation was evaluated in fixed cells after 6 h of WH.
Analysis of F-actin fibers at the ventral plane showed a strong alignment with the axis of locomotion in control conditions (**Fig. 18A, 18B**, *top panel*), which was confirmed through directionality analysis (**Fig. 18C**, *top panel*). TN-induced ER stress resulted in a strong perpendicular alignment of F-actin fibers (**Fig. 18A, 18B**, *middle panel*). Directionality analysis proved this observation with most analyzed fibers showing an orientation around 75°-110°

(**Fig. 18C**, *middle panel*). PERK-inhibition was successful in preventing this misalignment. Leader cells at the front showed most F-actin fibers aligned with the migratory axis (**Fig. 18A, 18B**, *bottom panel*) which was again corroborated by directionality analysis showing most F-actin fibers with an orientation of 0° and 180° (**Fig. 18C**, *bottom panel*).

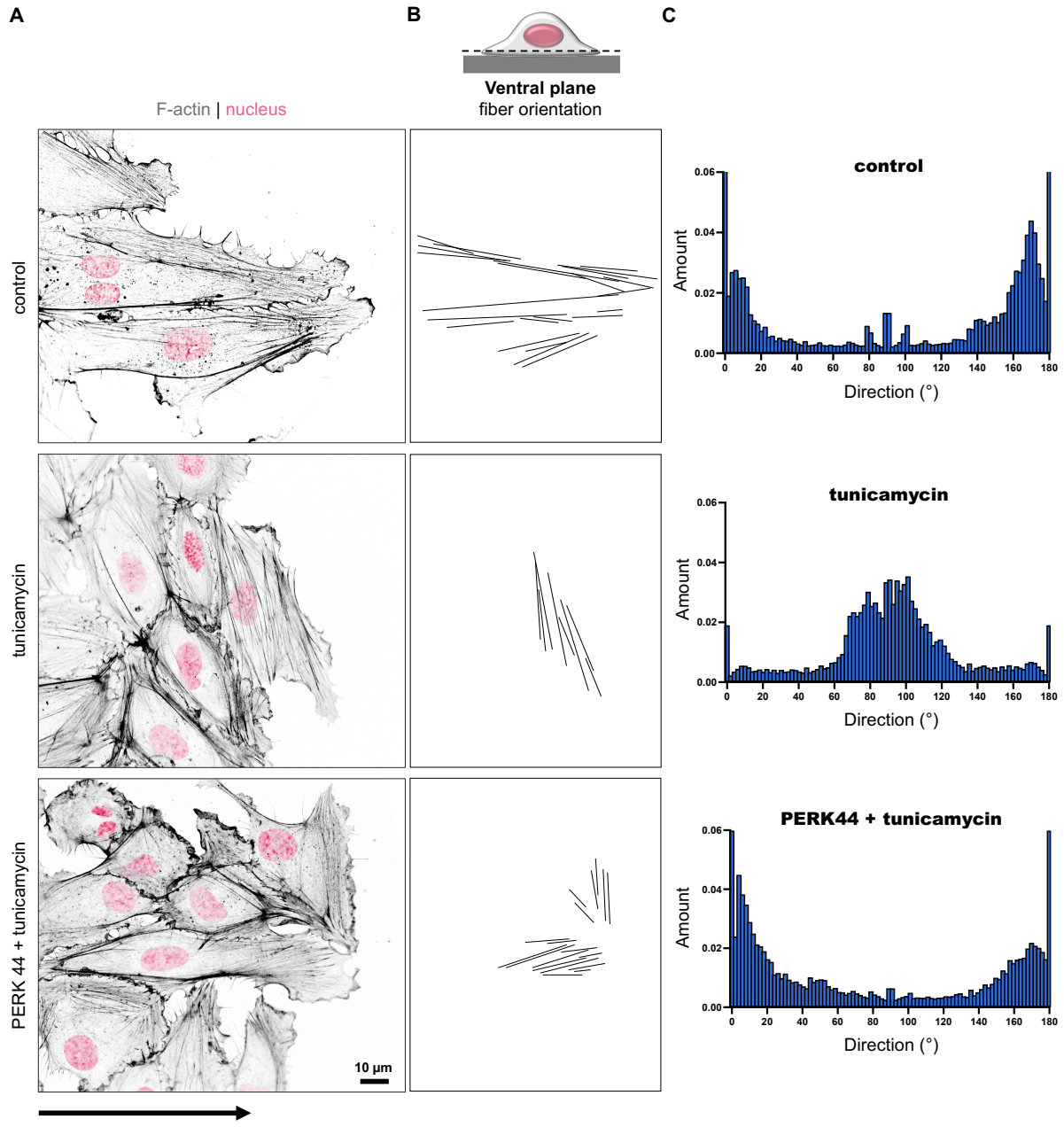

Figure 18: TN-treatment leads to a misalignment of F-actin fibers to the migratory axis.

(A) Representative confocal pictures of control cells (top panel), TN-treated cells (middle panel) and PERK44 + TN-treated cells (bottom panel) migrating towards the right. Cells were stained for F-actin (grey) and nucleus (pink), inverted LUT. Scale bar: 10 µm, same for each image. Black arrow indicates the direction of migration.
(B) Schematic pictures showing F-actin fibers visible in (A) to conceptualize the F-actin fibers at the ventral plane that were analyzed for their directionality.
(C) Directionality analysis of F-actin fibers at the ventral plane. Graphs show the average directionality of 10 analyzed cells for control (top panel), TN-treatment (middle panel) and PERK44 + TN-treatment (bottom panel) each. 0° and 180° correspond to a total alignment with the migratory axis, while 90° correspond to a perpendicular alignment.

In general, directionality analysis of F-actin fibers showed less fibers in total as it was limited to the fibers at the furthest ventral plane.
In addition, at the dorsal plane of the cell, F-actin fibers cover the nucleus and are aligned with the migratory axis (**Supplementary Fig. 2**, *left bottom panel*). These F-actin fibers, termed actin cables that form an actin cap, are reported to interact directly with proteins from the nuclear envelope allowing nuclear movement. In migrating cells, these actin cables are associated to the ER structure and its localization (Janota et al. 2022). Thus, the dorsal F-actin fibers were analyzed under TN-treatment and PERK44 pre-treatment conditions. Surprisingly, TN-treatment showed a strong reduction of these dorsal F-actin fibers. The F-actin present at the dorsal plane showed a perpendicular orientation (**Supplementary Fig. 2**, *middle bottom panel*), a response that was prevented by the inhibition of PERK (**Supplementary Fig. 2**, *right bottom panel*). PERK-inhibition was also successful in preventing the disappearance of F-actin cables at the dorsal plane. These results underline the hypothesis that ER stress modifies cytoskeleton dynamics – of actin and microtubules – which could lead to modifications in organelle positioning during cell migration.

Furthermore, the disruption of F-actin fiber alignment under ER stress would suggest a possible disturbance of membrane dynamics during directional migration. To explore these results in living cells, holotomographic imaging was performed. Different membrane dynamics were observed under control conditions, as well as TN-treatment. Under control conditions, the membrane spread out in the direction of migration and showed adherence to the substrate (**Fig. 19**, *top panel*). These stable protrusions were lamellipodia-like and were constantly turned over by new protrusions (**Fig. 19**, *top panel, e.g. transition from 00:36 min:sec to 01:24 min:sec*). TN-treatment showed accumulation of thicker and more dynamic protrusions (membrane “ruffles”), but less forward movement was observed. Even though the membrane was constantly turned over, TN-treated cells did not move forward and seemed stuck in the same place for longer time intervals (**Fig. 19**, *middle panel, e.g. transition from 01:24 min:sec to 02:12 min:sec*). PERK44 pre-treatment prevented the effect of TN-treatment. Leader cells at the front showed similar membrane dynamics to those observed under control conditions. The main protrusions remained flat and stable over time and showed alterations between protrusion and retraction of the membrane (**Fig. 19**, *bottom panel, e.g. transition from 00:00 min:sec to 00:36 min:sec*). Similar to fixed cells analyzed before, control cells and PERK44 pre-treated cells showed an alignment to the migratory axis.

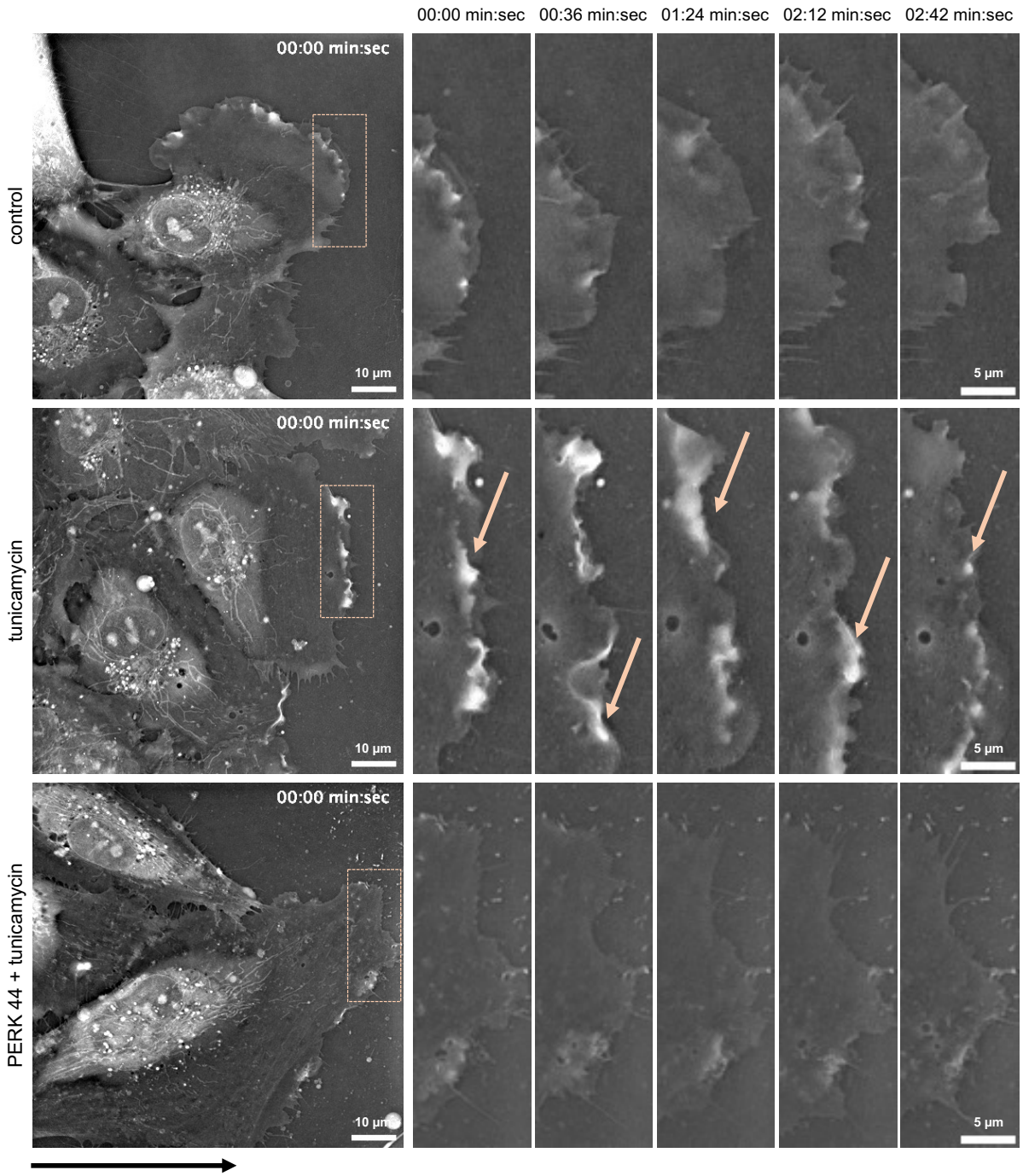

Figure 19: ER stress leads to non-productive membrane dynamics at the leading edge.

Holotomographic acquisition of control (top panel), TN-treated (middle panel) and PERK44 + TN-treated (bottom panel) cells during collective directional migration. Images were acquired every 2 s over a duration of 3 min to visualize membrane dynamics. Dashed boxes indicate the area of the zoom-in pictures on the right showing membrane dynamics at the leading edge for each cell under each condition at indicated time points. Scale bar whole field of view: 10 µm. Scale bar of zoom: 5 µm, same for each image.
Light orange arrows indicate thick membrane turn-over events (membrane ruffles) under TN-treatment. Black arrow indicates the direction of migration.

During collective mesenchymal cell migration in 2D, cells display strong interactions to the substrate through FAs. These FAs are dynamic in nature, switching between assembly and disassembly, a process that requires the actin cytoskeleton. The actin cytoskeleton is attached to integrins via proteins within FA structures and this attachment is critical in controlling the spatiotemporal dynamics of protrusions (extension and retraction). One of the proteins found in the FA complexes is paxillin which is also found in nascent adhesions (Le Clainche and Carlier 2008; Hu et al. 2014).

To examine whether the observed changes in membrane dynamics were a result of differential FA locations, fixed HUVECs were stained with an antibody against paxillin to visualize FA structures under control and ER stress conditions. Control HUVECs displayed FAs at the end of thick F-actin fibers that were aligned to the migratory axis. Because the paxillin staining created background noise, FA structures at the cell rear were less distinguishable (**Fig. 20**, *top panel*). FAs varied in size at the cell front with some FAs being well developed and larger (**Fig. 20**, *top panel, zoom 1*) while others looked smaller and associated with thinner F-actin fibers (**Fig. 20**, *top panel, zoom 2 and zoom 3*). TN-treated cells showed similar FA distributions, but a lower amount of FA spots at the front of the cell oriented towards the direction of migration suggesting a lower adhesive capacity. Because the F-actin fibers under ER stress were aligned perpendicular to the migratory axis, FAs showed the same misalignment, anchoring them antiparallel to the direction of locomotion (**Fig. 20**, *middle panel*). However, similar to control conditions, larger FA structures (**Fig. 20**, *middle panel, zoom 1 and zoom 2*) as well as smaller (**Fig. 20**, *middle panel, zoom 3*) FAs were observed. PERK inhibition prevented the misalignment of F-actin fibers showing F-actin organization and therefore FAs orientated towards the direction of migration (**Fig. 20**, *bottom panel*). Similar to control and TN-treated cells, FAs were associated with thicker F-actin stress fibers (**Fig. 20**, *bottom panel, zoom 1*) and smaller fibers at the leading edge of the cell (**Fig. 20**, *bottom panel, zoom 2 and zoom 3*). Altogether, these results suggest that while the structure of FAs under ER stress conditions is similar to those observed in control conditions, the dynamics of FA assembly and disassembly likely changed which remains to be studied.

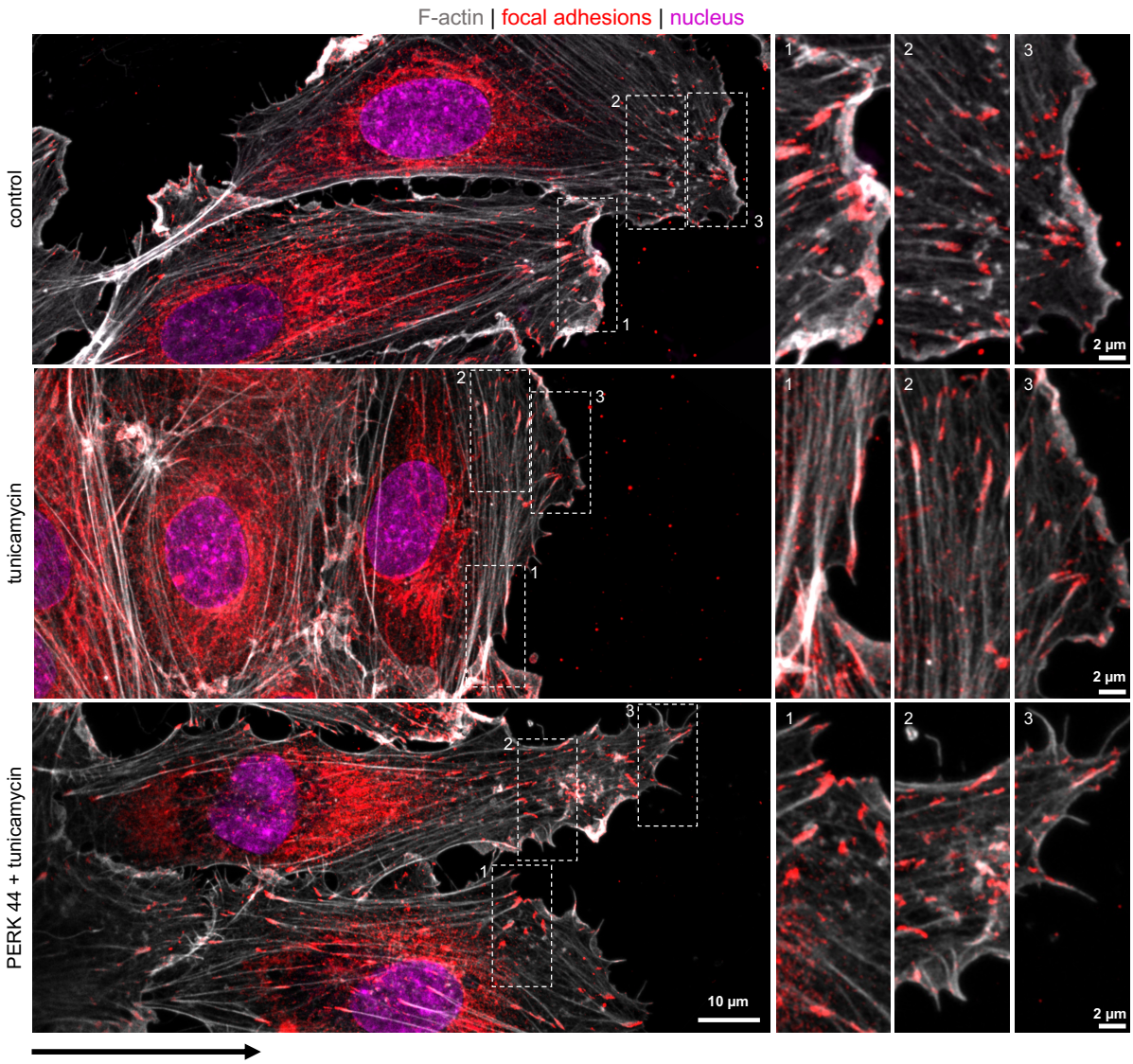

Figure 20: Focal adhesions link intracellular F-actin fibers to the extracellular matrix.

Representative confocal pictures of control cells (top panel), TN-treated cells (middle panel) and PERK44 + TN-treated cells (bottom panel) migrating towards the right. Cells were stained for F-actin (grey), focal adhesions (FAs, red) and nucleus (pink). Scale bar: 10 µm, same for each image.
Dashed boxes indicate the areas of the zoom-in pictures on the right showcasing FAs at the leading edge of each cell under each condition. Scale bar of zoom: 2 µm, same for each image.
Black arrow indicates the direction of migration.

Impact of ER stress on mitochondria organization and crosstalk

4. ER stress distorts mitochondria organization during collective cell migration

To summarize the findings of the first chapter: ER stress reduced mesenchymal cell migration in a PERK signalling-dependent manner which causes a distortion of the cytoskeletal organization. ER stress generated a misalignment of F-actin fibers leading to non-productive membrane dynamics at the leading edge of the cell. Moreover, PERK activation led to ER structure changes as a consequence of microtubule disorganization. Therefore, as the cytoskeleton, especially microtubules, is the main cellular network providing intracellular organization, stability and cell shape (Hohmann and Dehghani 2019), it is likely that other organelle dynamics, localization and crosstalk are impaired under ER stress conditions.

Interestingly, during visualizing of membrane dynamics during collective mesenchymal migration with holotomography, the dynamics of other cellular structures were also observed providing additional insights on the effects of ER stress. Focusing on the front part of the moving cell, string-like structures with a rather high RI were observed moving into the lamellipodial protrusion. These structures were identified as mitochondria (**Fig. 21**). While mitochondria under control conditions were dynamic and moved into the lamellipodium at the front of the cell (**Fig. 21**, *top panel*), mitochondria in TN-treated cells were less dynamic and were rarely found in the front area of the cell. While still showing movement inside the cell, the speed of mitochondria was slower and they showed less displacement over time compared to control conditions (**Fig. 21**, *middle panel*). Inhibition of PERK-signalling showed increased mitochondrial dynamics and movement towards the anterior part of the cell, similar to control conditions (**Fig. 21**, *bottom panel*).

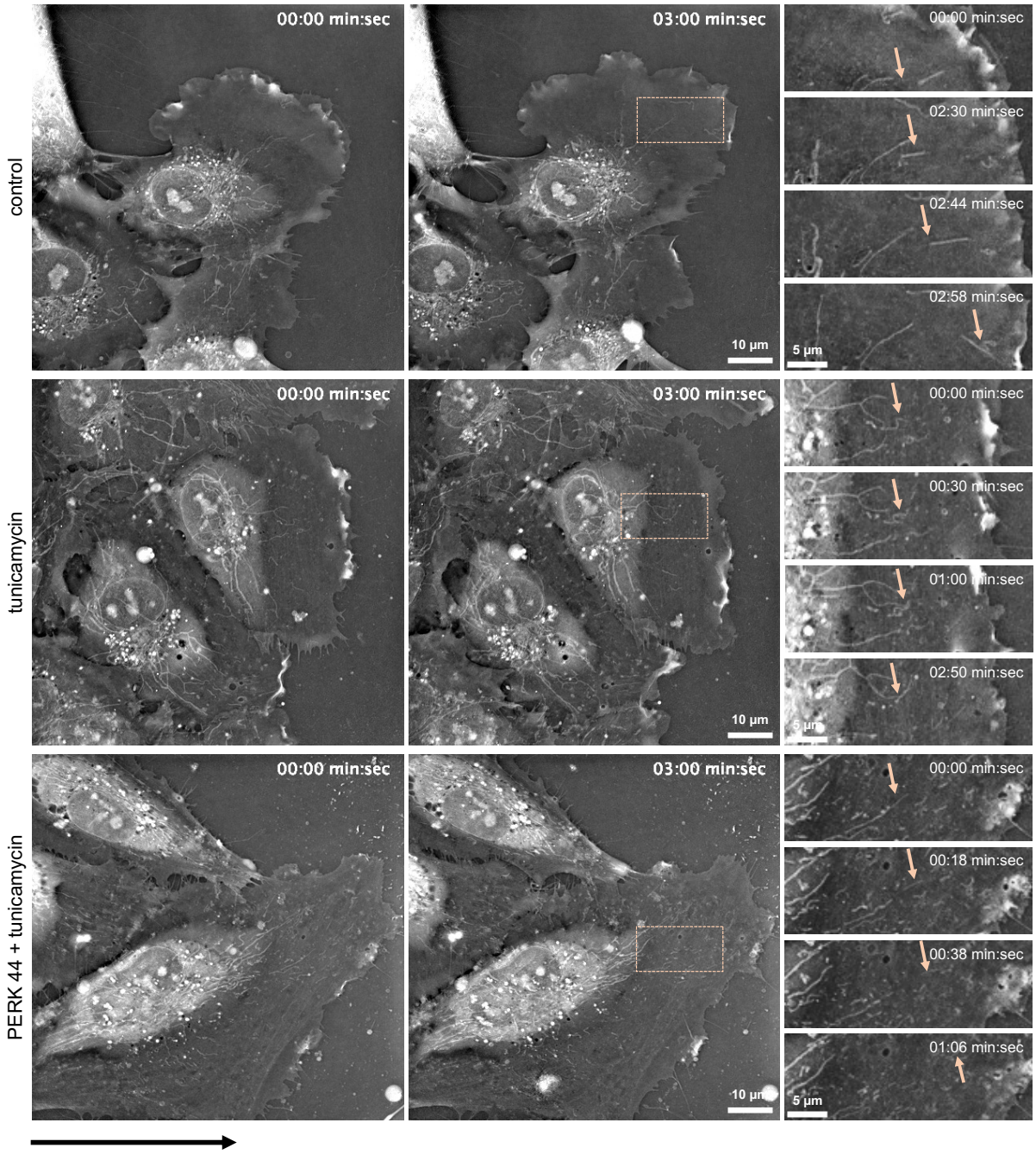

Figure 21: Mitochondria move into the protrusion of leader cells.

Holotomographic pictures of HUVECs migrating directionally at the front of the cell monolayer after WH. Pictures of refractive index (RI, greyscale) were taken in max-speed mode every 2 s over a duration of 3 min.
Top panel: HUVECs migrating under control conditions at the beginning and end of acquisition, scale bar: 10 µm, same for each image. Right panels show a zoom in (location indicated by dashed box) of mitochondria movement at the anterior part of the cell, scale bar: 5 µm, same for each image. Arrows point to single mitochondria over time.
Middle panel: HUVECs migrating after TN-treatment at the beginning and end of acquisition, scale bar: 10 µm, same for each image. Right panels show a zoom in of mitochondria movement at the anterior part of the cell, scale bar: 5 µm, same for each image. Arrows point to single mitochondria over time.
Bottom panel: HUVECs migrating after pre-treatment with PERK44 at the beginning and end of acquisition, scale bar: 10 µm, same for each image. Right panels show a zoom in of mitochondria movement at the anterior part of the cell, scale bar: 5 µm, same for each image. Arrows point to single mitochondria over time.
Black arrow indicates the direction of migration.

To analyze mitochondria organization in detail, HUVECs were fixed after 6 h of WH and stained with an antibody against TOM20. Mitochondrial intracellular distribution was examined with the directionality analysis previously described to compare their alignment to the migratory axis. Under control conditions, mitochondria showed an elongated phenotype and strong alignment to the axis of migration. Most mitochondria were found anterior to the nucleus and reached into the leading edge (**Fig. 22A**, *top panel*). Directionality analysis revealed that most mitochondria showed a direction of around 0° or 180°, confirming the visual finding of complete alignment with the migratory axis (**Fig. 22B**, *top panel*). TN-treatment led to a different phenotype of mitochondria inside the cell as they were found throughout the whole cell while showing a similar, more elongated phenotype. However, those mitochondria were distorted in comparison with the direction of migration (**Fig. 22A**, *middle panel*). Directionality analysis confirmed this misalignment by showing most mitochondria with a direction around 80° to 110° (**Fig. 22B**, *middle panel*). Pre-treatment with PERK44 was successful in preventing this misalignment, showing a phenotype similar to that found in control conditions. Elongated mitochondria were found at the leading edge of migrating cells (**Fig. 22A**, *bottom panel*). Analysis of directionality showed most mitochondria with a direction of 0° and 180°, proving the complete alignment to the axis of migration (**Fig. 22B**, *bottom panel*). As mentioned before, microtubules are actively involved in the distribution of membrane-bound organelles like the ER and mitochondria inside the cell (Tikhomirova et al. 2022). Long-distance transport of mitochondria inside the cell takes place on microtubule filaments via microtubule-based motor proteins, such as kinesins and dyneins. This direction of transport is dictated by microtubule filaments displaying an intrinsic polarity: plus-ends extend towards the cell periphery, while minus ends are anchored inside the MTOC (Melkov and Abdu 2018). Because of this strong interaction, microtubule distribution inside polarized HUVECs after 6 h of WH was investigated, as previously described (**Fig. 17**). Co-staining of microtubules and mitochondria showed a strong co-localization between the two (**Fig. 22C**). Both were aligned to the migratory axis and smaller mitochondria at the cell front showed association to microtubules close to the leading edge (**Fig. 22C**, *zoom 1 and zoom 2*).

It has been shown previously that mitochondria move and tether to FAs in NIH3T3 fibroblasts and regulate their size (Redaet et al. 2019). To examine whether a similar response takes place in HUVECs during mesenchymal migration, co-staining of FAs and mitochondria was performed after 6 h of WH (**Supplementary Fig. 3**). While mitochondria could be found in the vicinity of FAs under control conditions, only the smaller mitochondria at the leading edge could be hypothesized to co-localize with FAs (**Supplementary Fig. 3**, *top panel*). TN-treatment showed less proximity of mitochondria and FAs, especially at the part of the cell oriented towards the migratory axis (**Supplementary Fig. 3**, *middle panel*). PERK-inhibition was sufficient to re-direct mitochondria towards the front of the cell, where smaller fragmented

mitochondria were observed to co-localize with FAs (**Supplementary Fig. 3**, *bottom panel*). However, it remains to be studied whether a direct interaction of mitochondria and FAs plays a role in the observed dynamics of the cytoskeleton during mesenchymal cell migration.

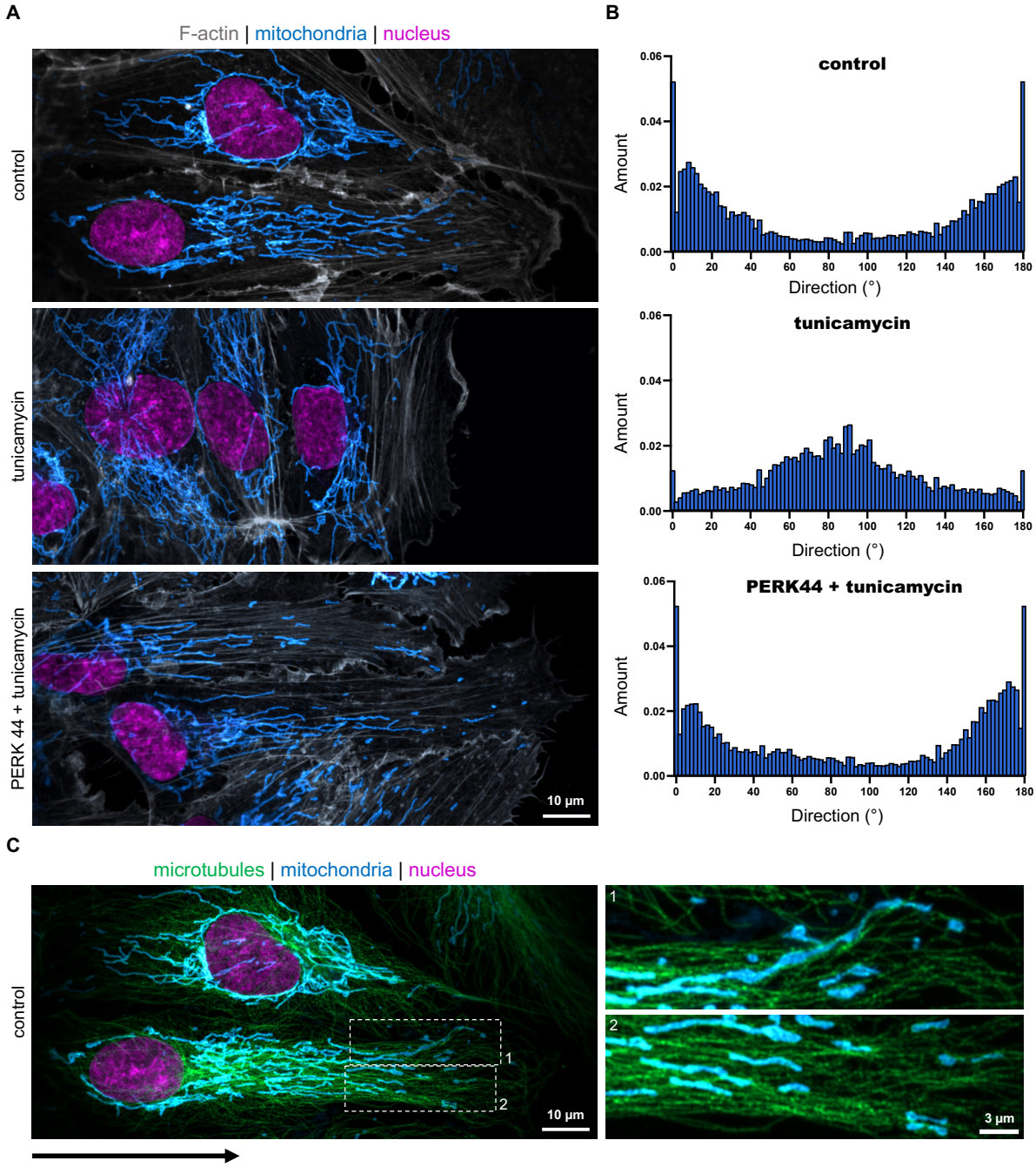

Figure 22: ER stress-induced mitochondria misalignment depends on PERK-signalling.

(A) Representative confocal pictures of control cells (top panel), TN-treated cells (middle panel) and PERK44 + TN-treated cells (bottom panel) migrating towards the right. Cells were stained for F-actin (grey), mitochondria (blue) and nucleus (pink). Scale bar: 10 µm, same for each image.
(B) Directionality analysis of mitochondria at the front of the cell. Graphs show the average directionality of 9 analyzed cells for control (top panel), TN-treatment (middle panel) and PERK44 + TN-treatment (bottom panel) each. 0° and 180° correspond to a total alignment with the migratory axis, while 90° correspond to a perpendicular alignment.
(C) Representative confocal pictures of control cells stained for microtubules (green), mitochondria (blue) and nucleus (pink). Scale bar: 10 µm. Dashed boxes indicate the areas of the zoom-in pictures on the right showcasing microtubule and mitochondria co-localization. Scale bar of zoom: 3 µm, same for each image. Black arrow indicates the direction of migration.

To study mitochondria organization during migration in a more controlled manner, micropatterns were used. Micropatterns of a circle, an ellipse and a crossbow were used to mimic possible orientation distributions in different polarized cell states. The circle pattern mimics a non-polarized state with zero cellular poles, the ellipse mimics a dual pole state where front and back are equally polarized, and the crossbow mimics one pole where the cell adopts a mono-polarized state (**Fig. 23A**, *top panel*). Because the cell could only attach inside the micropattern, live-cell imaging of organelle dynamics was simplified as the cell was unable to migrate out of view. Mitochondria inside the circle showed a distribution in every direction and no preferred alignment. Mitochondria inside the ellipse showed a distribution along one vertical axis connecting both poles. Mitochondria inside the crossbow pattern showed most mitochondria perinuclear with smaller mitochondria extending into the front area of the cell (**Fig. 23A**, *bottom panel*). Because the crossbow mimics a polarized cell during mesenchymal cell migration, this shape was chosen for live-cell imaging. During live-cell imaging, mitochondria under control conditions were aligned with the migratory axis and elongated to reach the front of the cell (**Fig. 23B**, *top panel*). Cells under ER stress showed mitochondria at the front of the cell, but displayed an orientation that was perpendicular to the axis of polarization **Fig. 23B**, *bottom panel*).

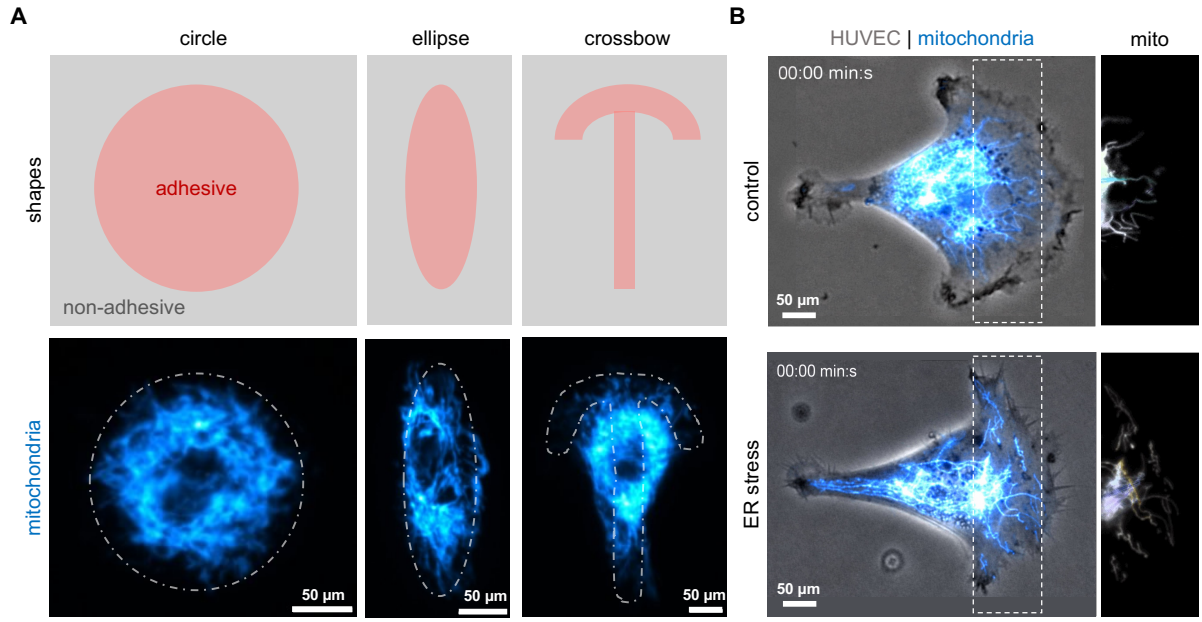

Figure 23: Mitochondria alignment along different poles, ER stress prevents alignment of mitochondria inside the cell front.

(A) *Top panel:* schematic depiction of micropatterns used to observe mitochondria organization in different polarized conditions. The red area corresponds to the adhesive pattern the cell attaches to, while the grey area is non-adhesive, preventing the cell to migrate out of the pattern. *Bottom panel:* Average mitochondria (stained with 100 nM TMRE, blue) distribution inside different micropatterns. Pictures show a z-projection of mitochondria from a minimum of 4 cells each. Scale bar: 50 µm.
(B) Composite picture of HUVEC (grey) and stained mitochondria (blue) for control conditions (top panel) and ER stress conditions (bottom panel) inside crossbow micropattern. Picture shows mitochondria distribution at the start of image acquisition. Dashed boxes indicate area of mitochondria analyzed for their orientation at the cell front.

The strong misalignment of organelles under ER stress conditions led to further investigation of the possible underlying crosstalk of the ER and other cellular components. Because the ER shows a strong association to mitochondria, forming physical connections via junctions termed mitochondria-associated membranes (MAMs) or mitochondria-ER contacts (MERCs) (Stacchiotti et al. 2019), ER and mitochondria dynamics inside migrating cells were analyzed. Co-staining of ER and mitochondria inside fixed cells showed a strong visual correlation between ER tubules and mitochondria. Under control conditions, the ER and mitochondria are aligned to the migratory axis, and high resolution microscopy strongly suggested the association between these organelles (**Fig. 24**, *top panel*). TN-treatment showed similar co-localization between ER and mitochondria, although both display an orientation antiparallel to the direction of locomotion (**Fig. 24**, *middle panel*). PERK-inhibition was sufficient to prevent the misalignment of both organelles, showing the ER and mitochondria aligned to the migratory axis. Because both organelles show association patterns on the same plane, contact between the two organelles is suggested (**Fig. 24**, *bottom panel*).

Because co-staining the two organelles does not prove contact, the PLA method was used to prove proximity between the two organelles. Under control conditions, PLA signals indicated strong proximity between ER and mitochondria as each signal technically proves contact between the two organelles (**Supplementary Fig. 4**, *left panel*). TN-treatment led to a strong reduction of PLA signals, indicating a reduction in MERCs (**Supplementary Fig. 4**, *middle panel*). PERK-inhibition restored the strong association observed under control conditions. The increase in PLA signals suggested an increased proximity between ER and mitochondria (**Supplementary Fig. 4**, *right panel*).

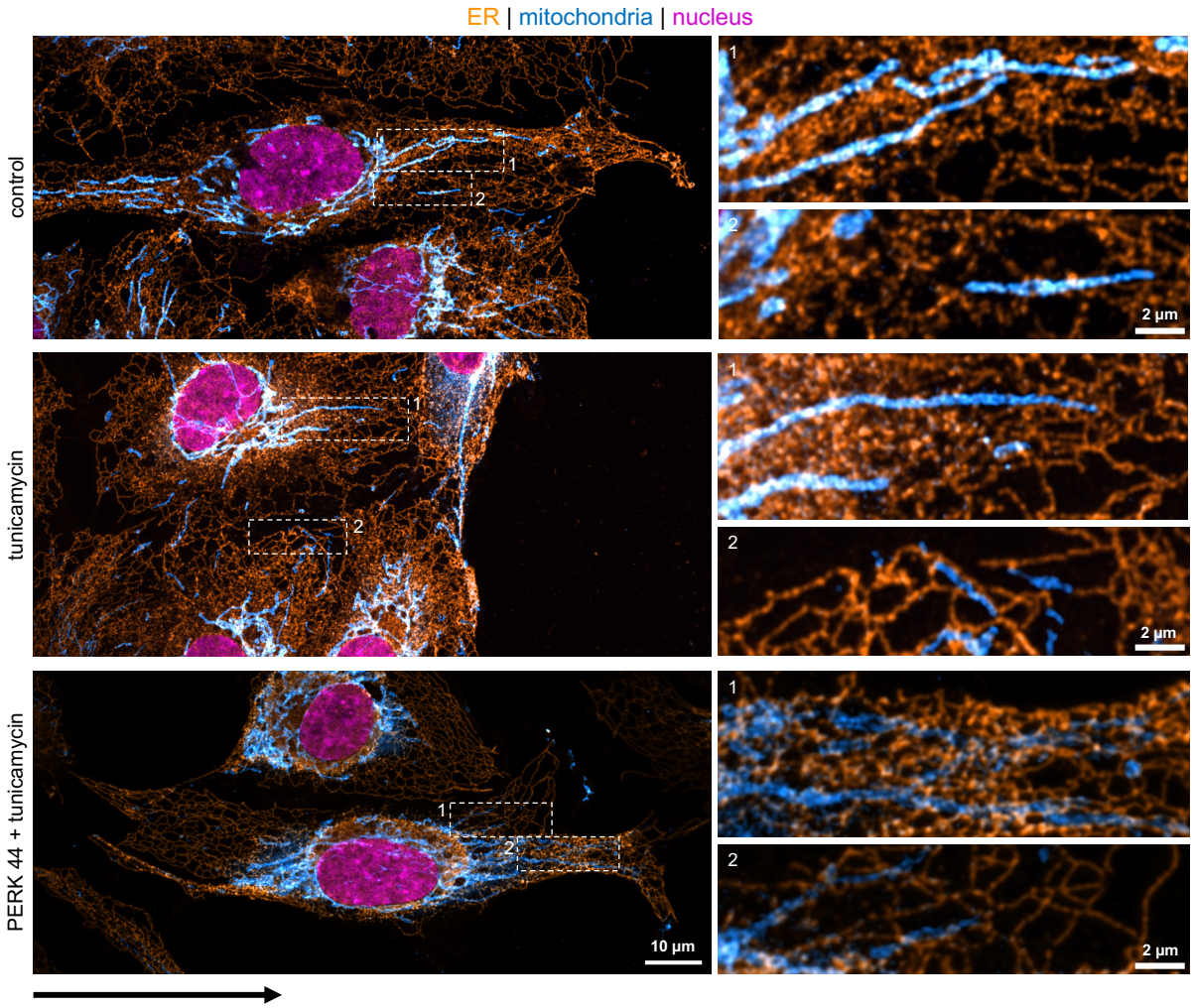

Figure 24: Co-localization between ER and mitochondria suggests contact.

Representative confocal pictures of control cells (top panel), TN-treated cells (middle panel) and PERK44 + TN-treated cells (bottom panel) migrating towards the right. Cells were stained for ER (orange), mitochondria (blue) and nucleus (pink). Scale bar: 10 µm, same for each image. Black arrow indicates the direction of migration.
Dashed boxes indicate area of the zoom-in pictures on the right of each large field of view, where ER and mitochondria association is shown. Scale bar: 2 µm, same for each image.

The PLA method is technically advanced and the method's high sensitivity can lead to positive signals even in the absence of interaction between the two proteins of interest (Tower and Chang 2025). To prove actual contact between the ER and mitochondria, ultrastructural analysis was done by visualizing these two organelles through electron microscopy. Electron micrographs of control cells revealed elongated mitochondria at the front of the cell. These mitochondria showed contact with ER tubules at different areas (**Fig. 25**, *top panel*). TN-treatment induced a morphology change, showing more fragmented mitochondria (**Fig. 25**, *middle panel*). Longer mitochondria showed misalignments to the direction of migration (**Fig. 25**, *middle panel, zoom 1*). Under ER stress, the distance between mitochondria and ER tubules seems to be increased. In control conditions, ER tubules are directly in contact with

the OMM, while cells after TN-treatment showed a slight distance between the two membranes. PERK-inhibition was successful in re-establishing direct contact between the two organelles. While mitochondria at the cell front were not as straight as mitochondria under control conditions, they were longer compared to the ones under ER stress (**Fig. 25**, *bottom panel*). Altogether, these data show that through the strong association between ER and mitochondria, ER stress induces morphological changes in mitochondria that could further lead to impaired mitochondrial function.

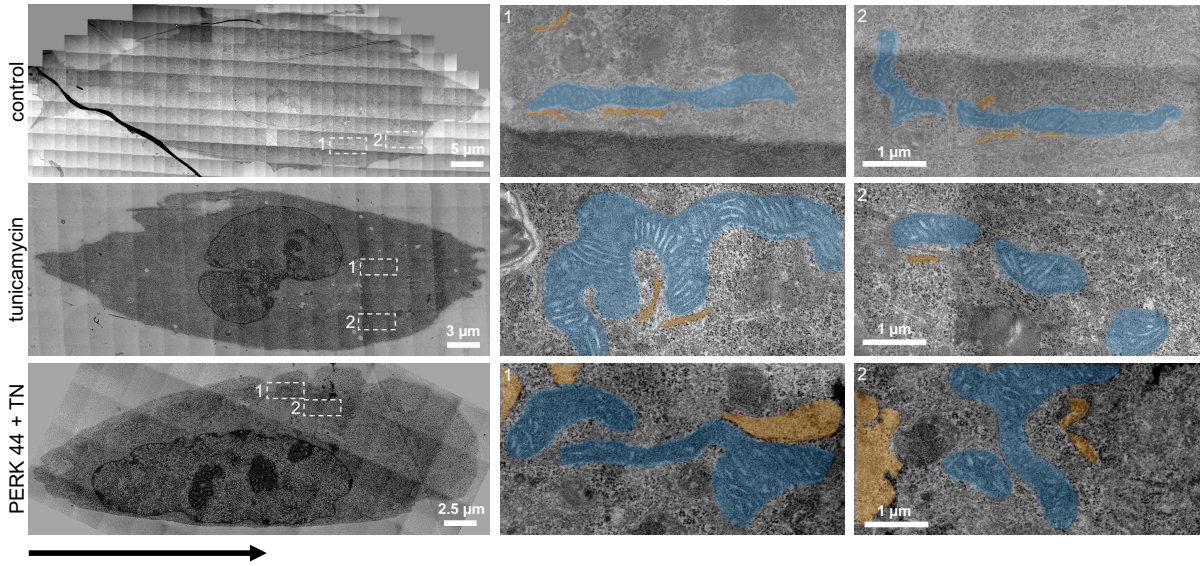

Figure 25: ER and mitochondria are in contact at the cell front of migrating cells.

Representative electron micrographs of control cells (top panel), TN-treated cells (middle panel) and PERK44 + TN-treated cells (bottom panel). One whole cell picture was reconstituted by stitching multiple smaller electron micrographs together. Scale bar: 5 µm for control, 3 µm for TN-treatment and 2.5 µm for PERK44 + TN-treatment. Black arrow indicates the direction of migration.
Dashed boxes indicate area of zoom-in pictures on the right showing direct contact between ER (orange) and mitochondria (blue). Scale bar: 1 µm, same for each image.

Single and collective mesenchymal cell migration and mitochondria function

5. Mitochondria anticipate the polarity axis during directional migration

After establishing that mitochondria organization is distorted under ER stress conditions which could be directly coupled to the observed migratory defects, the possible role of mitochondria during directional migration still needs to be investigated.

Observing mitochondria during random 2D live-cell migration revealed that mitochondria movement inside the cell is dynamic. While mitochondria could be found in all parts of the cell, it was shown that they accumulated inside cellular protrusions and were redirected to one protrusion that eventually determined the direction of migration (**Fig. 26**, *focus on 83:00 min:sec to 113:00 min:sec*). This data suggests a significant involvement of mitochondria in determining which direction the cell ends up migrating into.

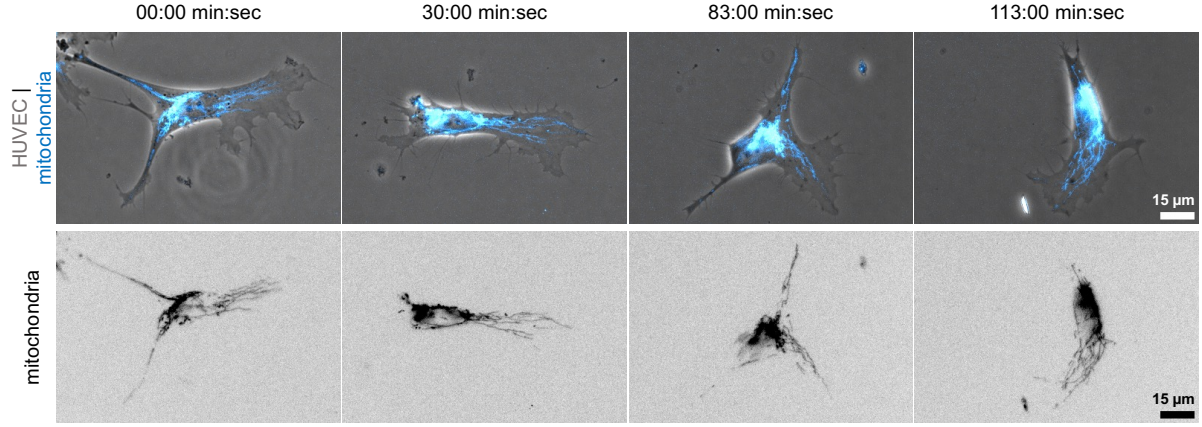

2D random free migration, duration 2 hours, pictures taken every 30 seconds with 40x magnification

Figure 26: Mitochondria align with the polarity axis during single random cell migration.

Single random cell migration in a 2D microenvironment was observed with a 40x objective over a duration of 2 hours.
Upper panel: Composite pictures of HUVEC (grey, phase contrast) and mitochondria (cyan, channel Cy3) at indicated timepoints. Scale bar: 15 µm, same for each image.
Lower panel: Pictures of single mitochondria (black) channel at indicated timepoints. Scale bar: 15 µm, same for each image.

One of the main roles of mitochondria is providing energy in the form of ATP synthesis through OXPHOS for various physiological processes including cell migration (Denisenko, Gorbunova, and Zhivotovsky 2019). During OXPHOS, the mitochondrial membrane potential ($\Delta\Psi$) that is generated by proton pumps is an essential component (Zorova et al. 2018). To visualize and quantify changes in membrane potential, fluorescent probes like TMRE are used. TMRE is a positively charged dye that accumulates in physiologically healthy mitochondria as their net negative charge is maintained around -180 mV (Crowley, Christensen, and Waterhouse 2016). Visualization of TMRE fluorescence changes allows to determine whether mitochondria display a higher or lower $\Delta\Psi$. While using TMRE as a tool to study $\Delta\Psi$, FCCP is used as a

control. FCCP as a protonophore uncouples OXPHOS by dissipating the proton gradient across the IMM and therefore eliminating the negative net charge. Treating cells with FCCP leads to strong depolarization events that are visualized by fluorescence signal loss of TMRE (Crowley, Christensen, and Waterhouse 2016). Staining mitochondria with TMRE in live-cells revealed dynamic changes in $\Delta\Psi$. While moving randomly, stochastic depolarization events were observed (**Fig. 27A**, *white arrows indicate depolarization events*). Acute addition of FCCP during live-cell acquisition led to a permanent depolarization of $\Delta\Psi$ which was not re-established over time. Upon FCCP addition to the full media, TMRE signal was fully lost after roughly 14 min of acquisition (**Fig. 27B**, *complete TMRE signal loss at 00:24 h:min*).

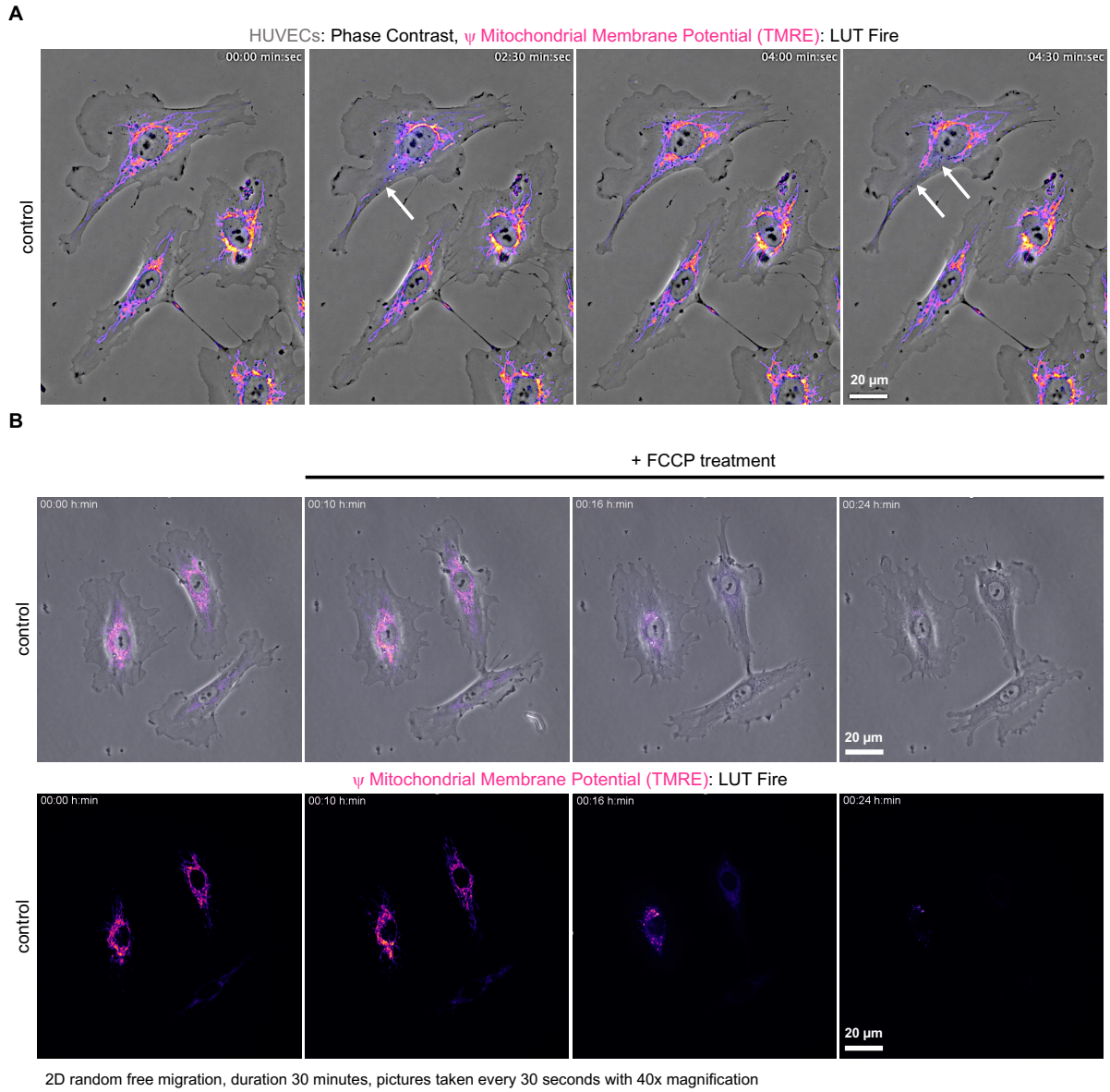

2D random free migration, duration 30 minutes, pictures taken every 30 seconds with 40x magnification

Figure 27: FCCP treatment induces strong, irreversible depolarization events.

(A) Composite pictures of HUVECs (grey, phase contrast) and mitochondria (TMRE staining depicted in LUT Fire, images acquired in channel Cy3) were taken every 30 s over a duration of 30 min. Dynamic TMRE signal is shown at indicated timepoints (white arrows). Scale bar: 20 µm for each image.
(B) HUVECs (grey, phase contrast) and mitochondria (TMRE staining depicted in LUT Fire, images acquired in channel Cy3) were observed for 30 min with pictures taken every 30 s. After 10 min of image acquisition, 50 µM FCCP treatment were added to the media and not washed out. Scale bar: 20 µm for each image. *Top panel:* Composite pictures of HUVECs and mitochondria at indicated time points. *Bottom panel:* Pictures of mitochondria stained with TMRE at indicated timepoints.

Considering that FCCP is a protonophore that uncouples OXPHOS, the effect of FCCP on collectively migrating HUVECs was analyzed. Two different concentrations of FCCP treatment – 10 µM and 50 µM – were added to full media and HUVECs were imaged during WH. As expected, 10 µM and 50 µM led to a significant reduction in overall speed of collective migration (**Fig. 28A**). Differentiating between random and directional movement, cells showed a significant reduction for speed in both migratory modes after FCCP treatment (**Fig. 28B**).

Treatment with 10 µM FCCP significantly reduced random (**Fig. 28C**, *top panel*), and directional migration (**Fig. 28C**, *bottom panel*). Surprisingly, despite a significant reduction in their motility capacity, cells treated with 50 µM FCCP remained motile throughout 20 h of acquisition time and exhibited both migratory modes: random and directional, but with a smaller magnitude (**Fig. 28C**).

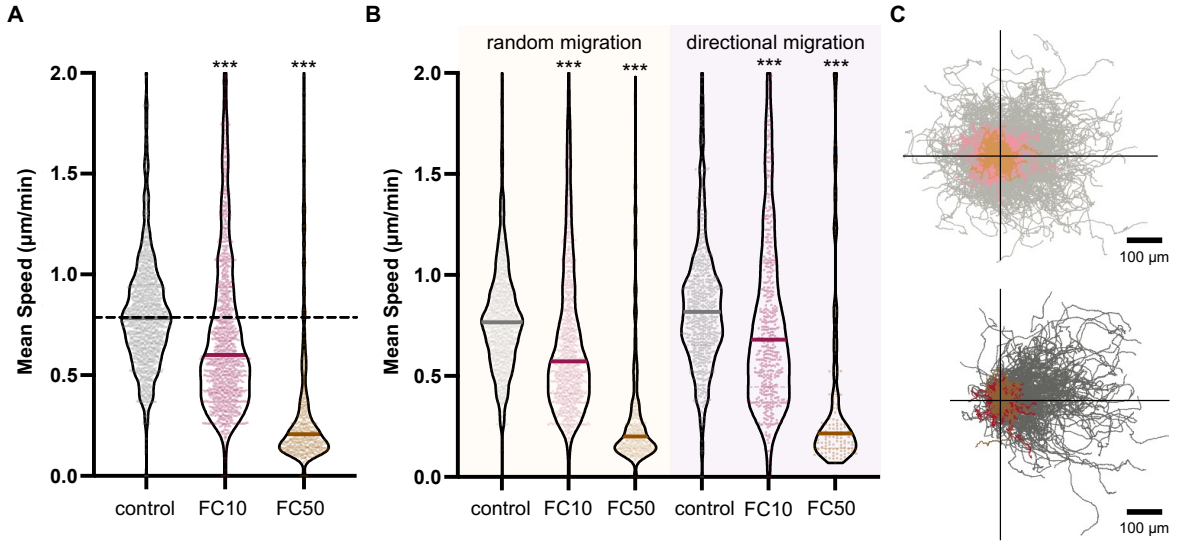

Figure 28: FCCP treatment reduces speed of collective migration, but cells stay motile.

(A) Graph shows the instantaneous mean speed of collectively migrating HUVECs in µm/min for control conditions (grey), 10 µM FCCP-treatment (dark red) and 50 µM FCCP-treatment (brown) as truncated violin plots. The dark lines indicate the median of each condition, the dotted line corresponds to the median of the control ***P < 0.001, Kruskal Wallis test. n > 500 cells each for overall motility.
(B) Graph shows the instantaneous mean speed of collectively migrating HUVECs in µm/min for control conditions (grey), 10 µM FCCP-treatment (dark red) and 50 µM FCCP-treatment (brown) for random migration (yellow) and directional migration (light purple) as truncated violin plots. The dark lines indicate the median of each condition.. ***P < 0.001, Kruskal Wallis test. n > 500 cells each for the two motility modes.
(C) *Top panel:* Track display of individual HUVECs moving randomly under control conditions (light grey), 10 µM FCCP-treatment (light red) and 50 µM FCCP-treatment (light brown). All track displays show individual tracks of n > 500 cells each. Scale bar: 100 µm. *Bottom panel:* Track display of individual HUVECs moving directionally under control conditions (dark grey), 10 µM FCCP-treatment (dark red) and 50 µM FCCP-treatment (dark brown). All track displays show individual tracks of n > 500 cells each. Scale bar: 100 µm.

To compare the effect of FCCP over collectively migrating cells with single cell migration, cells were treated with 50 µM FCCP during 2D random motility. While cells under control conditions displayed the already described membrane dynamics (see **Fig. 19**) of lamellipodia extension towards the direction of movement (**Fig. 29**, *top panel*), cells treated with FCCP showed almost no displacement of the cell body. However, while the cell body was not actually moving forward, the membrane was very dynamic, switching between phases of extension and retraction (**Fig. 29**, *bottom panel*). The observed membrane dynamics resembled those seen under ER stress conditions with thicker membrane "ruffles" (**Fig. 29**, *bottom panel, zoom at 02:23 min:sec*) and shuffling of the membrane over time without actually displacing further.

Overall, these data reveal that mitochondria activity is required for random and directional migration.

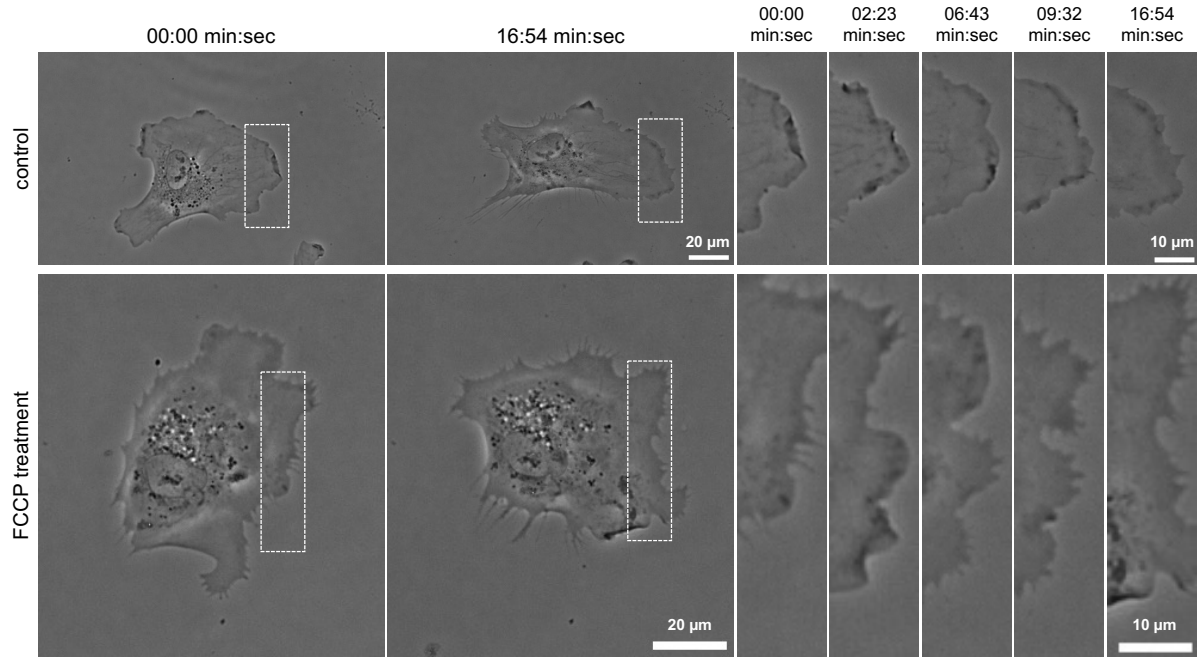

2D random free migration, duration 17 minutes, pictures taken every 13 seconds with 40x magnification

Figure 29: FCCP treatment induces membrane ruffles similar to TN-treatment.

Top panel: Membrane dynamics of HUVEC (grey) under control conditions at the start and end point of acquisition. Scale bar: 20 µm for both whole field of view pictures. Dashed boxes indicate the area of zoom-ins showcasing membrane dynamics at the leading edge at indicated time points. Scale bar: 10 µm for each zoom-in picture.
Bottom panel: Membrane dynamics of HUVEC (grey) after 50 µM FCCP-treatment at the start and end point of acquisition. Scale bar: 20 µm for both whole field of view pictures. Dashed boxes indicate the area of zoom-ins showcasing membrane dynamics at the leading edge at indicated time points. Scale bar: 10 µm for each zoom-in picture.

6. Higher frequency of depolarisation events occur during directional migration

After establishing that $\Delta\Psi$ is dynamic and showed fluctuations during random 2D migration, $\Delta\Psi$ was monitored in cells via live-cell acquisition of HUVECs during WH. To guarantee that the observed fluctuations in TMRE signal are the result of depolarization events of $\Delta\Psi$ and not mitochondria moving out of focus, HUVECs were transfected with a plasmid for mitochondria that shows stable fluorescent signal that is independent of $\Delta\Psi$, mitoGFP. This way, depolarization events could be depicted by pseudo-ratiometric measurement by overlapping the two fluorescent signals (TMRE will be shown as a blue color, stable plasmid fluorescence will be shown as a red color): If a depolarization occurs, the blue TMRE signal will be reduced, whereas the red signal will be unaffected, allowing to monitor mitochondrial location. This method was used to observe changes in $\Delta\Psi$ under control conditions as well as ER stress conditions.

Under control conditions, TMRE signal was dynamic and random depolarization events occurred in every cell. However, it became evident that polarized cells migrating directionally showed repeated depolarization events, especially in mitochondria oriented in the direction of migration. These cells were found at the front of the cell monolayer. While some cells were elongated, others were smaller, but still polarized in their shape (**Fig. 30A**, *zoom of cell 1 smaller, but polarized; and zoom of cell 2, elongated shape*).

Quantification of TMRE signal and therefore changes in $\Delta\Psi$ was technically very challenging, as the segmentation did not allow to distinguish between single mitochondria and mitochondria networks. Thus, to depict the changes in $\Delta\Psi$, especially the depolarization events, 3D surface plot profiles of an area of mitochondria were generated. For optimal visualization, the mitochondria analyzed were turned to be orientated downward. The 3D surface plot allowed for visualization of the fluctuations both signals (TMRE and mitoGFP) depict. One representative time frame per cell was shown to prove depolarization events over time. The main depolarization event during directional movement of cell 1 lasted roughly 1 min 50 sec (**Fig. 30B**, *time frame from 02:50 min:sec till 04:40 min:sec*). While the mitoGFP signal stayed consistent during that time period (**Fig. 30B**, *bottom panel, area marked with dashed box for mitoGFP*), a small mitochondria population showed strong depolarization events which were quantified by complete signal loss of TMRE signal. While TMRE fluorescence was still present at 02:50 min:sec for that mitochondria population, the signal was lost for around 40 sec (*time frame 03:30 min:sec till 04:10 min:sec*), and re-established around 04:40 min:sec, showing repolarisation events (**Fig. 30B**, *top panel, area marked with dashed box for TMRE*).

Cell 2 showed another, less strong depolarization pattern. TMRE signal was present from 08:30 min:sec onwards and showed a slight decrease at 08:40 min:sec, which increased again at 09:50 min:sec (**Fig. 30C**, *top panel, area marked with dashed box for TMRE*). The main depolarization event happened at 10:00 min:sec, with the TMRE signal of those mitochondria completely lost. The mitoGFP signal for those mitochondria stayed consistent over time (**Fig. 30C**, *bottom panel, area marked with dashed box for mitoGFP*), proving fluctuations in $\Delta\Psi$ that were either very strong with complete signal loss of TMRE or weaker with only small decreases in TMRE fluorescence signal.

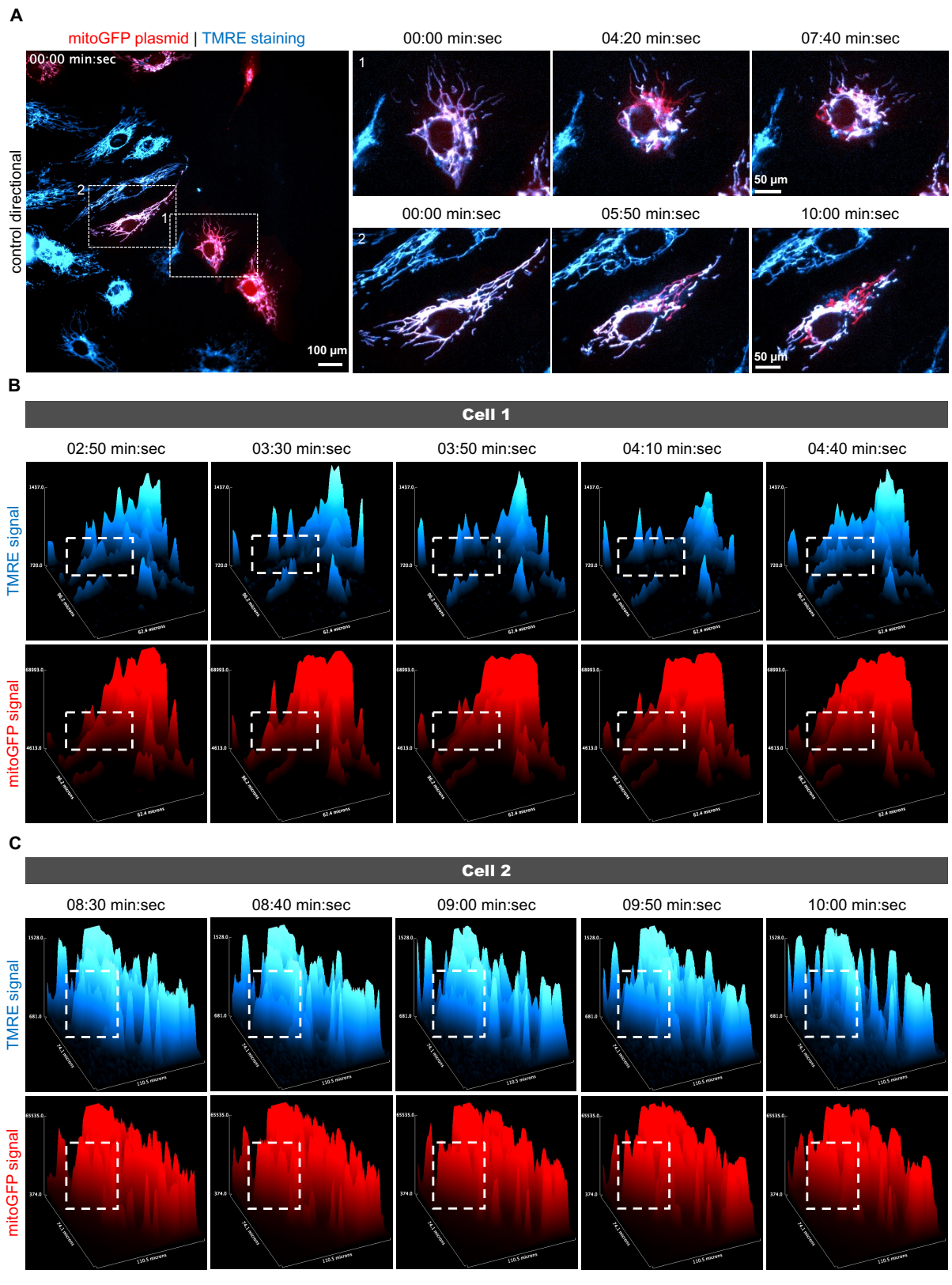
A
mitoGFP plasmid | TMRE staining
00:00 min:sec
04:20 min:sec
07:40 min:sec
control directional
00:00 min:sec
100 µm
50 µm
00:00 min:sec
05:50 min:sec
10:00 min:sec
50 µm
B
Cell 1
02:50 min:sec
03:30 min:sec
03:50 min:sec
04:10 min:sec
04:40 min:sec
TMRE signal
mitoGFP signal
C
Cell 2
08:30 min:sec
08:40 min:sec
09:00 min:sec
09:50 min:sec
10:00 min:sec
TMRE signal
mitoGFP signal

Figure 30: High frequency of depolarization events during directional migration.

(A) Composite pictures of control HUVECs mitochondria transfected with mitoGFP (red) and stained with TMRE (blue) during directional migration. Pictures were taken every 10 s over a duration of 10 min. Scale bar: 100 µm. Dashed boxes indicate area of zoom-in pictures of two chosen cells showing depolarization events at indicated timepoints. Scale bar: 50 µm, same for each image.
(B) 3D surface plots of one mitochondria population at the cell front of cell 1 (same as in (A)) for TMRE signal (blue plots) and mitoGFP signal (red plots) at indicated time points. Dashed boxes indicate mitochondria displaying depolarization events during acquisition.
(C) 3D surface plots of one mitochondria population at the cell front of cell 2 (same as in (A)) for TMRE signal (blue plots) and mitoGFP signal (red plots) at indicated time points. Dashed boxes indicate mitochondria displaying depolarization events during acquisition.

TN-treatment induced changes in the duration of depolarization events. While $\Delta\Psi$ was still dynamic and TMRE signal showed fluctuations in most cells, the signal loss indicating depolarizations was significantly longer compared to control conditions. Cells were analyzed during collective migration at the front of the cell monolayer. While some cells appeared polarized and displaced over time (**Fig. 31A**, *zoom of cell 1*), others were enlarged and showed little displacement over time (**Fig. 31A**, *zoom of cell 2*). Consequently, the depolarizations occurred in different mitochondria populations. The more motile cells showed main depolarization events in mitochondria oriented towards the direction of movement, while the more sessile cell showed strong depolarization events all over the cell (**Fig. 31A**, *comparison between cell 1 over time and cell 2 over time*).

Quantification of $\Delta\Psi$ changes over time was done as previously described through 3D surface plot visualization. While the surface plot analysis revealed similar changes in both TMRE signal and mitoGFP signal, the depolarization lasted longer in both cell types after TN-treatment. The main depolarization event of cell 1 during movement lasted roughly 06 min 50 sec (**Fig. 31B**, *time frame from 00:00 min:sec till 06:50 min:sec, top panel, area marked with dashed box for TMRE*). TMRE signal re-appeared slightly around 02:00 min:sec, but was lost again at 02:50 min:sec. In comparison, mitoGFP signal stayed consistent over time for mitochondria populations analyzed (**Fig. 31B**, *bottom panel, area marked with dashed box for mitoGFP*). It should be mentioned that depolarization events occurred mostly in the same mitochondria populations. While the main depolarization depicted through 3D surface plot reconstruction lasted longer for about 06:50 min:sec, the same mitochondria population showed another depolarization event at 09:00 min:sec (**Fig. 31A**, *zoom of cell 1 at last indicated timepoint*).

Similar observations were made for the less motile cell 2. The main depolarization event shown lasted around 02:30 min:sec with small TMRE fluctuation changes at 01:50 min:sec (**Fig. 31C**, *time frame from 00:00 min:sec till 02:30 min:sec, top panel, area marked with dashed box for TMRE*). The same mitochondria populations showed another depolarisation event at 05:10 min:sec (**Fig. 31A**, *zoom of cell 2 at last indicated timepoint*). Here, mitoGFP

signal stayed consistent over time for all mitochondria populations analyzed as well, ruling out potential changes in focus or other microscopy-related artifacts (**Fig. 31C**, *bottom panel, area marked with dashed box for mitoGFP*).

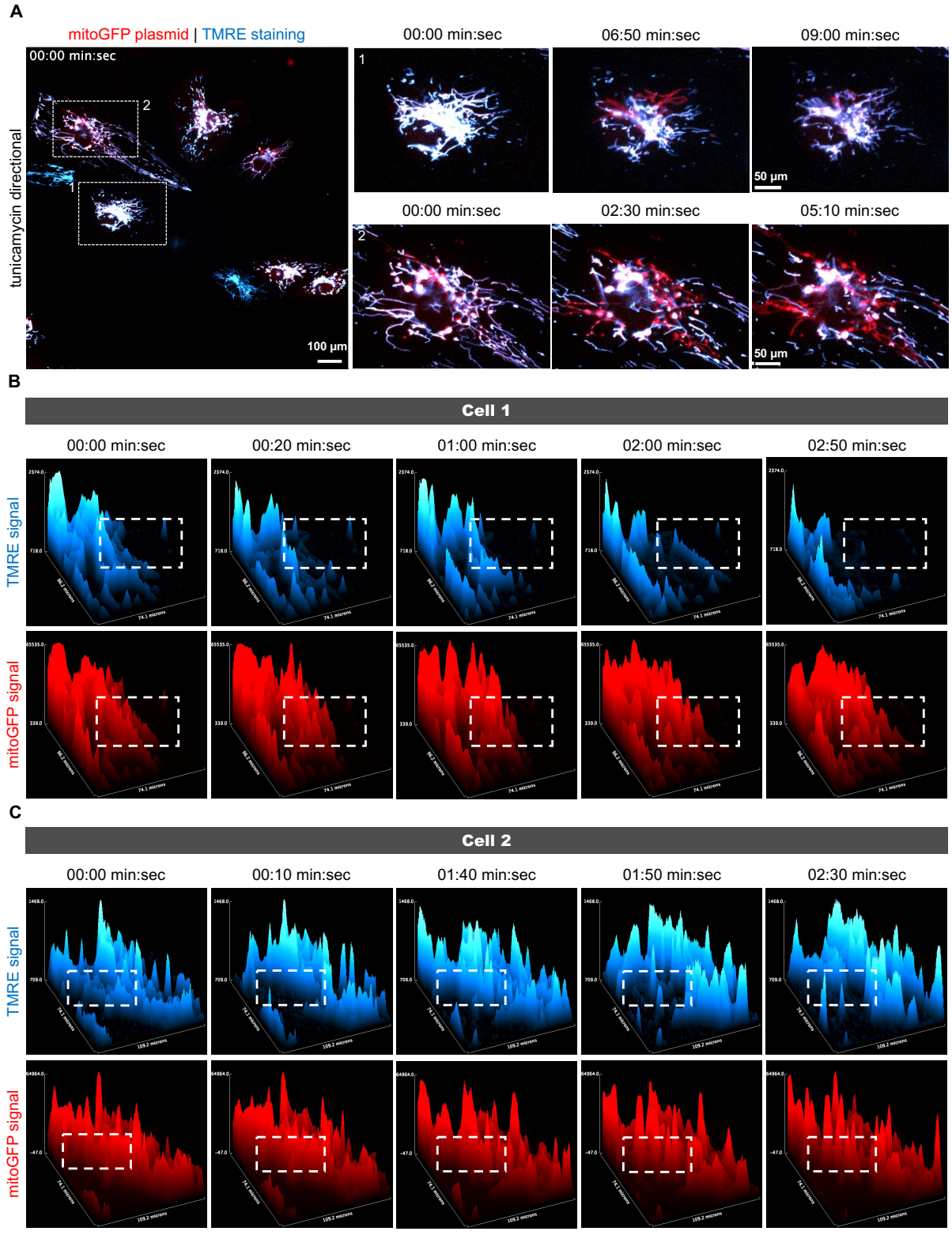

Figure 31: ER stress leads to longer depolarization events during directional migration.

A) Composite pictures of TN-treated HUVECs mitochondria transfected with mitoGFP (red) and stained with TMRE (blue) during directional migration. Pictures were taken every 10 s over a duration of 10 min. Scale bar: 100 µm. Dashed boxes indicate area of zoom-in pictures of two chosen cells showing depolarization events at indicated timepoints. Scale bar: 50 µm, same for each image.
(B) 3D surface plots of one mitochondria population at the cell front of cell 1 (same as in (A)) for TMRE signal (blue plots) and mitoGFP signal (red plots) at indicated time points. Dashed boxes indicate mitochondria displaying depolarization events during acquisition.
(C) 3D surface plots of one mitochondria population at the cell front of cell 2 (same as in (A)) for TMRE signal (blue plots) and mitoGFP signal (red plots) at indicated time points. Dashed boxes indicate mitochondria displaying depolarization events during acquisition.

PERK-inhibition led to similar depolarization patterns observed under control conditions. $\Delta\Psi$ was dynamic and stochastic depolarization events occurred in every cell. To show changes during directional migration, polarized motile cells at the front of the cell monolayer were analysed. PERK-inhibition led to polarized cell states with different cell sizes. While some cells were smaller, others were well-polarized and elongated in the direction of migration (**Fig. 32A**). As mentioned before, the main depolarization events occurred in the same mitochondria populations over time (**Fig. 32A**, *zoom of cell 1 and cell 2 during directional movement at indicated time points*).

Reconstruction of fluorescent signal changes over time through 3D surface plots showed depolarization patterns similar to those observed in control conditions, with depolarization events lasting slightly longer. The main depolarization event in cell 1 lasted around 2 min (**Fig. 32B**, *time frame from 07:30 min:sec till 10:00 min:sec, top panel, area marked with dashed box for TMRE*). Before the main depolarization event with complete TMRE signal loss, a slight reduction in $\Delta\Psi$ occurred around 07:00 min:sec, with re-establishment of $\Delta\Psi$ at 07:30 min:sec (**Fig. 32B**, *top panel, area marked with dashed box for TMRE*). MitoGFP signal stayed consistent over the indicated timepoints (**Fig. 32B**, *bottom panel, area marked with dashed box for mitoGFP*).

Cell 2 showed similar depolarization patterns with the main depolarization of $\Delta\Psi$ lasting around 1 min (**Fig. 32C**, *depolarization shown from 09:40 min:sec till 10:00 min:sec, top panel, area marked with dashed box for TMRE*). Again, a slight reduction in $\Delta\Psi$ occurred before the complete signal loss at 07:20 min:sec and TMRE signal was not completely re-established to the one observed before the slight reduction (**Fig. 32C**, *top panel, comparison between 07:10 min:sec and 08:30 min:sec*). MitoGFP signal showed no significant changes over time, proving that the observed changes in TMRE signal are $\Delta\Psi$-dependent and results of depolarization events happening over time (**Fig. 32C**, *bottom panel, area marked with dashed box for mitoGFP*).

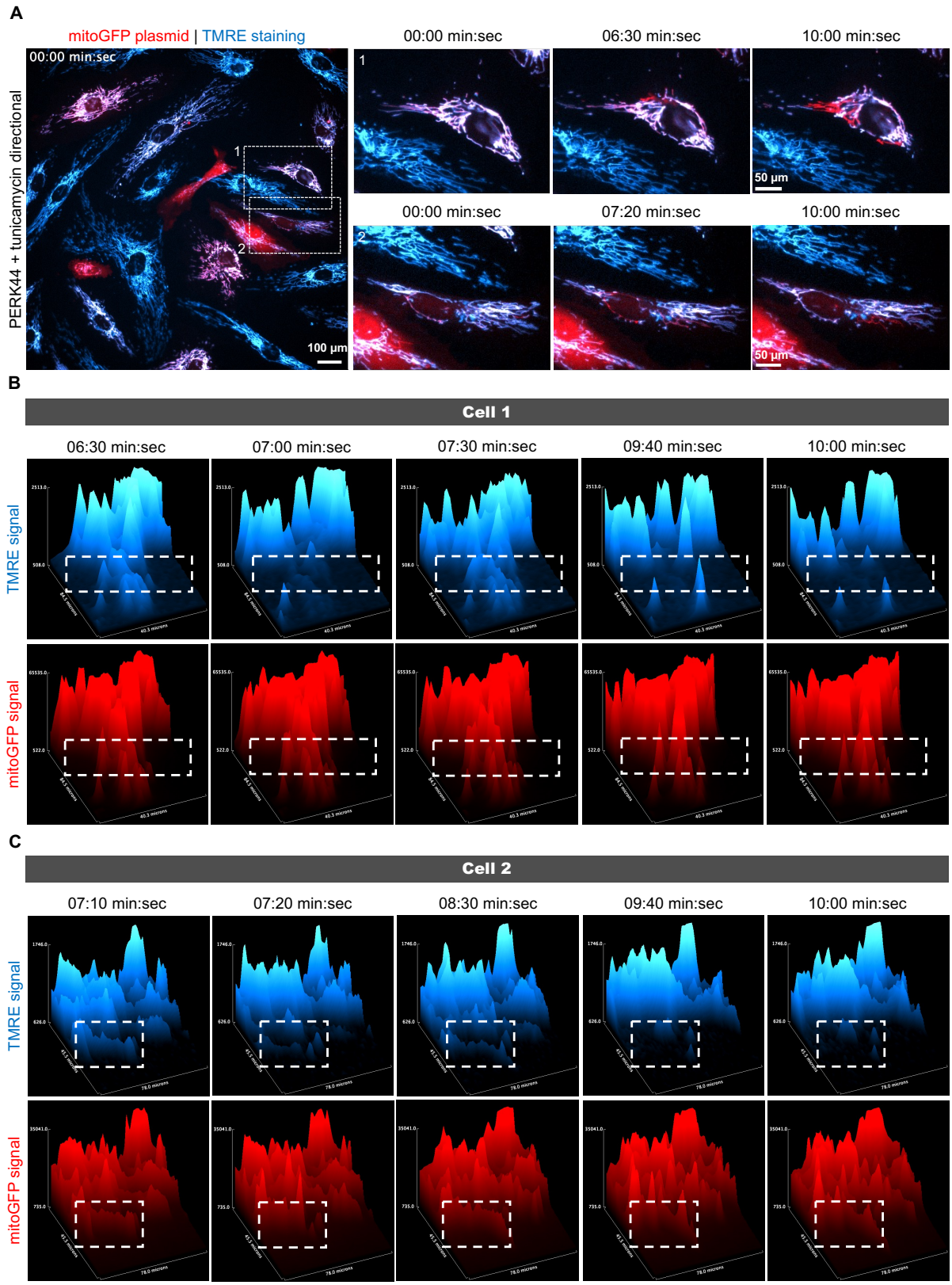
A
mitoGFP plasmid | TMRE staining
00:00 min:sec
06:30 min:sec
10:00 min:sec
PERK44 + tunicamycin directional
00:00 min:sec
100 µm
1
2
50 µm
00:00 min:sec
07:20 min:sec
10:00 min:sec
50 µm
B
Cell 1
06:30 min:sec
07:00 min:sec
07:30 min:sec
09:40 min:sec
10:00 min:sec
TMRE signal
mitoGFP signal
C
Cell 2
07:10 min:sec
07:20 min:sec
08:30 min:sec
09:40 min:sec
10:00 min:sec
TMRE signal
mitoGFP signal

Figure 32: PERK-inhibition prevents prolonged duration of depolarization events during directional migration.

A) Composite pictures of PERK 44 + TN-treated HUVECs mitochondria transfected with mitoGFP (red) and stained with TMRE (blue) during directional migration. Pictures were taken every 10 s over a duration of 10 min. Scale bar: 100 µm. Dashed boxes indicate area of zoom-in pictures of two chosen cells showing depolarization events at indicated timepoints. Scale bar: 50 µm, same for each image.
(B) 3D surface plots of one mitochondria population at the cell front of cell 1 (same as in (A)) for TMRE signal (blue plots) and mitoGFP signal (red plots) at indicated time points. Dashed boxes indicate mitochondria displaying depolarization events during acquisition.
(C) 3D surface plots of one mitochondria population at the cell front of cell 2 (same as in (A)) for TMRE signal (blue plots) and mitoGFP signal (red plots) at indicated time points. Dashed boxes indicate mitochondria displaying depolarization events during acquisition.

To summarize the observations made for depolarisation events during directional migration, a time frame of 3 min was chosen to compare the depolarisation durations in the different conditions (**Fig. 33A**). The main depolarisation event under control conditions lasted around 1 min 50 sec, with repolarisation occurring shortly after (**Fig. 33A**, *top panel*). In comparison, the depolarisation under TN-induced ER stress lasted significantly longer with 6 min 50 sec (see **Fig. 31B**) and no repolarisation could be observed during the 3 min time frame (**Fig. 33A**, *middle panel*). PERK inhibition prevented the increase in depolarisation duration with the main depolarisation lasting around 2 min (**Fig. 32B**), but repolarisations occurring in between (**Fig. 33A**, *bottom panel*).

To examine possible ion channel candidates that could play a role in the observed ER-mitochondria dynamics and the changes in $\Delta\Psi$ under ER stress conditions, a new pipeline for protein interaction inside tissues, termed multiplexing, was developed (method described in: (Kuehl et al. 2025). Standard pipelines use acquisition of cells or tissues incubated with antibodies of interest, then thresholding and segmentation of the acquired images to show interactions between proteins of interest. The new pipeline uses dimensionality reduction to blur the acquired images. This reduction allows for recognition of broader clusters or patterns of proteins. Applying this new pipeline to healthy tissue and tissues associated with ER stress conditions, a relevant cluster was found linking transient receptor potential channel type 6 (TRPC6) signalling to mitochondrial and ER stress, and further to changes in cell migration (**Fig. 33B**). Because TRPC6 was found as a key link between mitochondria stress and ER stress, HUVECs were stained with a TRPC6 antibody which has been previously validated (Kuehl et al. 2025). TRPC6 is mainly responsible for regulating calcium influx into the cytoplasm (M. Wang et al. 2024). Surprisingly, TRPC6 was not only found at the plasma membrane, but also in some places co-localizing with mitochondria (**Fig. 33C**).

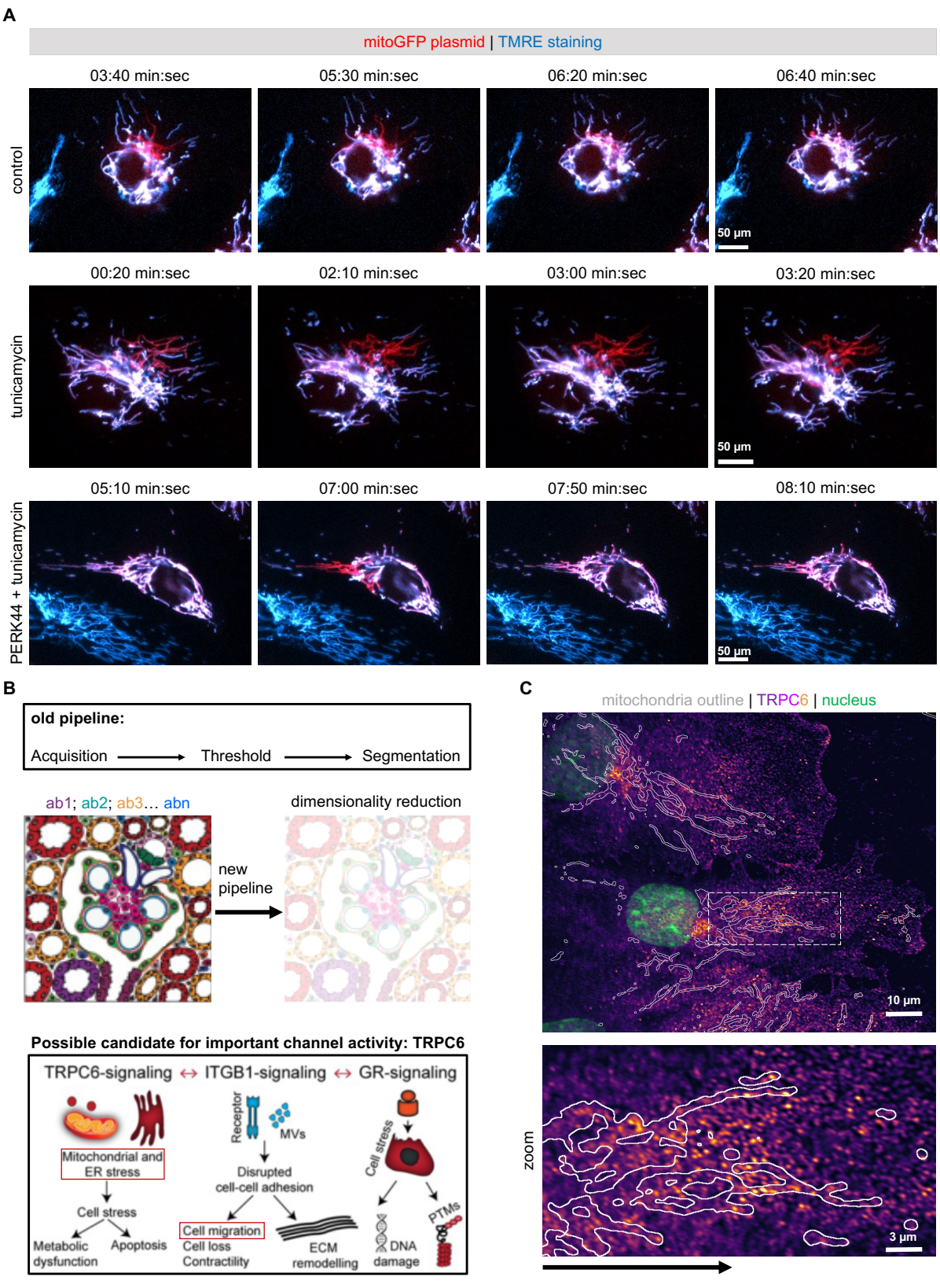
A
mitoGFP plasmid | TMRE staining
03:40 min:sec
05:30 min:sec
06:20 min:sec
06:40 min:sec
control
50 µm
00:20 min:sec
02:10 min:sec
03:00 min:sec
03:20 min:sec
tunicamycin
50 µm
05:10 min:sec
07:00 min:sec
07:50 min:sec
08:10 min:sec
PERK44 + tunicamycin
50 µm
B
old pipeline:
Acquisition
Threshold
Segmentation
ab1; ab2; ab3… abn
dimensionality reduction
new pipeline
Possible candidate for important channel activity: TRPC6
TRPC6-signaling ↔ ITGB1-signaling ↔ GR-signaling
Mitochondrial and ER stress
Cell stress
Metabolic dysfunction
Apoptosis
Receptor
MVs
Disrupted cell-cell adhesion
Cell migration
Cell loss
Contractility
ECM remodelling
Cell stress
DNA damage
PTMs
C
mitochondria outline | TRPC6 | nucleus
10 µm
zoom
3 µm

Figure 33: TRPC6 as a possible candidate linking mitochondria function to ER stress.

(A) Representative composite pictures of depolarization events in control cells (top panel), TN-treated cells (middle panel) and PERK44 + TN-treated cells (bottom panel). Cells were transfected with mitoGFP (red) and stained with TMRE (blue). Depolarisation events are shown over a duration of 3 min at indicated timepoints. Scale bar: 50 µm, same for each image per condition.
(B) Old pipeline to reveal protein interactions: Image acquisition, image thresholding and image segmentation. New multiplexing pipeline uses dimensionality reduction to recognize broader clusters or patterns of protein interaction. Multiplexing revealed a cluster linking TRPC6 signalling to mitochondrial and ER stress and further to disruptions in cell migration (red boxes).
(C) Representative confocal pictures of control cells migrating towards the right. Cells were stained for mitochondria (outline shown in white), TRPC6 (LUT fire), and nucleus (green). Scale bar: 10 µm. Dashed box indicates area of zoom-in below showing TRPC6 signal co-localizing with mitochondria. Scale bar: 3 µm. Black arrow indicates the direction of migration.

To test whether inhibition of TRPC6 could rescue the migratory defect found in ER stress conditions, HUVECs were pre-treated with two different inhibitors of TRPC6, GsMTx4 (a broad blocker of ion channels like Piezo and TRPC6) and BI-749327 (a highly selective blocker of TRPC6). Pre-treatment with both TRPC6 blockers was not able to fully prevent the reduction in motility induced by TN-treatment (**Fig. 34A**), but several interesting observations were made. Broad blocker GsMTx4 prevented the effect of TN under random, but not directional migration (**Fig. 34B**, *green plots in yellow and violet area*). These data suggest that the ion channels involved in random migration are different from those required for directional migration. To test the specific contribution of TRPC6, different concentrations of BI-749327 were tested. Interestingly, the effects of TRPC6 inhibition were different under random and directional migration conditions. While TN-treatment led to reduced speed of randomly migrating cells (**Fig. 34B**, *yellow area, violet plot*), treatment with 1 µM BI-749327 and 10 µM BI-749327 led to random migration speeds similar to those observed under control conditions (**Fig. 34B**, *yellow area, blue plots*). This effect, however, was lost during directional migration. Neither pre-treatment with 10 µM nor 5 µM and 1 µM BI-749327 was successful in preventing the loss of migration speed observed during ER stress conditions (**Fig. 34B**, *light violet area, blue plots*).

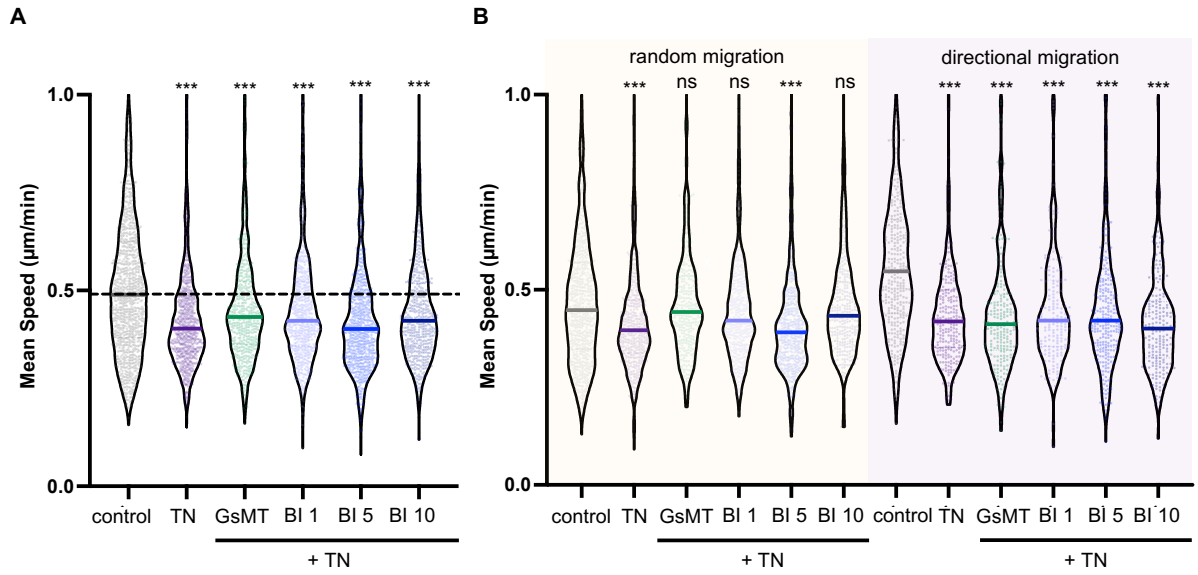

Figure 34: Inhibition of TRPC6 does not prevent the migratory effects observed under ER stress conditions.

(A) Graph shows the instantaneous mean speed of collectively migrating HUVECs in µm/min for control conditions (grey), TN-treatment (purple), GsMTx4 + TN-treatment (green), and 1 µM, 5 µM and 10 µM BI-749327 + TN-treatment (different shades of blue) as truncated violin plots. The dark lines indicate the median of each condition, the dotted line corresponds to the median of the control ***P < 0.001, Kruskal Wallis test. n > 500 cells each for overall motility.
(B) Graph shows the instantaneous mean speed of collectively migrating HUVECs in µm/min for control conditions (grey), TN-treatment (purple), GsMTx4 + TN-treatment (green), and 1 µM, 5 µM and 10 µM BI-749327 + TN-treatment (different shades of blue) for random migration (yellow) and directional migration (light purple) as truncated violin plots. The dark lines indicate the median of each condition. ***P < 0.001, Kruskal Wallis test, ns = not significant. n > 500 cells each for the two motility modes.

The expression of TRPC6 in HUVECs is unclear as its functional expression has been shown (Ge et al. 2009; Weber et al. 2015), whereas in other conditions its expression has not been detected (Bruneel et al. 2003).

Since the previous observations showed that the reduction in migration related to ER stress does not depend on TRPC6, the function of other key mitochondrial ion channels was explored. Voltage-dependent anion channel 1 (VDAC1) is present in the outer membrane of mitochondria, plays a role in the flux of metabolites regulating OXPHOS as well as in regulating Ca^{2+} uptake and ROS release (Shoshan-Barmatz, Maldonado, and Krelin 2017). Its presence in HUVECs (Groten et al. 2024) and its important role in mitochondrial health makes him an interesting candidate to study for its impact on collective mesenchymal cell migration. VBIT-12 was used as a selective oligomerization inhibitor for VDAC1 to test whether pre-treatment with VBIT-12 would have protective effects for ER stress induction.

Pre-treatment with VBIT-12 at different concentrations – 10 µM, 20 µM and 50 µM – had no significant protective effects against the reduction in motility induced by ER stress. Independent of the concentration used, inhibition of VDAC1 oligomerization was not successful in preventing the reduction in speed of collective mesenchymal migration after TN-

treatment (**Fig. 35A**, *pink plots*). Of note, VDAC1 function inhibition significantly reduced speed during collective mesenchymal migration (**Fig. 35A**, *red plot*). Distinguishing between random and directional migration showed no differences compared to overall motility. Cells migrating randomly as well as directionally showed no rescue effect of VDAC1 function inhibition during ER stress conditions. In both migratory populations, inhibition of VDAC1 led to a significant decrease in speed as well (**Fig. 35B**, *yellow and light violet areas*). These observations suggest that VDAC1 is required for the spontaneous migration of HUVECs, without playing a significant role during ER stress.

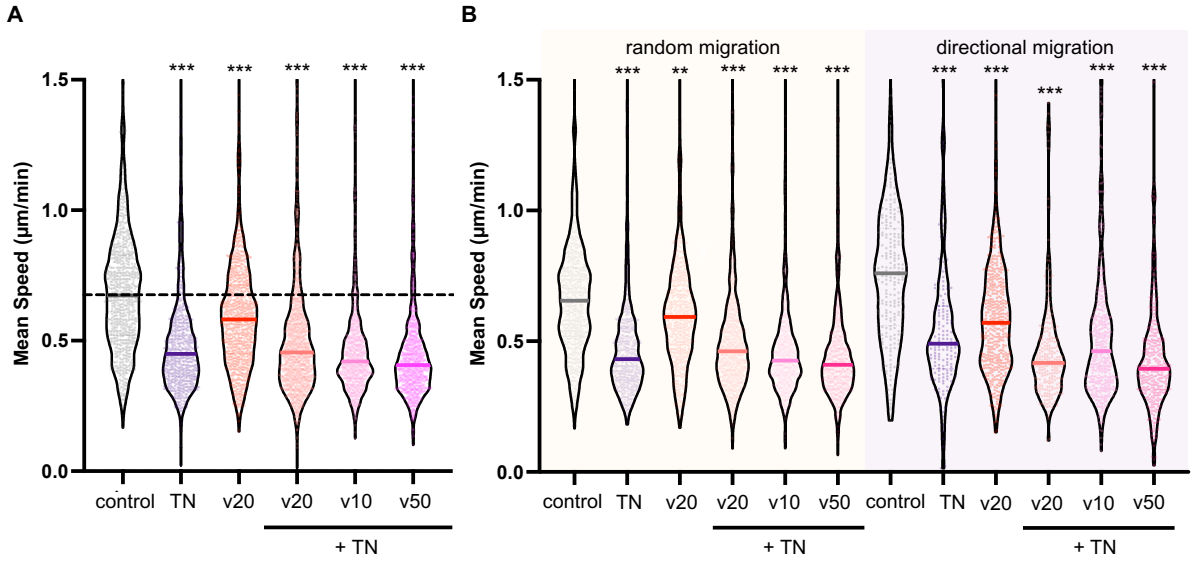

Figure 35: VDAC1 functions as a key regulator of collective migration in resting conditions.

(A) Graph shows the instantaneous mean speed of collectively migrating HUVECs in µm/min for control conditions (grey), TN-treatment (purple), VBIT-12 (red), and 20 µM, 10 µM and 50 µM VBIT-12 + TN-treatment (different shades of pink) as truncated violin plots. The dark lines indicate the median of each condition, the dotted line corresponds to the median of the control ***P < 0.001, Kruskal Wallis test. n > 500 cells each for overall motility.
(B) Graph shows the instantaneous mean speed of collectively migrating HUVECs in µm/min for control conditions (grey), TN-treatment (purple), VBIT-12 (red), and 20 µM, 10 µM and 50 µM VBIT-12 + TN-treatment (different shades of pink) for random migration (yellow) and directional migration (light purple) as truncated violin plots. The dark lines indicate the median of each condition. ***P < 0.001, **P < 0.01, Kruskal Wallis test. n > 500 cells each for the two motility modes.

To summarize, induction of ER stress leads to extreme changes in overall cell shape and intracellular distributions of organelles. These changes result in migratory defects with cells losing their capacity to properly polarize and migrate in a directional manner. The strong association between the ER and mitochondria makes mitochondria an important organelle to study for their contribution to the observed effects that happen under ER stress. Because mitochondria are the main organelles providing energy, and this energy productions depends strongly on $\Delta\Psi$, the connection between mitochondria metabolism and ER signalling needs to be further investigated in HUVECs, as inhibition of some of the relevant ion channels was unable to rescue the effect of induced ER stress on the collective migration of endothelial cells. This suggests that a cryptic protein controls both mitochondria membrane potential and directional migration.

Discussion

Endothelial dysfunction is a characteristic of different diseases, ranging from obesity and diabetes to atherosclerosis and insulin resistance (Rajendran et al. 2013). It has been shown that many of these diseases show a disproportionate activation of the ER stress triggered UPR which further contributes to endothelial dysfunction (Cimellaro et al. 2016). This endothelial dysfunction corresponds to vascular dysfunction and distorted angiogenesis (Sáez et al. 2014). As endothelial cells have to migrate during angiogenesis (Auerbach et al. 2003), this thesis aimed at determining the role of ER stress on endothelial migration. To monitor endothelial migration, HUVECs were observed during single and collective migration in different microenvironments. During collective mesenchymal migration in 2D, two distinct migratory phenotypes were observed under control conditions: directionally migrating cells close to the wounded area, and randomly migrating cells behind. These migratory behaviours correspond to the leader-follower model where leader cells occupy the leading edge and determine the speed and direction of collective migration. Follower cells comprise the majority of the moving group and show different FA and adherent protein distributions (Qin et al. 2021; Haeger et al. 2015; Mayor and Etienne-Manneville 2016).

Using TN to mimic maternal obesity-induced ER stress *in vitro*, it was shown that ER stress induction led to a significant decrease in speed during single and collective mesenchymal cell migration in 2D. Further, cells under ER stress were unable to migrate directionally and showed no acceleration capacity compared to control conditions. During single migration in a 1D microenvironment ER stress induction led to lower directional persistence and, compared to control cells in 1D, TN-treated cells showed more sessile phases. One of the main functions of endothelial cells is angiogenesis, the formation of new vessels from pre-existing ones (Auerbach et al. 2003). To corroborate whether findings in 1D and 2D microenvironments could be extended to a 3D microenvironment, tubule formation under control and ER stress conditions inside a Matrigel was visualized to test whether ER stress also affects endothelial cell migration in 3D. Interestingly, TN-induced ER stress did not prevent the initial formation of 3D structures (tube formation). However, while control cells were still organized in tubes 72 h later (**Fig. 36**, *top panel*), neither TN-treated cells nor PERK44 pre-treated cells were able to keep the tube organization, showing clusters of rounded cells (**Fig. 36**, *middle and bottom panel*). Compared to treatment with 50 µM FCCP in which cells completely failed to form any type of collective structure (**Supplementary Fig. 5**), cells under ER stress were able to line up inside the Matrigel and form polygonal tube structures, showing that VEGF-A signalling was still intact under ER stress. The inability to maintain the tube formation suggests perturbation in the cell-cell adhesions which are mediated through cellular junctions mainly

composed of vascular endothelial cadherin (VE-cadherin)-based adherens junctions, and tight junctions (primarily through the proteins claudins and occludins) (Schimmel and Gordon 2018). VE-cadherin is found in the junctions between ECs and it is crucial in maintaining vascular integrity and regulating endothelial permeability (Nan et al. 2023). These findings are in line with previous research showing that ER stress in human retinal endothelial cells led to increased addition of N-acetyl-glucosamine acylation to serine/threonine residues of VE-cadherin affected barrier integrity (Lenin et al. 2019).

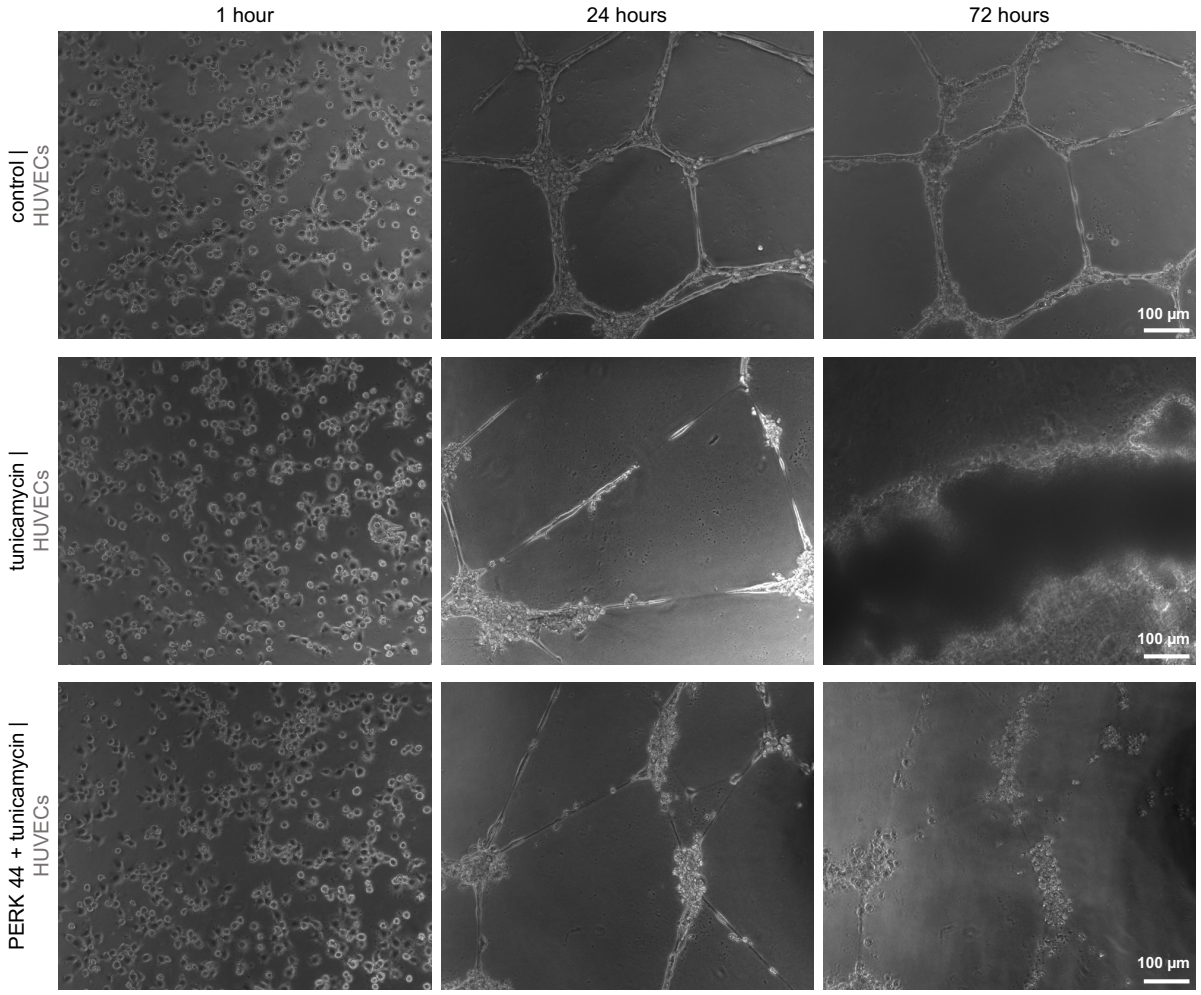

Figure 36: ER stress impacts stability of three-dimensional tube formation.

Representative pictures of control cells (top panel), TN-treated cells (middle panel) and PERK44 + TN-treated cells (bottom panel) during tube formation [angiogenesis assay] at indicated timepoints. Cells were plated inside a Matrigel with media containing VEGF-A, and tube formation was observed by taking pictures every 20 min. Scale bar: 100 µm, same for every image per condition.

ER stress affected endothelial cell behaviour across different migratory strategies (single vs. collective) in every dimension. Distorted collective migration in 2D was exclusively dependent on PERK-signalling as inhibition of PERK prevented the decrease in speed and directionality. After activation of PERK upon ER stress induction, PERK phosphorylates eIF2α leading to the attenuation of global translation which reduces the folding demand on the ER. Phosphorylated eIF2α also leads to the translation of ATF4. ATF4 as a transcription factor induces the expression of genes involved in protein folding, amino-acid metabolism, the antioxidant response, autophagy and apoptosis. Under prolonged ER stress, the PERK-eIF2α pathway activates ATF4/CHOP expression and induces apoptosis of the cell (Limia et al. 2019). Inhibition of PERK with PERK44 showed positive effects in HUVECs during collective mesenchymal migration. In contrast, inhibiting ATF6 or IREα with Ceapin A7 or AMG 18 hydrochloride, respectively, negatively impacted collective migration showing an even further decrease in speed after ER stress reduction. These findings suggest that ATF6 and IRE1α signalling are required in HUVECs for collective migration whereas PERK signalling negatively impacts migration in terms of speed and directionality after ER stress induction.

Intracellular analysis of cells during collective migration revealed that all cytoskeletal components, in particular the actin cytoskeleton and FAs, showed strong misalignments to the migratory axis. F-actin fibers on the ventral and dorsal plane were orientated perpendicular to the migratory axis. The distortion in actin cytoskeleton and FA dynamics led to non-productive membrane dynamics in TN-treated HUVECs. Interestingly, cells under ER stress showed more dynamic protrusions and a constant turnover of the membrane (membrane “ruffles”), yet the cells did not move forward and seemed stuck in place for longer time periods (a similar phenotype to the one observed during single migration on 1D micropatterned lines). As TN-treatment reduced the number of FA spots at the leading edge, it can be hypothesized that the membrane at the front is less anchored to the ECM explaining the observed increase in membrane dynamics. Further, missing adhesions at the front prevent the capacity of the cell to generate traction forces and move forward. The central transducer of forces that controls FA assembly and disassembly is FAK (Hu et al. 2014). FAK regulates important mechanosignalling pathways like RhoA and ROCK, but also mechanosensitive ion channel components (e.g. Piezo1). Recently, the mechanism by which force generation at FAs increases FAK phosphorylation and therefore activity was revealed (Fernández-Yagüe et al. 2025). FAK activity showed a highly polarized pattern where high traction forces generated by growing FAs at the leading edge precede FAK activity. In summary, traction forces and higher FAK activity is found at the leading edge, while smaller FAs at the rear exhibit reduced traction forces and less FAK activity (Fernández-Yagüe et al. 2025).

It can be suggested that ER stress induction affects the speed of migration through a combination of misaligned F-actin fibers, decreased FA size and therefore likely less FAK activity at the front. Since actin retrograde flow is also required for efficient migration (Hohmann and Dehghani 2019), aligned F-actin fibers and FAs at the front provide the necessary protrusion forces for efficient migration under control conditions. The misaligned F-actin fibers could slow down the actin retrograde flow and in combination with smaller FAs and less traction force prevent successful movement forwards.

PERK inhibition prevented this misalignment, suggesting that PERK signalling directly affects cytoskeletal dynamics. Previous studies support this notion as PERK was shown to directly interact with the actin regulator filamin A in other cellular models. Filamin A interacts with the F-actin cytoskeleton, forming crosslinked, orthogonal networks (van Vliet and Agostinis 2017). Filamins are known regulators of plasma membrane-localized Ca^{2+} receptors and connect the ER to the actin cytoskeleton. In HEK293T cells, PERK deficiency led to a peripheral and strong cortical distribution of F-actin, suggesting that PERK signalling influences actin polymerization and polarization through filamin A. F-actin deposition directly underneath the plasma membrane was found in PERK-lacking cells, which led to a significant reduction in ER-plasma membrane contacts. Interestingly, this study found an unprecedented role of PERK in the regulation of the actin cytoskeleton and ER-plasma membrane signalling (van Vliet et al. 2017). While this would suggest that PERK inhibition further disturbs the actin cytoskeleton organization, it should be mentioned that the interaction of PERK and filamin A in this study was proven in an UPR-independent context. It should therefore be evaluated, if the same signalling pathways occur during ER stress conditions and whether PERK inhibition would result in a decrease in ER-plasma membrane contacts in HUVECs during collective migration as well. ER-plasma membrane contacts have already been proven to play a role during persistent directional migration. The contact gradient was shown to be proportionate to the migration speed, with contacts predominantly found at the leading edge. Loss of the contact gradient played an inhibitory role in cell migration (Gong et al. 2024). Taken together, these findings suggest that ER stress induction leads to a decrease in ER association to the plasma membrane.

A compelling new study revealed different ER-cytoskeleton dynamics depending on the edge curvature of the surrounding cell monolayer. While lamellipodia crawling is found at convex edges, string-like movements occur at concave edges. During lamellipodia crawling, epithelial cells display branched actin polymerization and FAs that are oriented perpendicularly. String-like movements happen through actin bundle formation and parallely oriented FAs. Upon inspection of the organelle response to the large-scale geometrical cue, the authors found that especially the ER showed a significant change in morphology with ER tubule formation

observed at convex edges and ER sheet-like morphology found at concave edges which proves a clear curvature-dependent structural organization of the ER (Rawal et al. 2025). While this data was obtained in epithelial cells without the context of ER stress induction, it suggests an interesting correlation between the intracellular organization and the morphology of the cell monolayer. It should be considered that while ER stress induces morphological changes in cytoskeleton distribution and organelle organization, the large-scale geometrical cues might play into the misalignments observed during collective migration under ER stress. In addition, this organization can emerge from single cell signalling dependent on the ER, e.g. the ER frequently reaches the plasma membrane at the cell front of leader cells. This could lead to local and global Ca^{2+} signalling, as recently shown (Benedetti et al. 2025), which is known to control cytoskeleton and membrane dynamics providing an alternative mechanism for this response.

In this thesis, PERK-dependent ER stress was shown to impact cytoskeletal dynamics. The misalignments of the F-actin cytoskeleton together with a change in FA dynamics led to changes in migratory speed, while the disturbed orientation of microtubules impacted cell polarity and directionality of cell migration. Microtubule organization is essential for proper intracellular organelle distribution and polarized trafficking to the cell front and cell rear (Wehrle-Haller and Imhof 2003). Microtubules directly interact with organelles like the ER and mitochondria (Tikhomirova et al. 2022). ER stress induction distorted microtubule organization and consequently organelle distribution inside the cell. Though ER morphology did not change significantly, with ER sheet and ER tubules still being distinguishable, ER alignment mirrored the misalignment already described for the cytoskeleton: ER tubules were oriented perpendicular to the migratory axis, a distortion that could be prevented through PERK inhibition. Previous studies support the connection between ER and microtubule organization showing PERK as direct regulator of ER distribution. Using different epithelial cells (MCF10A, HeLa and MDA-MB231), the study reported that PERK depletion resulted in an impairment of ER subcellular distribution upon TN-treatment. As several ER membrane proteins engage with microtubules, e.g. ribosome-binding protein 1 (RRBP1) and Climp63, the interaction between ER and microtubules was shown. The authors found that ER-microtubule anchoring occurs through RRBP1/p180-αtubulin interaction. This interaction is decreased upon TN-treated ER stress induction and increased after PERK knockdown in epithelial cells (Sánchez-Álvarez et al. 2025). While the same impaired ER subcellular distribution could not be observed in HUVECs during directional migration, the connection between ER and microtubules should be considered for further evaluation. This thesis clearly showed that the misalignment observed for ER tubules was also found in microtubule distribution. The anchoring between

ER and microtubules indicates a coordinated phenotype with microtubule organization influencing ER distribution and vice versa.

Mitochondria showed the same perpendicular orientation which is consequent with the ER and microtubule misalignments. The interest in the mechanisms that regulate mitochondria dynamics under ER stress has grown in recent years. It was shown that the PERK arm of the UPR was responsible for the adaptive remodelling of phosphatidic acid in the OMM which results in protective mitochondria elongation upon acute ER stress. This elongation aims at reducing premature mitochondria fragmentation and keeps mitochondrial respiratory chain activity intact (Perea et al. 2023). A previous study found a similar phenotype of ER stress-induced mitochondrial hyperfusion being dependent on PERK signalling. Here, pharmacological or genetic inhibition of PERK leads to increased mitochondria fragmentation and impaired mitochondria activity (Lebeau et al. 2018). Both of these studies reported PERK-dependent changes in mitochondria morphology in HeLa cells upon ER stress reduction. While the phenotype of hyperfused mitochondria could be suggested in HUVECs after TN-treatment, blockade of PERK activation was insufficient to prevent this response, suggesting that other signalling pathways activated by ER stress are required for mitochondria fusion.

As ER and mitochondria are closely associated and form direct contacts (MERCs), the question arises how ER stress influences the signalling between these organelles. ER and mitochondria are known to interact. Both use microtubules for transport (Tikhomirova et al. 2022), so changes in microtubule organization and ER distribution strongly suggest that the interaction patterns of MERCs are also changed under the ER stress phenotype. The data obtained in this thesis proves that ER stress leads to a decrease in the number of MERCs. Ultrastructural analysis of MERCs also indicates that the distance between ER and mitochondria is increased upon ER stress induction with TN-treatment. Previous studies already investigated the relationship between MERCs under different conditions. MERCs play an important role in different cellular processes like Ca^{2+} transfer, lipid metabolism, mitochondrial dynamics and cell death through apoptosis and autophagy (C. Chen et al. 2025). One study found that ER stress promoted the Ca^{2+} transfer from the ER to mitochondria which led to Ca^{2+} overload, decreased mitochondria membrane potential, increased mitochondrial fission and mitophagy. Further, depolarisation is known to fragment mitochondria, leading to smaller mitochondria. Damaged or dysfunctional mitochondria undergo increased fragmentation from the healthy mitochondrial network to keep mitochondria homeostasis intact (C. Li et al. 2022). These findings are in line with the results of this thesis and offer a potential explanation for the changes in $\Delta\Psi$ observed during ER stress. TN-treatment led to an increased duration of depolarization events during directional migration. The observed

mitochondrial “flickers” were reduced upon ER stress induction as repolarisation events occurred less frequently compared to control conditions. Even though PLA and ultrastructural analysis suggest less contact between ER and mitochondria, the increased Ca^{2+} leak though remaining contacts could be responsible for the longer depolarizations observed. Another study further reported that the distance between ER and mitochondria is a critical parameter for optimal Ca^{2+} transfer efficiency. The Ca^{2+} transfer occurs through ER-located inositol-1,4,5-trisphosphate receptors (IP_3Rs) on the ER membrane and VDAC1 on the OMM. Interestingly, the study revealed that there is an optimal distance for high efficient Ca^{2+} transfer of 20 nm. A distance of 10 nm still allowed Ca^{2+} transfer, but it was significantly less efficient (Dematteis et al. 2024). To put these findings in the context of the observed MERC dynamics upon ER stress induction, it could be hypothesized that the increase in MERC distance after TN-treatment observed in ultrastructural analysis leads to more “efficient” Ca^{2+} leak from ER to mitochondria even if the number of MERCs is reduced. Taking Ca^{2+} signalling into consideration, it should be mentioned that while the ER stress in this thesis was induced through TN-treatment which directly affects protein binding, changes in the Ca^{2+} homeostasis of the ER are also a known inducer of ER stress. As the ER is the main intracellular store for Ca^{2+}, consequently even moderate changes in Ca^{2+} concentration have been shown as ER stress inducers. Inhibitors like thapsigargin act on the sarcoplasmic/endoplasmic reticulum Ca^{2+}-ATPase (SERCA) pump and prevent Ca^{2+} uptake from the cytosol into the ER therefore depleting the ER’s luminal Ca^{2+} concentration (Abdullahi et al. 2017). IRE1α and PERK sense these changes in luminal Ca^{2+} and initiate the UPR. While IRE1α reacts more rapidly than PERK, it is feasible that the observed dynamics in MERCs upon TN-treatment might ultimately affect the ER luminal Ca^{2+} concentration leading to a positive feedback loop and continuous ER stress induction over time.

As key ion channels like TRPC6 (predominantly found in the plasma membrane) and VDAC1 are known players in the intracellular Ca^{2+} signalling, their contribution to the observed migratory changes was determined. Neither inhibition of TRPC6 nor VDAC1 was successful in preventing the decrease in speed and directionality upon ER stress induction. However, it was found that inhibition of VDAC1 in absence of ER stress led to a significant decrease in speed during collective mesenchymal cell migration. This suggests that VDAC1 activity is required for directional migration under resting conditions. Consequently, inhibition of VDAC1 could not restore the reduced migration during ER stress, as both individually negatively impact collective migration. Using both a broad blocker of Piezo and TRPC6 and a selective blocker for TRPC6 showed that while neither were effective in preventing the reduction in directional migration after TN-treatment, they effectively prevented the decrease in speed

during random migration. This suggests the contribution of TRPC6 during random migration, proposing that the role of these channels is more prominent in follower cells than in leader cells. However, how these and other channels differentially regulate the behaviour of leader and follower cells during directional and random migration, respectively, should be further explored.

When evaluating mitochondria function, it is important to mention the contributions of organelle pH. In mitochondria, the transmembrane pH gradient is used together with the electrical gradient ($\Delta\Psi$) to generate ATP through OXPHOS. Until very recently, pH within a single organelle was assumed to be uniform. Using a new pH-sensitive reporter called SeRapHin and targeting it to mitochondria made it possible to map the pH in single mitochondria. Preliminary experiments with this reporter obtained during the internship at the laboratory of Yamuna Krishnan (University of Chicago) showed that SeRapHin can be targeted to mitochondria and allows long-term pH mapping (**Fig. 37A**). To calibrate SeRapHin and avoid interference of the probe with autofluorescence, it was targeted to the cell surface where it showed different fluorescent properties depending on the extracellular pH (**Fig. 37B**). The detailed method to analyze the fluorescent ratios obtained during pH mapping is described in this recently published study (Lee et al. 2025). Importantly, this study revealed that single mitochondria do not harbour a uniform pH, but rather display up to 4-fold variation in pH spanning from pH 7.8-8.4 (Lee et al. 2025). These pH variations are in line with previous report proving that individual cristae in the same mitochondria harbour different $\Delta\Psi$ and act functionally independent from each other (Wolf et al. 2019). Overall, these findings suggest that more than the contribution of single distinct proteins, the observed changes in directional migration upon ER stress induction might emerge from a combination of spatially distributed changes in pH and $\Delta\Psi$ that lead to alternate mitochondria functions compared to the ones observed under control conditions. The latter means that several ion channels, transporters and enzymes could contribute to this response, and therefore the blockade or perturbations in the expression of single proteins might mask their contribution by the functional compensation of other clusters of proteins.

Recently, the concept of mechano-metabolism has been used to define the relation between the mechanical sensing of the microenvironment (mechanobiology) and its coupling to the energetic state of the cell or metabolism (Dupont 2025).The data obtained during this thesis suggest that the mechano-metabolic profile of migrating cells is changed during ER stress, which leads to changes in mitochondrial structure and function downstream of the UPR. One of the key enzymes that control the mechano-metabolism signalling required for cell migration is AMP-activated protein kinase (AMPK), as shown recently (Crosas-Molist et al. 2023;

reviewed in: Fabiano, Poole, and Reinhart-King 2025). Interestingly, AMPK activation is, in general, associated with prevention or alleviation of ER stress (Dong et al. 2010). Therefore, it would be interesting to test whether more than specific mitochondrial ion channels, the activation of this pathway could restore the migratory capacity of HUVECs.

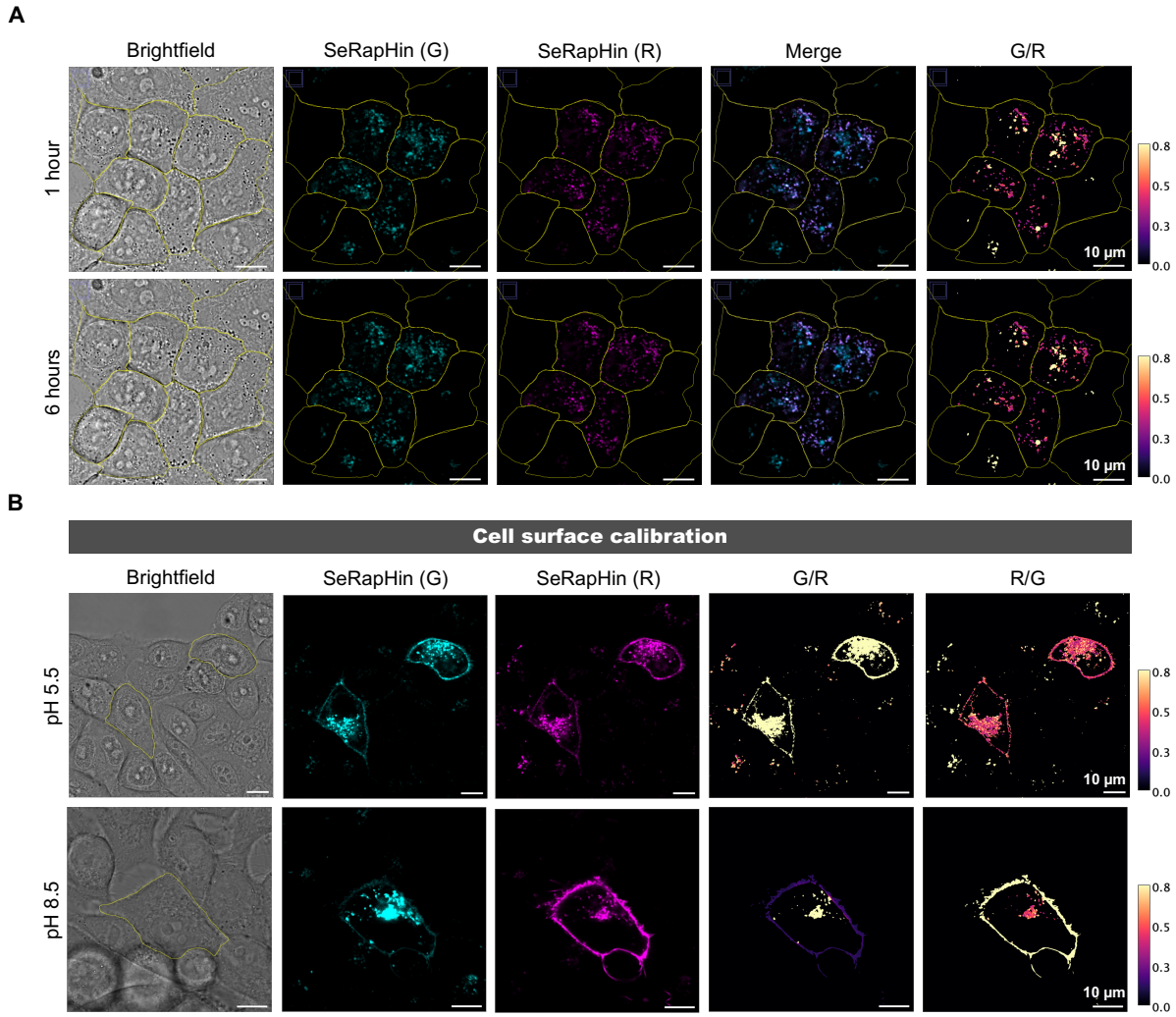

Figure 37: SeRapHin maps intracellular pH changes.

(A) Representative pictures of control HeLa cells 1 hour (top panel) and 6 hours (bottom panel) after SeRapHin incubation. Pictures show HeLa cells in brightfield, SeRapHin signal in the green channel (G) and red channel (R), a merge of (G) and (R) and the generated G/R value.
(B) Representative pictures of control HeLa cells at extracellular pH 5.5 (top panel) and pH 8.5 (bottom panel). To calibrate SeRapHin signal, the reporter was targeted to the cell surface. Pictures show HeLa cells in brightfield, SeRapHin signal in the green channel (G) and red channel (R), a merge of (G) and (R) and the generated G/R and R/G values, respectively.
These pictures show preliminary results obtained during an internship at the Krishnan laboratory at the University of Chicago. HeLa cell pictures and analysis of G/R and R/G values were generated with the help of Sangyoon Lee.
For a brief explanantion: (G) shows a higher fluorescence at acidic pH values, while (R) shows a higher fluorescence at basic pH values. The generated G/R or R/G calibration curve allows for pH mapping of pH in the range of pH 5.5-10.5. Lee et al. (2025).

Outlook

The results of this thesis suggest a key role for mitochondria during single and collective migration, in particular during directional migration. Cells migrating in a complex microenvironment, e.g. during branching in angiogenesis, often face obstacles like bifurcating junctions where they have to decide on one direction to continue their migration. Until recently, it was unknown how cells behave when encountering a symmetric bifurcation without any external cue or geometrical constraints (Ron et al. 2024). *In vitro* studies have shown that while deciding on a path inside a junction, cells form multiple protrusions that explore the possible arms of each junction. A new theoretical framework predicts that these polarization events inside a symmetric Y-shaped junction undergo deterministic actin-dependent oscillations of the plasma membrane, which result in cycles of elongation and retraction of the protrusive fronts. The dynamics of each protrusive arm are described by (1) arm length, (2) local actin polymerization speed at the leading edge, and (3) concentration of adhesions at the leading edge. This model predicted that cells with lower actin polymerization speed tend to get trapped inside a junction and directional decision-making takes longer compared to cells with a higher actin polymerization speed (HUVECs vs. human glioma propagating cells, respectively) (Ron et al. 2024). Very recently, this theoretical model was extended to describe cells that simultaneously span multiple junctions and display a highly branched phenotype. Effectively, the advanced model revealed a trade-off between local exploration and the efficiency of long-range cell migration. Indeed, while a larger number of cellular branches increases local sensing and exploration of the microenvironment, it reduces cell polarity resulting in less motility (Liu et al. 2026).

Both models focus on the protrusion dynamics at the leading edge during directional migration and emphasize the importance of the actin polymerization speed. While these findings highlight the significance of the actin cytoskeleton during directional migration, they do not yet address the relevance of membrane-bound organelles, such as mitochondria. As shown in this thesis, mitochondria accumulate inside the protrusion that ends up determining the direction of migration during single random migration. Further, they were shown to move into the leading edge and display deterministic depolarization events. Monitoring mitochondria dynamics during directional migration inside symmetric Y-shaped junctions (20 µm hexagonal micropattern) revealed that mitochondria depolarize at the cell front before and during the decision-making process (**Fig. 38**). While there were still depolarizations observed in the losing arm, it can be speculated that while being trapped inside the junction, each arm explores the possible paths and as mitochondria are present in each exploring arm, the arm with more mitochondria content and higher depolarization events ends up deciding the direction (**Fig. 38**, *zoom 02:42:30 h:min:sec and zoom 02:50:30 h:min:sec*). In addition, since mitochondria

are associated with FAs, it is conceivable that the arm with more mitochondria will have more stable protrusions, more energy available, and therefore will become the winning arm. Extending the current models with these preliminary observations will significantly advance the field by incorporating concepts of mechano-metabolism during cell migration.

Finally, this thesis has opened several unexplored questions about the interplay between the cytoskeleton, membrane-bound organelles, and signalling, proving that directional migration, especially directional decision-making, is a very complex process where multiple intracellular networks are finely tuned in order to determine the direction of migration.

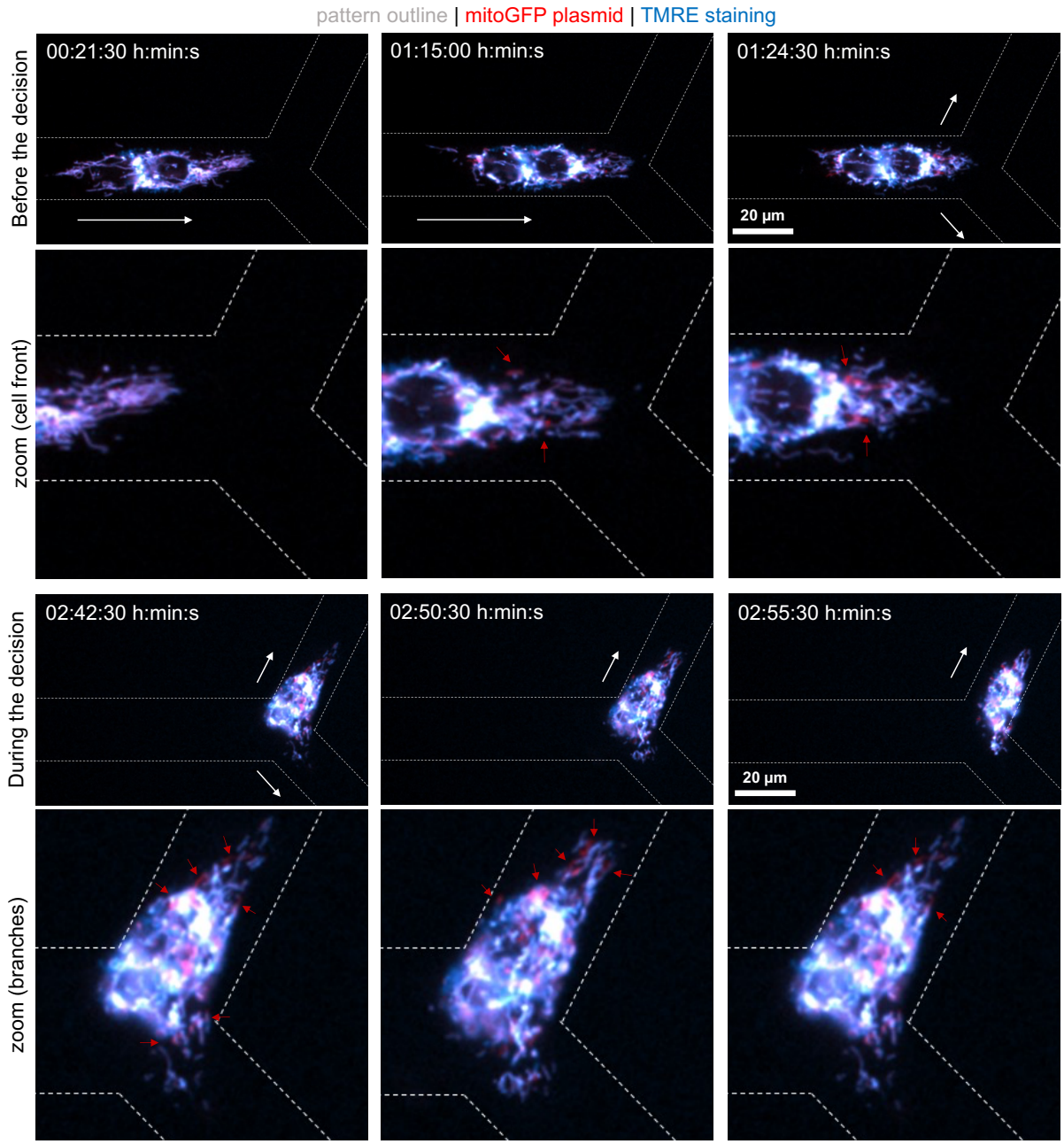

Figure 38: Mitochondria activity is increased during directional decision-making.

Composite pictures of mitochondria transfected with mitoGFP (red) and stained with TMRE (blue) observed during migration over a 1D micropatterned symmetric Y-junction (hexagon shape). Mitochondria activity is shown at indicated timepoints, depolarisation events are indicated with red arrows, the direction of migration is indicated with white arrows. The zoom-in pictures on the bottom, respectively, show mitochondria activity at the cell front at indicated timepoints. Scale bar: 20 µm for whole-field of view.

Supplementary information

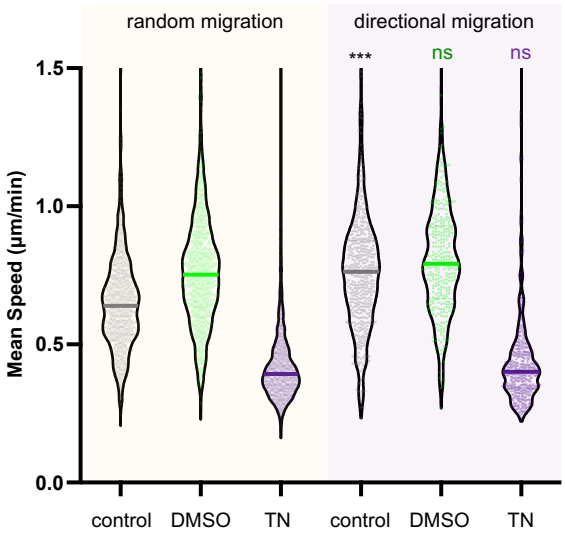

Supplementary Figure 1: Vehicle DMSO does not induce significant changes in directional migration.

Graph shows the instantaneous mean speed of collectively migrating HUVECs in µm/min for control conditions (grey), DMSO-treated (vehicle, green) and TN-treated cells (purple). Yellow area shows violin plots for random migration, light purple area for directional migration. Statistical analysis was performed for plots of the same condition, random and directional migration was compared. Cells under control conditions were the only ones showing a significant increase in speed during directional migration. ***P < 0.001, Kruskal Wallis test. n > 1000 cells for each condition.

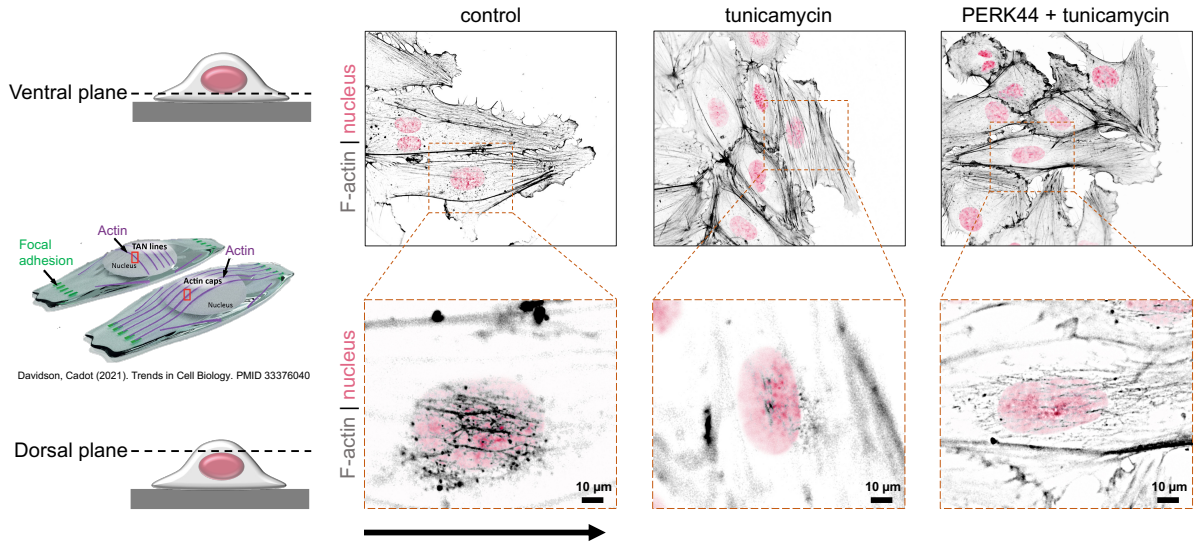

Supplementary Figure 2: ER stress disrupts actin cables over the nucleus.

Top panel: Representative confocal pictures of control cells (left), TN-treated cells (middle) and PERK44 + TN-treated cells (right) migrating towards the right. Cells were stained for F-actin (grey) and nucleus (pink), inverted LUT. Top panel shows the F-actin fibers on the ventral plane underneath the nucleus.
Middle panel: Scheme depicting the differences in actin fibers over the nucleus: actin caps over the nucleus are aligned with the cell polarity axis and anchored to focal adhesions at the front and rear part. TAN lines over the nucleus show a perpendicular orientation to the cell polarity axis and are not associated to focal adhesions.
Bottom panel: Representative confocal pictures of control cells (left), TN-treated cells (middle) and PERK44 + TN-treated cells (right) migrating towards the right. Cells were stained for F-actin (grey) and nucleus (pink), inverted LUT. Top panel shows the F-actin fibers on the dorsal plane over the nucleus. Scale bars: 10 µm for every corresponding picture. Black arrows indicated the direction of migration.

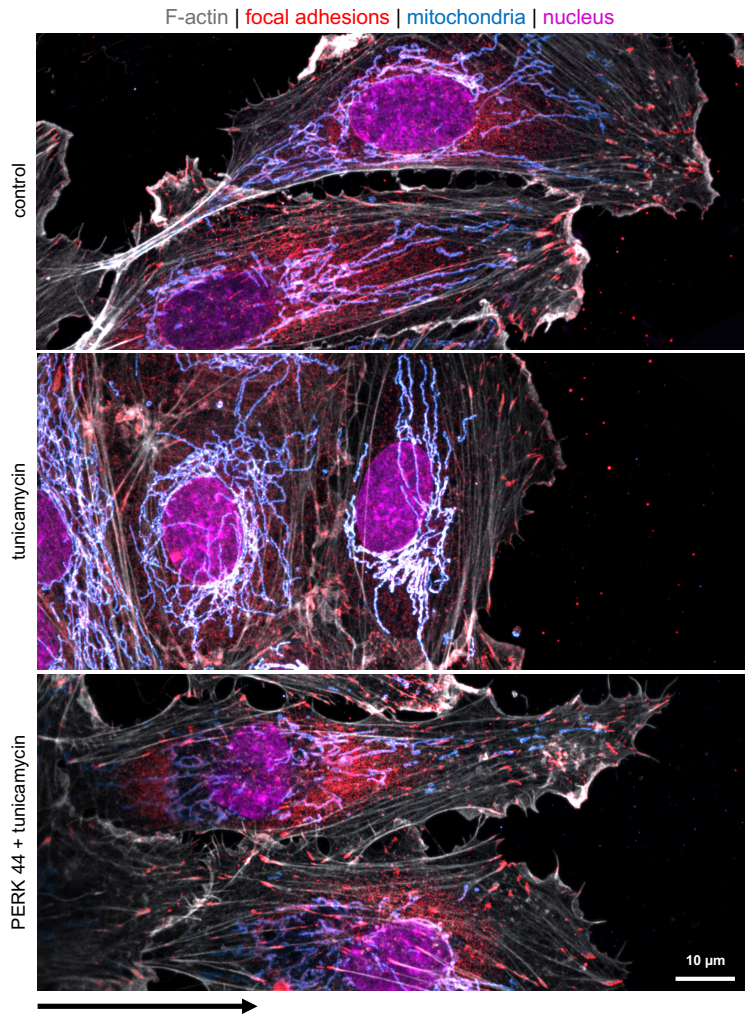

Supplementary Figure 3: Smaller mitochondria co-localize with focal adhesion at the cell front.

Representative confocal pictures of control cells (top panel), TN-treated cells (middle panel) and PERK44 + TN-treated cells (bottom panel) migrating towards the right. Cells were stained for F-actin (grey), FAs (red), mitochondria (blue) and nucleus (pink). Scale bar: 10 um, same for each image.
Black arrow indicates the direction of migration.

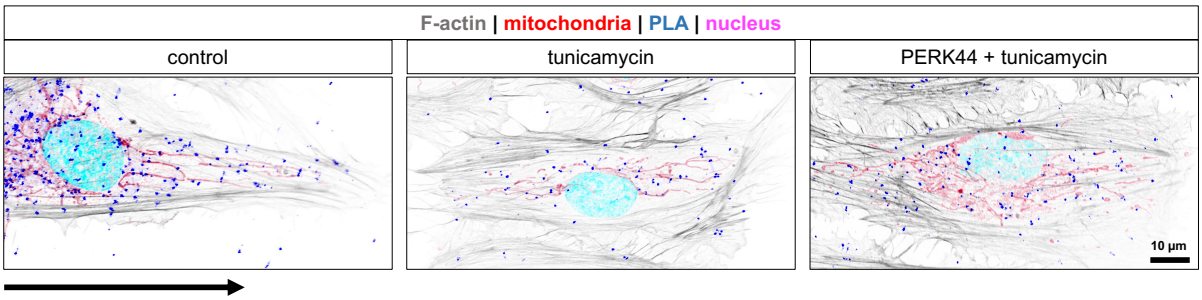

Supplementary Figure 4: ER stress reduces mitochondria-ER contacts (MERCs).

Representative confocal pictures of control cells (left panel), TN-treated cells (middle panel) and PERK44 + TN-treated cells (right panel) migrating towards the right. Cells were stained for F-actin (grey), mitochondria (red) and nucleus (pink). Proximity Ligation Assay is depicted through dots (blue). Each dot corresponds to protein contact between mitochondria (TOM20) and ER (NOGO). Scale bar: 10 µm, same for each image. Black arrow indicated the direction of migration.

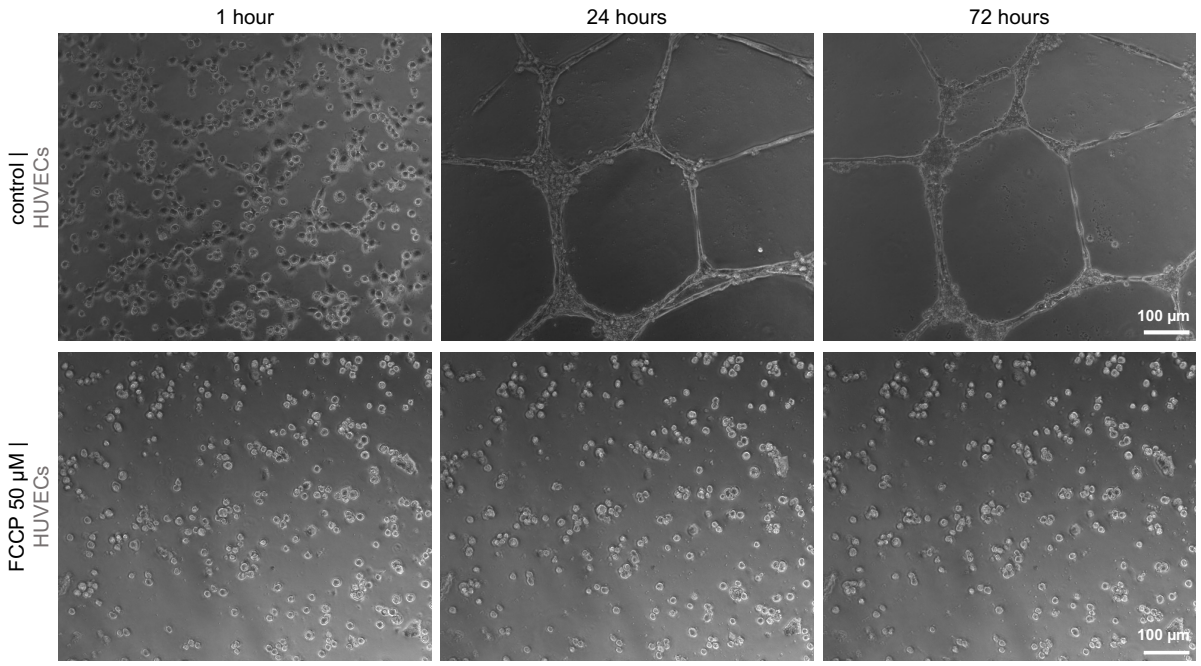

Supplementary Figure 5: FCCP treatment prevents tube formation during angiogensis.

Representative pictures of control cells (top panel) and 50 µM FCCP-treated cells (bottom panel) during tube formation [angiogenesis assay] at indicated timepoints. Cells were plated inside a Matrigel with media containing VEGF-A, and tube formation was observed by taking pictures every 20 min. Scale bar: 100 µm, same for every image per condition.

References

Abdullahi, Abdikarim, Mile Stanojcic, Alexandra Parousis, David Patsouris, and Marc G. Jeschke. 2017. “MODELING ACUTE ER STRESS in VIVO and in VITRO.” *Shock* 47 (4): 506–13. https://doi.org/10.1097/SHK.0000000000000759.

Adebayo, Mary, Seema Singh, Ajay Pratap Singh, and Santanu Dasgupta. 2021. “Mitochondrial Fusion and Fission: The Fine-Tune Balance for Cellular Homeostasis.” *The FASEB Journal* 35 (6): e21620. https://doi.org/https://doi.org/10.1096/fj.202100067R.

Adel, Ali, and Mahmood Abduljabar. 2020. “Microbial Pathogenesis Inhibition of N-Linked Glycosylation by Tunicamycin May Contribute to The Treatment of SARS-CoV-2.” *Microbial Pathogenesis* 149 (October): 104586. https://doi.org/10.1016/j.micpath.2020.104586.

Akhmanova, Anna, Samantha J. Stehbens, and Alpha S. Yap. 2009. “Touch, Grasp, Deliver and Control: Functional Cross-Talk between Microtubules and Cell Adhesions.” *Traffic* 10 (3): 268–74. https://doi.org/10.1111/j.1600-0854.2008.00869.x.

Alam, Muhammad S. 2018. “Proximity Ligation Assay (PLA)” 123: 1–8. https://doi.org/10.1002/cpim.58.

Auerbach, Robert, Rachel Lewis, Brenda Shinners, Louis Kubai, and Nasim Akhtar. 2003. “Angiogenesis Assays : A Critical Overview” 40: 32–40.

Bear, James E., and Jason M. Haugh. 2014. “Directed Migration of Mesenchymal Cells: Where Signaling and the Cytoskeleton Meet.” *Current Opinion in Cell Biology* 30 (1): 74–82. https://doi.org/10.1016/j.ceb.2014.06.005.

Becchetti, Andrea, and Annarosa Arcangeli. 2010. “Integrins and Ion Channels in Cell Migration: Implications for Neuronal Development, Wound Healing and Metastatic Spread.” *Advances in Experimental Medicine and Biology* 674: 107–23. https://doi.org/10.1007/978-1-4419-6066-5_10.

Benedetti, Lorena, Ruolin Fan, Aubrey V. Weigel, Andrew S. Moore, Patrick R. Houlihan, Mark Kittisopikul, Grace Park, et al. 2025. “Periodic ER-Plasma Membrane Junctions Support Long-Range Ca2+ Signal Integration in Dendrites.” *Cell* 188 (2): 484-500.e22. https://doi.org/10.1016/j.cell.2024.11.029.

Bergeijk, Petra van, Casper C. Hoogenraad, and Lukas C. Kapitein. 2016. “Right Time, Right Place: Probing the Functions of Organelle Positioning.” *Trends in Cell Biology* 26 (2): 121–34. https://doi.org/10.1016/j.tcb.2015.10.001.

Bi, Jianlei, Yincong Sun, Meihua Guo, Xiaoxin Sun, Jie sun, Rujiao Jiang, Ning Wang, and Gena Huang. 2025. “Lysosomes: Guardians and Healers within Cells- Multifaceted Perspective and Outlook from Injury Repair to Disease Treatment.” *Cancer Cell International* 25 (1). https://doi.org/10.1186/s12935-025-03771-5.

Bliek, Alexander M. van der, Qinfang Shen, and Sumihiro Kawajiri. 2013. “Mechanisms of Mitochondrial Fission and Fusion.” *Cold Spring Harbor Perspectives in Biology* 5 (6). https://doi.org/10.1101/cshperspect.a011072.

Bola, Becky, and Viki Allan. 2009. “How and Why Does the Endosplasmic Reticulum Move?” *Biochemical Society Transactions* 37 (5): 961–65. https://doi.org/10.1042/BST0370961.

Bretou, Marine, Pablo J. Sáez, Doriane Sanséau, Mathieu Maurin, Danielle Lankar, Melanie Chabaud, Carmine Spampanato, et al. 2017. “Lysosome Signaling Controls the Migration of Dendritic Cells.” *Science Immunology* 2 (16). https://doi.org/10.1126/sciimmunol.aak9573.

Brocard, Jacques B., Gordon L. Rintoul, and Ian J. Reynolds. 2003. “New Perspectives on Mitochondrial Morphology in Cell Function.” *Biology of the Cell* 95 (5): 239–42. https://doi.org/10.1016/S0248-4900(03)00062-5.

Bruneel, Arnaud, Valérie Labas, Agnès Mailloux, Sanjiv Sharma, Joelle Vinh, Michel Vaubourdolle, and Bruno Baudin. 2003. “Proteomic Study of Human Umbilical Vein Endothelial Cells in Culture.” *Proteomics* 3 (5): 714–23. https://doi.org/10.1002/pmic.200300409.

Calero-Cuenca, Francisco J., Cátia S. Janota, and Edgar R. Gomes. 2018. “Dealing with the Nucleus during Cell Migration.” *Current Opinion in Cell Biology* 50: 35–41. https://doi.org/10.1016/j.ceb.2018.01.014.

Canales Coutiño, Brenda, and Roberto Mayor. 2021. “Mechanosensitive Ion Channels in Cell Migration.” *Cells and Development* 166 (April). https://doi.org/10.1016/j.cdev.2021.203683.

Canales, Jimena, Diego Morales, Constanza Blanco, Jose Rivas, Nicolas Diaz, Ioannis Angelopoulos, and Oscar Cerda. 2019. “A Tr(i)p to Cell Migration: New Roles of Trp

Channels in Mechanotransduction and Cancer." *Frontiers in Physiology* 10 (JUN): 1–14. https://doi.org/10.3389/fphys.2019.00757.

Chalmers, Susan, Christopher D. Saunter, John M. Girkin, and John G. McCarron. 2016. "Age Decreases Mitochondrial Motility and Increases Mitochondrial Size in Vascular Smooth Muscle." *Journal of Physiology* 594 (15): 4283–95. https://doi.org/10.1113/JP271942.

Chambliss, Allison B., Shyam B. Khatau, Nicholas Erdenberger, D. Kyle Robinson, Didier Hodzic, Gregory D. Longmore, and Denis Wirtz. 2013. "The LINC-Anchored Actin Cap Connects the Extracellular Milieu to the Nucleus for Ultrafast Mechanotransduction." *Scientific Reports* 3: 1–9. https://doi.org/10.1038/srep01087.

Chen, Chen, Guohua Dai, Maoxia Fan, Xingmeng Wang, Kaibin Niu, and Wulin Gao. 2025. "Mitochondria-Associated Endoplasmic Reticulum Membranes and Myocardial Ischemia: From Molecular Mechanisms to Therapeutic Strategies." *Journal of Translational Medicine* 23 (1). https://doi.org/10.1186/s12967-025-06262-3.

Chen, Ziming, Peilin Chen, Jiayue Li, Euphemie Landao-Bassonga, John Papadimitriou, Junjie Gao, Delin Liu, et al. 2025. "External Strain on the Plasma Membrane Is Relayed to the Endoplasmic Reticulum by Membrane Contact Sites and Alters Cellular Energetics." *Sci. Adv* 11 (June): 6132. https://doi.org/10.1126/sciadv.ads6132.

Cimellaro, A., M. Perticone, T. V. Fiorentino, A. Sciacqua, and M. L. Hribal. 2016. "Role of Endoplasmic Reticulum Stress in Endothelial Dysfunction." *Nutrition, Metabolism and Cardiovascular Diseases* 26 (10): 863–71. https://doi.org/10.1016/j.numecd.2016.05.008.

Clainche, Christophe Le, and Marie France Carlier. 2008. "Regulation of Actin Assembly Associated with Protrusion and Adhesion in Cell Migration." *Physiological Reviews* 88 (2): 489–513. https://doi.org/10.1152/physrev.00021.2007.

Conza, Giusy Di, and Ping Chih Ho. 2020. "ER Stress Responses: An Emerging Modulator for Innate Immunity." *Cells* 9 (3): 1–11. https://doi.org/10.3390/cells9030695.

Coq, Johanne Le, Iván Acebrón, Bárbara Rodrigo Martin, Pilar López Navajas, and Daniel Lietha. 2022. "New Insights into FAK Structure and Function in Focal Adhesions." *Journal of Cell Science* 135 (20). https://doi.org/10.1242/jcs.259089.

Cramer, Louise P. 2010. "Forming the Cell Rear First: Breaking Cell Symmetry to Trigger Directed Cell Migration." *Nature Cell Biology* 12 (7): 628–32.

https://doi.org/10.1038/ncb0710-628.

Crosas-Molist, Eva, Vittoria Graziani, Oscar Maiques, Pahini Pandya, Joanne Monger, Remi Samain, Samantha L. George, et al. 2023. “AMPK Is a Mechano-Metabolic Sensor Linking Cell Adhesion and Mitochondrial Dynamics to Myosin-Dependent Cell Migration.” *Nature Communications* 14 (1): 1–22. https://doi.org/10.1038/s41467-023-38292-0.

Crowley, Lisa C., Melinda E. Christensen, and Nigel J. Waterhouse. 2016. “Measuring Mitochondrial Transmembrane Potential by TMRE Staining.” *Cold Spring Harbor Protocols* 2016 (12): 1092–96. https://doi.org/10.1101/pdb.prot087361.

Cui, Chao, Chenglu Sun, Peng Yuan, Shibo Tian, Hailong Xie, Funeng Xu, and Haohuan Li. 2025. “The Golgi Apparatus as a Strategic Target in Cancer: Mechanisms, Diagnosis and Therapeutic Opportunities.” *Journal of Drug Targeting* 0 (0): 1–15. https://doi.org/10.1080/1061186X.2025.2527867.

Daniilidis, Melina, Umut Günsel, Georgios Broutzakis, Kira D. Leitl, Robert Janowski, Kai Fredriksson, Dierk Niessing, Christos Gatsogiannis, and Franz Hagn. 2025. “Structural Basis of Apoptosis Induction by the Mitochondrial Voltage-Dependent Anion Channel.” *Nature Communications* 16 (1). https://doi.org/10.1038/s41467-025-65363-1.

Davidson, Patricia M., and Bruno Cadot. 2021. “Actin on and around the Nucleus.” *Trends in Cell Biology* 31 (3): 211–23. https://doi.org/10.1016/j.tcb.2020.11.009.

Day, Kasey J., L. Andrew Staehelin, and Benjamin S. Glick. 2013. “A Three-Stage Model of Golgi Structure and Function.” *Histochemistry and Cell Biology* 140 (3): 239–49. https://doi.org/10.1007/s00418-013-1128-3.

Dematteis, Giulia, Laura Tapella, Claudio Casali, Maria Talmon, Elisa Tonelli, Simone Reano, Adele Ariotti, et al. 2024. “ER-Mitochondria Distance Is a Critical Parameter for Efficient Mitochondrial Ca2+ Uptake and Oxidative Metabolism.” *Communications Biology* 7 (1): 1–15. https://doi.org/10.1038/s42003-024-06933-9.

Denisenko, Tatiana V., Anna S. Gorbunova, and Boris Zhivotovsky. 2019. “Mitochondrial Involvement in Migration, Invasion and Metastasis.” *Frontiers in Cell and Developmental Biology* 7 (December): 1–17. https://doi.org/10.3389/fcell.2019.00355.

Dong, Yunzhou, Miao Zhang, Bin Liang, Zhonglin Xie, Zhengxing Zhao, Sima Asfa, Hyoung Chul Choi, and Ming Hui Zou. 2010. “Reduction of AMP-Activated Protein Kinase A2 Increases Endoplasmic Reticulum Stress and Atherosclerosis in Vivo.” *Circulation* 121

(6): 792–803. https://doi.org/10.1161/CIRCULATIONAHA.109.900928.

Doyle, Andrew D., Ryan J. Petrie, Matthew L. Kutys, and Kenneth M. Yamada. 2013. “Dimensions in Cell Migration.” *Current Opinion in Cell Biology* 25 (5): 642–49. https://doi.org/10.1016/j.ceb.2013.06.004.

Dupont, Sirio. 2025. “Mechano-Metabolism on the Rise.” *Current Opinion in Cell Biology* 95: 102529. https://doi.org/10.1016/j.ceb.2025.102529.

Edwards, Ruairidh, Ross Eaglesfield, and Kostas Tokatlidis. 2021. “The Mitochondrial Intermembrane Space: The Most Constricted Mitochondrial Sub-Compartment with the Largest Variety of Protein Import Pathways.” *Open Biology* 11 (3). https://doi.org/10.1098/rsob.210002.

Ershov, Dmitry, Minh Son Phan, Joanna W. Pylvänäinen, Stéphane U. Rigaud, Laure Le Blanc, Arthur Charles-Orszag, James R.W. Conway, et al. 2022. “TrackMate 7: Integrating State-of-the-Art Segmentation Algorithms into Tracking Pipelines.” *Nature Methods* 19 (7): 829–32. https://doi.org/10.1038/s41592-022-01507-1.

Fabiano, Emily D., Jenna M. Poole, and Cynthia A. Reinhart-King. 2025. “Mechanometabolism: Recent Findings on the Intersection of Cell Adhesion, Cell Migration, and Metabolism.” *American Journal of Physiology - Cell Physiology* 328 (6): C1866–79. https://doi.org/10.1152/ajpcell.00892.2024.

Feng, Qian, and Benoît Kornmann. 2018. “Mechanical Forces on Cellular Organelles.” *Journal of Cell Science* 131 (21). https://doi.org/10.1242/jcs.218479.

Fernández-Yagüe, Marc A., Elijah N. Marquez, Chetan S. Poojari, Jianping Fu, Yingxiao Wang, Aránzazu Del Campo, and Andrés J. García. 2025. “Mechanochemical Waves in Focal Adhesions during Cell Migration.” *Science Advances* 11 (40): eadw6425. https://doi.org/10.1126/sciadv.adw6425.

Fletcher, Daniel A., and R. Dyche Mullins. 2010. “Cell Mechanics and the Cytoskeleton.” *Nature* 463 (7280): 485–92. https://doi.org/10.1038/nature08908.

Frakes, Ashley E., and Andrew Dillin. 2017. “The UPRER: Sensor and Coordinator of Organismal Homeostasis.” *Molecular Cell* 66 (6): 761–71. https://doi.org/10.1016/j.molcel.2017.05.031.

Freeman, Spencer A., Sergio Grinstein, and John Orlowski. 2023. “DETERMINANTS,

MAINTENANCE, AND FUNCTION OF ORGANELLAR PH." *Physiological Reviews* 103 (1): 515–606. https://doi.org/10.1152/physrev.00009.2022.

Galloway, Chad A., and Yisang Yoon. 2013. "Mitochondrial Morphology in Metabolic Diseases." *Antioxidants and Redox Signaling* 19 (4): 415–30. https://doi.org/10.1089/ars.2012.4779.

Gant Luxton, G. W., Edgar R. Gomes, Eric S. Folker, Howard J. Worman, and Gregg G. Gundersen. 2011. "TAN Lines: A Novel Nuclear Envelope Structure Involved in Nuclear Positioning." *Nucleus* 2 (3): 173–81. https://doi.org/10.4161/nucl.2.3.16243.

Garcin, Clare, and Anne Straube. 2019. "Microtubules in Cell Migration." *Essays in Biochemistry* 63 (5): 509–20. https://doi.org/10.1042/EBC20190016.

Gardel, Margaret L., Ian C. Schneider, Yvonne Aratyn-Schaus, and Clare M. Waterman. 2010. "Mechanical Integration of Actin and Adhesion Dynamics in Cell Migration." *Annual Review of Cell and Developmental Biology* 26: 315–33. https://doi.org/10.1146/annurev.cellbio.011209.122036.

Ge, Ruiliang, Yilin Tai, Yuanyuan Sun, Kechun Zhou, Shenglian Yang, Tianlin Cheng, Qifei Zou, Feng Shen, and Yizheng Wang. 2009. "Critical Role of TRPC6 Channels in VEGF-Mediated Angiogenesis." *Cancer Letters* 283 (1): 43–51. https://doi.org/10.1016/j.canlet.2009.03.023.

Giorgi, Carlotta, Diego De Stefani, Angela Bononi, Rosario Rizzuto, and Paolo Pinton. 2009. "Structural and Functional Link between the Mitochondrial Network and the Endoplasmic Reticulum." *International Journal of Biochemistry and Cell Biology* 41 (10): 1817–27. https://doi.org/10.1016/j.biocel.2009.04.010.

Gong, Bo, Jake D. Johnston, Alexander Thiemicke, Alex de Marco, and Tobias Meyer. 2024. "Endoplasmic Reticulum–Plasma Membrane Contact Gradients Direct Cell Migration." *Nature* 631 (8020): 415–23. https://doi.org/10.1038/s41586-024-07527-5.

Grada, Ayman, Marta Otero-Vinas, Francisco Prieto-Castrillo, Zaidal Obagi, and Vincent Falanga. 2017. "Research Techniques Made Simple: Analysis of Collective Cell Migration Using the Wound Healing Assay." *Journal of Investigative Dermatology* 137 (2): e11–16. https://doi.org/10.1016/j.jid.2016.11.020.

Groten, Stijn A., Eva R. Smit, Maartje van den Biggelaar, and Arie J. Hoogendijk. 2024. "The Proteomic Landscape of in Vitro Cultured Endothelial Cells across Vascular Beds."

Communications Biology 7 (1). https://doi.org/10.1038/s42003-024-06649-w.

Gupton, Stephanie L., Karen L. Anderson, Thomas P. Kole, Robert S. Fischer, Aaron Ponti, Sarah E. Hitchcock-DeGregori, Gaudenz Danuser, et al. 2005. “Cell Migration without a Lamellipodium: Translation of Actin Dynamics into Cell Movement Mediated by Tropomyosin.” *Journal of Cell Biology* 168 (4): 619–31. https://doi.org/10.1083/jcb.200406063.

Haeger, Anna, Katarina Wolf, Mirjam M. Zegers, and Peter Friedl. 2015. “Collective Cell Migration: Guidance Principles and Hierarchies.” *Trends in Cell Biology* 25 (9): 556–66. https://doi.org/10.1016/j.tcb.2015.06.003.

Hao, Huiwen, Jiahao Niu, Boxin Xue, Qian Peter Su, Menghan Liu, Junsheng Yang, Jinshan Qin, Shujuan Zhao, Congying Wu, and Yujie Sun. 2020. “Golgi-associated Microtubules Are Fast Cargo Tracks and Required for Persistent Cell Migration.” *EMBO Reports* 21 (3): 1–16. https://doi.org/10.15252/embr.201948385.

Harris, Andrew R., Pamela Jreij, and Daniel A. Fletcher. 2018. “Mechanotransduction by the Actin Cytoskeleton: Converting Mechanical Stimuli into Biochemical Signals.” *Annual Review of Biophysics* 47: 617–31. https://doi.org/10.1146/annurev-biophys-070816-033547.

Heath, J P, and G A Dunn. 1978. “Cell to Substratum Contacts of Chick Fibroblasts and Their Relation to the Microfilament System. A Correlated Interference-Reflexion and High-Voltage Electron-Microscope Study.” *Journal of Cell Science* 29 (February): 197–212. https://doi.org/10.1242/jcs.29.1.197.

Herrmann, Johannes M., and Jan Riemer. 2010. “The Intermembrane Space of Mitochondria.” *Antioxidants and Redox Signaling* 13 (9): 1341–58. https://doi.org/10.1089/ars.2009.3063.

Hertzog, Maud, and Fabian Erdel. 2023. “The Material Properties of the Cell Nucleus: A Matter of Scale.” *Cells* 12 (15). https://doi.org/10.3390/cells12151958.

Heyn, Johannes C.J., Joachim O. Rädler, and Martin Falcke. 2024. “Mesenchymal Cell Migration on One-Dimensional Micropatterns.” *Frontiers in Cell and Developmental Biology* 12 (April): 1–16. https://doi.org/10.3389/fcell.2024.1352279.

His, W. 1865. *Die Häute Und Höhlen Des Körpers: Academisches Programm*. Schweighauserische Universitäts-Buchdruckerei.

https://books.google.de/books?id=ML1AAQAAMAAJ.

Hohmann, Tim, and Faramarz Dehghani. 2019. “The Cytoskeleton—a Complex Interacting Meshwork.” *Cells* 8 (4): 1–55. https://doi.org/10.3390/cells8040362.

Hong, Yu Ah, and Reiko Inagi. 2025. “Endoplasmic Reticulum-Mediated Organelle Crosstalk in Kidney Disease.” *Nature Reviews Nephrology*. https://doi.org/10.1038/s41581-025-00989-4.

Hotulainen, Pirta, and Pekka Lappalainen. 2006. “Stress Fibers Are Generated by Two Distinct Actin Assembly Mechanisms in Motile Cells.” *Journal of Cell Biology* 173 (3): 383–94. https://doi.org/10.1083/jcb.200511093.

Hu, Ying Li, Shaoying Lu, Kai W. Szeto, Jie Sun, Yingxiao Wang, Juan C. Lasheras, and Shu Chien. 2014. “FAK and Paxillin Dynamics at Focal Adhesions in the Protrusions of Migrating Cells.” *Scientific Reports* 4: 1–7. https://doi.org/10.1038/srep06024.

Huang, Jingjing, Hanhui Shi, Jiaying Shang, Gongrui Fu, and Pingzheng Zhou. 2025. “Ion Channels of the Plasma Membrane and Endolysosomes: Roles in Osmoregulation and Volume Regulation in Immune Cells.” *Pharmacological Research* 221 (September): 107951. https://doi.org/10.1016/j.phrs.2025.107951.

Jain, Arjun. 2013. “Endothelin-1-Induced Endoplasmic Reticulum Stress in Disease.” *The Journal of Pharmacology and Experimental Therapeutics* 346 (2): 163–72. https://doi.org/10.1124/jpet.113.205567.

Janota, Cátia Silva, Andreia Pinto, Anna Pezzarossa, Pedro Machado, Judite Costa, Pedro Campinho, Cláudio A. Franco, and Edgar R. Gomes. 2022. “Shielding of Actin by the Endoplasmic Reticulum Impacts Nuclear Positioning.” *Nature Communications* 13 (1). https://doi.org/10.1038/s41467-022-30388-3.

Jerka, Dominika, Klaudia Bonowicz, Klaudia Piekarska, Seyda Gokyer, Utku Serhat Derici, Osama Ali Hindy, Baris Burak Altunay, et al. 2024. “Unraveling Endothelial Cell Migration: Insights into Fundamental Forces, Inflammation, Biomaterial Applications, and Tissue Regeneration Strategies.” *ACS Applied Bio Materials* 7 (4): 2054–69. https://doi.org/10.1021/acsabm.3c01227.

Kaverina, Irina, and Anne Straube. 2011. “Regulation of Cell Migration by Dynamic Microtubules.” *Seminars in Cell and Developmental Biology* 22 (9): 968–74. https://doi.org/10.1016/j.semcdb.2011.09.017.

Khalil, Antoine A., and Peter Friedl. 2010. “Determinants of Leader Cells in Collective Cell Migration.” *Integrative Biology* 2 (11–12): 568–74. https://doi.org/10.1039/c0ib00052c.

Kim, Jeong Ki, Arghavan Louhghalam, Geonhui Lee, Benjamin W. Schafer, Denis Wirtz, and Dong Hwee Kim. 2017. “Nuclear Lamin A/C Harnesses the Perinuclear Apical Actin Cables to Protect Nuclear Morphology.” *Nature Communications* 8 (1): 1–13. https://doi.org/10.1038/s41467-017-02217-5.

Kodakandla, Goutham, Askar M. Akimzhanov, and Darren Boehning. 2023. “Regulatory Mechanisms Controlling Store-Operated Calcium Entry.” *Frontiers in Physiology* 14 (December). https://doi.org/10.3389/fphys.2023.1330259.

Koksal, Ali Riza, George Nicholas Verne, and QiQi Zhou. 2021. “Endoplasmic Reticulum Stress in Biological Processing and Disease.” *Journal of Investigative Medicine* 69 (2): 309–15. https://doi.org/10.1136/jim-2020-001570.

Kramer, Nina, Angelika Walzl, Christine Unger, Margit Rosner, Georg Krupitza, Markus Hengstschläger, and Helmut Dolznig. 2013. “In Vitro Cell Migration and Invasion Assays.” *Mutation Research - Reviews in Mutation Research* 752 (1): 10–24. https://doi.org/10.1016/j.mrrev.2012.08.001.

Krüger-Genge, Anne, Anna Blocki, Ralf-Peter Franke, and Friedrich Jung. 2019. “Molecular Sciences Vascular Endothelial Cell Biology: An Update.” *International Journal of Molecular Sciences* 20: 4411. www.mdpi.com/journal/ijms.

Kuehl, Malte, Yusuke Okabayashi, Milagros N. Wong, Lukas Gernhold, Gabriele Gut, Nico Kaiser, Maria Schwerk, et al. 2025. “Pathology-Oriented Multiplexing Enables Integrative Disease Mapping.” *Nature* 644 (8076): 516–26. https://doi.org/10.1038/s41586-025-09225-2.

Kumari, Reena, Katharina Ven, Megan Chastney, Shrikant B. Kokate, Johan Peränen, Jesse Aaron, Konstantin Kogan, et al. 2024. “Focal Adhesions Contain Three Specialized Actin Nanoscale Layers.” *Nature Communications* 15 (1). https://doi.org/10.1038/s41467-024-46868-7.

Kupfer, A., G. Dennert, and S. J. Singer. 1983. “Polarization of the Golgi Apparatus and the Microtubule-Organizing Center within Cloned Natural Killer Cells Bound to Their Targets.” *Proceedings of the National Academy of Sciences of the United States of America* 80 (23 I): 7224–28. https://doi.org/10.1073/pnas.80.23.7224.

Lamalice, Laurent, Fabrice Le Boeuf, and Jacques Huot. 2007. “Endothelial Cell Migration during Angiogenesis.” *Circulation Research* 100 (6): 782–94. https://doi.org/10.1161/01.RES.0000259593.07661.1e.

Lebeau, Justine, Jaclyn M. Saunders, Vivian W.R. Moraes, Aparajita Madhavan, Nicole Madrazo, Mary C. Anthony, and R. Luke Wiseman. 2018. “The PERK Arm of the Unfolded Protein Response Regulates Mitochondrial Morphology during Acute Endoplasmic Reticulum Stress.” *Cell Reports* 22 (11): 2827–36. https://doi.org/10.1016/j.celrep.2018.02.055.

Lee, Sangyoon, Sandip Chakraborty, Soyoung Kim, Asif Ali, and Koushambi Mitra. 2025. “Organelles Harbour PH Gradients.”

Lenin, Raji, Peter G. Nagy, Kumar Abhiram Jha, and Rajashekhar Gangaraju. 2019. “GRP78 Translocation to the Cell Surface and O-GlcNAcylation of VE-Cadherin Contribute to ER Stress-Mediated Endothelial Permeability.” *Scientific Reports* 9 (1): 1–14. https://doi.org/10.1038/s41598-019-47246-w.

Li, Anqi, Meng Gao, Wenting Jiang, Yuan Qin, and Guohua Gong. 2020. “Mitochondrial Dynamics in Adult Cardiomyocytes and Heart Diseases.” *Frontiers in Cell and Developmental Biology* 8 (December): 1–14. https://doi.org/10.3389/fcell.2020.584800.

Li, Chengfei, Yikai Pan, Yingjun Tan, Yongchun Wang, and Xiqing Sun. 2022. “PINK1-Dependent Mitophagy Reduced Endothelial Hyperpermeability and Cell Migration Capacity Under Simulated Microgravity.” *Frontiers in Cell and Developmental Biology* 10 (July): 1–19. https://doi.org/10.3389/fcell.2022.896014.

Li, Xiaoquan, Joseph Dale Combs, Khalid Salaita, and Xiaokun Shu. 2023. “Polarized Focal Adhesion Kinase Activity within a Focal Adhesion during Cell Migration.” *Nature Chemical Biology* 19 (12): 1458–68. https://doi.org/10.1038/s41589-023-01353-y.

Limia, Celia Maria, Chloé Sauzay, Hery Urra, Claudio Hetz, Eric Chevet, and Tony Avril. 2019. “Emerging Roles of the Endoplasmic Reticulum Associated Unfolded Protein Response in Cancer Cell Migration and Invasion.” *Cancers* 11 (5): 1–25. https://doi.org/10.3390/cancers11050631.

Lindsay, Karen L., Claudia Buss, Pathik D. Wadhwa, and Sonja Entringer. 2019. “The Interplay Between Nutrition and Stress in Pregnancy: Implications for Fetal Programming of Brain Development.” *Biological Psychiatry* 85 (2): 135–49. https://doi.org/10.1016/j.biopsych.2018.06.021.

Liu, Jiayi, Javier Boix-, Jonathan E Ron, Johan M Kux, and Magdalena E M Oremek. 2026. “Trade- - off between Branching and Polarity Controls Making during Cell Migration” 2734 (January): 1–14. https://doi.org/10.1126/sciadv.ads2734.

Lomakin, A. J., C. J. Cattin, D. Cuvelier, Z. Alraies, M. Molina, G. P.F. Nader, N. Srivastava, et al. 2020. “The Nucleus Acts as a Ruler Tailoring Cell Responses to Spatial Constraints.” *Science* 370 (6514). https://doi.org/10.1126/science.aba2894.

Luo, Zhen, Jianbo Yao, Zhe Wang, and Jianxiong Xu. 2023. “Mitochondria in Endothelial Cells Angiogenesis and Function: Current Understanding and Future Perspectives.” *Journal of Translational Medicine* 21 (1): 1–28. https://doi.org/10.1186/s12967-023-04286-1.

Makhoul, Christian, Prajakta Gosavi, and Paul A. Gleeson. 2019. “Golgi Dynamics: The Morphology of the Mammalian Golgi Apparatus in Health and Disease.” *Frontiers in Cell and Developmental Biology* 7 (July): 1–7. https://doi.org/10.3389/fcell.2019.00112.

Malhotra, Jyoti D., and Randal J. Kaufman. 2011. “ER Stress and Its Functional Link to Mitochondria: Role in Cell Survival and Death.” *Cold Spring Harbor Perspectives in Biology* 3 (9): 1–13. https://doi.org/10.1101/cshperspect.a004424.

Martucciello, Stefania, Milena Masullo, Antonietta Cerulli, and Sonia Piacente. 2020. “Natural Products Targeting ER Stress, and the Functional Link to Mitochondria.” *International Journal of Molecular Sciences* 21 (6). https://doi.org/10.3390/ijms21061905.

Marwaha, Rituraj, Diya Manoj, Simran Rawal, Purnati Khuntia, Sanak Banerjee, Praver Gupta, Basil Thurakkal, Manish Jaiswal, and Tamal Das. 2025. “Mechanosensitive Dynamics of Lysosomes along Microtubules Regulate Leader Cell Emergence during Collective Cell Migration.” *Nature Communications*. https://doi.org/10.1038/s41467-025-67645-0.

Marziano, Corina, Gael Genet, and Karen K. Hirschi. 2021. “Vascular Endothelial Cell Specification in Health and Disease.” *Angiogenesis* 24 (2): 213–36. https://doi.org/10.1007/s10456-021-09785-7.

Mastronarde, David N. 2005. “Automated Electron Microscope Tomography Using Robust Prediction of Specimen Movements.” *Journal of Structural Biology* 152 (1): 36–51. https://doi.org/10.1016/j.jsb.2005.07.007.

Mastronarde, David N., and Susannah R. Held. 2017. “Automated Tilt Series Alignment and Tomographic Reconstruction in IMOD.” *Journal of Structural Biology* 197 (2): 102–13. https://doi.org/10.1016/j.jsb.2016.07.011.

Matrullo, Gianmarco, Giuseppe Filomeni, and Salvatore Rizza. 2025. “Redox Regulation of Focal Adhesions.” *Redox Biology* 80 (November 2024): 103514. https://doi.org/10.1016/j.redox.2025.103514.

Mayor, Roberto, and Sandrine Etienne-Manneville. 2016. “The Front and Rear of Collective Cell Migration.” *Nature Reviews Molecular Cell Biology* 17 (2): 97–109. https://doi.org/10.1038/nrm.2015.14.

McCarron, John G., Calum Wilson, Mairi E. Sandison, Marnie L. Olson, John M. Girkin, Christopher Saunter, and Susan Chalmers. 2013. “From Structure to Function: Mitochondrial Morphology, Motion and Shaping in Vascular Smooth Muscle.” *Journal of Vascular Research* 50 (5): 357–71. https://doi.org/10.1159/000353883.

Mehta, Kritika, Leeba Ann Chacko, Manjyot Kaur Chug, Siddharth Jhunjhunwala, and Vaishnavi Ananthanarayanan. 2019. “Association of Mitochondria with Microtubules Inhibits Mitochondrial Fission by Precluding Assembly of the Fission Protein Dnm1.” *Journal of Biological Chemistry* 294 (10): 3385–96. https://doi.org/10.1074/jbc.RA118.006799.

Meldi, Lauren, and Jason H. Brickner. 2011. “Compartmentalization of the Nucleus.” *Trends in Cell Biology* 21 (12): 701–8. https://doi.org/10.1016/j.tcb.2011.08.001.

Melkov, Anna, and Uri Abdu. 2018. “Regulation of Long-Distance Transport of Mitochondria along Microtubules.” *Cellular and Molecular Life Sciences* 75 (2): 163–76. https://doi.org/10.1007/s00018-017-2590-1.

Meusser, Birgit, Christian Hirsch, Ernst Jarosch, and Thomas Sommer. 2005. “ERAD: The Long Road to Destruction.” *Nature Cell Biology* 7 (8): 766–72. https://doi.org/10.1038/ncb0805-766.

Millarte, Valentina, and Hesso Farhan. 2012. “The Golgi in Cell Migration: Regulation by Signal Transduction and Its Implications for Cancer Cell Metastasis.” *The Scientific World Journal* 2012. https://doi.org/10.1100/2012/498278.

Missiroli, Sonia, Simone Patergnani, Natascia Caroccia, Gaia Pedriali, Mariasole Perrone, Maurizio Previati, Mariusz R. Wieckowski, and Carlotta Giorgi. 2018. “Mitochondria-Associated Membranes (MAMs) and Inflammation.” *Cell Death and Disease* 9 (3). https://doi.org/10.1038/s41419-017-0027-2.

Nan, Weijin, Yuxi He, Shurong Wang, and Yan Zhang. 2023. “Molecular Mechanism of VE-

Cadherin in Regulating Endothelial Cell Behaviour during Angiogenesis." *Frontiers in Physiology* 14 (August): 1–12. https://doi.org/10.3389/fphys.2023.1234104.

Navarro, Alexandra P., Mary Ann Collins, and Eric S. Folker. 2016. "The Nucleus Is a Conserved Mechanosensation and Mechanoresponse Organelle." *Cytoskeleton* 73 (2): 59–67. https://doi.org/10.1002/cm.21277.

Nemethova, Maria, Sonja Auinger, and J. Victor Small. 2008. "Building the Actin Cytoskeleton: Filopodia Contribute to the Construction of Contractile Bundles in the Lamella." *Journal of Cell Biology* 180 (6): 1233–44. https://doi.org/10.1083/jcb.200709134.

Nixon-Abell, Jonathon, Christopher J. Obara, Aubrey V. Weigel, Dong Li, Wesley R. Legant, C. Shan Xu, H. Amalia Pasolli, et al. 2016. "Increased Spatiotemporal Resolution Reveals Highly Dynamic Dense Tubular Matrices in the Peripheral ER." *Science* 354 (6311). https://doi.org/10.1126/science.aaf3928.

Novikoff, Alex B., H. Beaufay, and C. De Duve. 1956. "Electron Microscopy of Lysosome-Rich Fractions from Rat Liver." *Journal of Cell Biology* 2 (4): 179–84. https://doi.org/10.1083/jcb.2.4.179.

Oakes, Scott A., and Feroz R. Papa. 2015. "The Role of Endoplasmic Reticulum Stress in Human Pathology." *Annual Review of Pathology: Mechanisms of Disease* 10: 173–94. https://doi.org/10.1146/annurev-pathol-012513-104649.

Oslowski, Christine M., and Fumihiko Urano. 2011. "Measuring ER Stress and the Unfolded Protein Response Using Mammalian Tissue Culture System." *Methods in Enzymology* 490 (C): 71–92. https://doi.org/10.1016/B978-0-12-385114-7.00004-0.

Pascalis, Chiara De, and Sandrine Etienne-Manneville. 2017. "Single and Collective Cell Migration: The Mechanics of Adhesions." *Molecular Biology of the Cell* 28 (14): 1833–46. https://doi.org/10.1091/mbc.E17-03-0134.

Paupe, Vincent, and Julien Prudent. 2018. "New Insights into the Role of Mitochondrial Calcium Homeostasis in Cell Migration." *Biochemical and Biophysical Research Communications* 500 (1): 75–86. https://doi.org/10.1016/j.bbrc.2017.05.039.

Pawluchin, Anna, and Milos Galic. 2022. "Moving through a Changing World: Single Cell Migration in 2D vs. 3D." *Frontiers in Cell and Developmental Biology* 10 (December): 1–14. https://doi.org/10.3389/fcell.2022.1080995.

Peng, Shuang, Jian Gao, Darko Stojkov, Shida Yousefi, and Hans-Uwe Simon. 2023. “Established and Emerging Roles for Mitochondria in Neutrophils.” *Immunological Reviews* 314 (1): 413–26. https://doi.org/10.1111/imr.13158.

Perea, Valerie, Christian Cole, Justine Lebeau, Vivian Dolina, Kelsey R Baron, Aparajita Madhavan, Jeffery W Kelly, Danielle A Grotjahn, and R Luke Wiseman. 2023. “ PERK Signaling Promotes Mitochondrial Elongation by Remodeling Membrane Phosphatidic Acid .” *The EMBO Journal* 42 (15): 1–14. https://doi.org/10.15252/embj.2023113908.

Perry, Seth W., John P. Norman, Justin Barbieri, Edward B. Brown, and Harris A. Gelbard. 2011. “Mitochondrial Membrane Potential Probes and the Proton Gradient: A Practical Usage Guide.” *BioTechniques* 50 (2): 98–115. https://doi.org/10.2144/000113610.

Phillips, Melissa J., and Gia K. Voeltz. 2016. “Structure and Function of ER Membrane Contact Sites with Other Organelles.” *Nature Reviews Molecular Cell Biology* 17 (2): 69–82. https://doi.org/10.1038/nrm.2015.8.

Potter, Huntington, and Richard Heller. 2018. “Transfection by Electroporation,” 1–13. https://doi.org/10.1002/cpmb.48.

Preibisch, Stephan, Stephan Saalfeld, and Pavel Tomancak. 2009. “Globally Optimal Stitching of Tiled 3D Microscopic Image Acquisitions.” *Bioinformatics* 25 (11): 1463–65. https://doi.org/10.1093/bioinformatics/btp184.

Pu, Jing, Carlos M. Guardia, Tal Keren-Kaplan, and Juan S. Bonifacino. 2016. “Mechanisms and Functions of Lysosome Positioning.” *Journal of Cell Science* 129 (23): 4329–39. https://doi.org/10.1242/jcs.196287.

Qin, Lei, Dazhi Yang, Weihong Yi, Huiling Cao, and Guozhi Xiao. 2021. “Roles of Leader and Follower Cells in Collective Cell Migration.” *Molecular Biology of the Cell* 32 (14): 1267–72. https://doi.org/10.1091/mbc.E20-10-0681.

Qiu, Ruoyi, and Richard S. Lewis. 2019. “Structural Features of STIM and Orai Underlying Store-Operated Calcium Entry.” *Current Opinion in Cell Biology* 57: 90–98. https://doi.org/10.1016/j.ceb.2018.12.012.

Rajendran, Peramaiyan, Thamaraiselvan Rengarajan, Jayakumar Thangavel, Yutaka Nishigaki, Dhanapal Sakthisekaran, Gautam Sethi, and Ikuo Nishigaki. 2013. “The Vascular Endothelium and Human Diseases.” *International Journal of Biological Sciences* 9 (10): 1057–69. https://doi.org/10.7150/ijbs.7502.

Rao, R. V., H. M. Ellerby, and D. E. Bredesen. 2004. “Coupling Endoplasmic Reticulum Stress to the Cell Death Program.” *Cell Death and Differentiation* 11 (4): 372–80. https://doi.org/10.1038/sj.cdd.4401378.

Rawal, Simran, Pradeep Keshavanarayana, Diya Manoj, Purnati Khuntia, Sanak Banerjee, Basil Thurakkal, Rituraj Marwaha, Fabian Spill, and Tamal Das. 2025. “Edge Curvature Drives Endoplasmic Reticulum Reorganization and Dictates Epithelial Migration Mode.” *Nature Cell Biology* 27 (10): 1660–75. https://doi.org/10.1038/s41556-025-01729-3.

Read, Adam, and Martin Schröder. 2021. “The Unfolded Protein Response: An Overview.” *Biology* 10 (5): 1–10. https://doi.org/10.3390/biology10050384.

Redaet, Daniel, Abebech Mengeta, Patricia Bilodeau, and Jonathan M. Lee. 2019. “Mitochondria Tether to Focal Adhesions during Cell Migration and Regulate Their Size. Running.” *BioRxiv Preprint*, 1–23.

Renkawitz, Jörg, Aglaja Kopf, Julian Stopp, Ingrid de Vries, Meghan K. Driscoll, Jack Merrin, Robert Hauschild, et al. 2019. “Nuclear Positioning Facilitates Amoeboid Migration along the Path of Least Resistance.” *Nature* 568 (7753): 546–50. https://doi.org/10.1038/s41586-019-1087-5.

Roest, Gemma, Evelien Hesemans, Kirsten Welkenhuyzen, Tomas Luyten, Nikolai Engedal, Geert Bultynck, and Jan B Parys. 2018. “The ER Stress Inducer L -Azetidine-2-Carboxylic Acid Elevates the Levels of Phospho-EIF2 α and of LC3-II in a Ca 2 + -Dependent Manner” 1. https://doi.org/10.3390/cells7120239.

Ron, Jonathan E., Michele Crestani, Johan M. Kux, Jiayi Liu, Nabil Al-Dam, Pascale Monzo, Nils C. Gauthier, Pablo J. Sáez, and Nir S. Gov. 2024. “Emergent Seesaw Oscillations during Cellular Directional Decision-Making.” *Nature Physics* 20 (3): 501–11. https://doi.org/10.1038/s41567-023-02335-6.

Rosen, Mary Ellen, and J. C. Dallon. 2022. “A Mathematical Analysis of Focal Adhesion Lifetimes and Their Effect on Cell Motility.” *Biophysical Journal* 121 (6): 1070–80. https://doi.org/10.1016/j.bpj.2022.02.003.

Rube, Daniel A., and Alexander M. van der Bliek. 2004. “Mitochondrial Morphology Is Dynamic and Varied.” *Molecular and Cellular Biochemistry* 256–257 (1–2): 331–39. https://doi.org/10.1023/b:mcbi.0000009879.01256.f6.

Sáez, Pablo J., Roberto Villalobos-Labra, Francisco Westermeier, Luis Sobrevia, and Marcelo

Farías-Jofré. 2014. “Modulation of Endothelial Cell Migration by ER Stress and Insulin Resistance: A Role during Maternal Obesity?” *Frontiers in Pharmacology* 5 AUG (August): 1–10. https://doi.org/10.3389/fphar.2014.00189.

Sánchez-Álvarez, Miguel, Fidel Nicolás Lolo, Heba Sailem, Giulio Fulgoni, Patricia Pascual-Vargas, Lucía Agüera, Mauro Catalá-Montoro, et al. 2025. “PERK-Dependent Reciprocal Crosstalk between ER and Non-Centrosomal Microtubules Coordinates ER Architecture and Cell Shape.” *Cell Reports* 44 (5). https://doi.org/10.1016/j.celrep.2025.115590.

Sánchez-Álvarez, Miguel, Fidel Lolo, Heba Sailem, Patricia Pascual-Vargas, Giulio Fulgoni, Mar Arias-García, Miguel Ángel del Pozo, and Chris Bakal. 2021. “PERK-Dependent Reciprocal Crosstalk between ER and Non-Centrosomal Microtubules Coordinates ER Architecture and Cell Shape.” *BioRxiv*, 2021.01.19.426991. https://www.biorxiv.org/content/10.1101/2021.01.19.426991v1%0Ahttps://www.biorxiv.org/content/10.1101/2021.01.19.426991v1.abstract.

Sandoz, Patrick A., Christopher Tremblay, F. Gisou van der Goot, and Mathieu Frechin. 2019. “Image-Based Analysis of Living Mammalian Cells Using Label-Free 3D Refractive Index Maps Reveals New Organelle Dynamics and Dry Mass Flux,” 1–22. https://doi.org/https://doi.org/10.1371/journal.pbio.3000553.

Santo-Domingo, Jaime, and Nicolas Demaurex. 2012. “Perspectives on: SGP Symposium on Mitochondrial Physiology and Medicine: The Renaissance of Mitochondrial PH.” *Journal of General Physiology* 139 (6): 415–23. https://doi.org/10.1085/jgp.201110767.

Saraswathibhatla, Aashrith, Dhiraj Indana, and Ovijit Chaudhuri. 2023. “Cell–Extracellular Matrix Mechanotransduction in 3D.” *Nature Reviews Molecular Cell Biology* 24 (7): 495–516. https://doi.org/10.1038/s41580-023-00583-1.

Schaks, Matthias, Grégory Giannone, and Klemens Rottner. 2019. “Actin Dynamics in Cell Migration.” *Essays in Biochemistry* 63 (5): 483–95. https://doi.org/10.1042/EBC20190015.

Schimmel, Lilian, and Emma Gordon. 2018. “The Precise Molecular Signals That Control Endothelial Cell–Cell Adhesion within the Vessel Wall.” *Biochemical Society Transactions* 46 (6): 1673–80. https://doi.org/10.1042/BST20180377.

Schwab, Albrecht, Anke Fabian, Peter J. Hanley, and Christian Stock. 2012. “Role of Ion Channels and Transporters in Cell Migration.” *Physiological Reviews* 92 (4): 1865–1913. https://doi.org/10.1152/physrev.00018.2011.

Schwarz, Dianne S., and Michael D. Blower. 2016. “The Endoplasmic Reticulum: Structure, Function and Response to Cellular Signaling.” *Cellular and Molecular Life Sciences* 73 (1): 79–94. https://doi.org/10.1007/s00018-015-2052-6.

Scorrano, Luca. 2013. “Keeping Mitochondria in Shape: A Matter of Life and Death.” *European Journal of Clinical Investigation* 43 (8): 886–93. https://doi.org/10.1111/eci.12135.

Seetharaman, Shailaja, and Sandrine Etienne-Manneville. 2020. “Cytoskeletal Crosstalk in Cell Migration.” *Trends in Cell Biology* 30 (9): 720–35. https://doi.org/10.1016/j.tcb.2020.06.004.

SenGupta, Shuvasree, Carole A. Parent, and James E. Bear. 2021. “The Principles of Directed Cell Migration.” *Nature Reviews Molecular Cell Biology* 22 (8): 529–47. https://doi.org/10.1038/s41580-021-00366-6.

Shibuya, Masabumi. 2011. “Vascular Endothelial Growth Factor (VEGF) and Its Receptor (VEGFR) Signaling in Angiogenesis: A Crucial Target for Anti- and Pro-Angiogenic Therapies.” *Genes and Cancer* 2 (12): 1097–1105. https://doi.org/10.1177/1947601911423031.

Shin, Jay W., Reto Huggenberger, and Michael Detmar. 2008. “Transcriptional Profiling of VEGF-A and VEGF-C Target Genes in Lymphatic Endothelium Reveals Endothelial-Specific Molecule-1 as a Novel Mediator of Lymphangiogenesis.” *Blood* 112 (6): 2318–26. https://doi.org/10.1182/blood-2008-05-156331.

Shoshan-Barmatz, Varda, Eduardo N. Maldonado, and Yakov Krelin. 2017. “VDAC1 at the Crossroads of Cell Metabolism, Apoptosis and Cell Stress.” *Cell Stress* 1 (1): 11–36. https://doi.org/10.15698/cst2017.10.104.

Silva, André Ferreira Da, Francesca Romana Mariotti, Valdemar Máximo, and Silvia Campello. 2014. “Mitochondria Dynamism: Of Shape, Transport and Cell Migration.” *Cellular and Molecular Life Sciences* 71 (12): 2313–24. https://doi.org/10.1007/s00018-014-1557-8.

Small, J. Victor, Theresia Stradal, Emmanuel Vignal, and Klemens Rottner. 2002. “The Lamellipodium: Where Motility Begins.” *Trends in Cell Biology* 12 (3): 112–20. https://doi.org/10.1016/S0962-8924(01)02237-1.

Stacchiotti, Alessandra, Gaia Favero, Antonio Lavazza, Raquel Garcia-Gomez, Maria Monsalve, and Rita Rezzani. 2019. “Perspective: Mitochondria-ER Contacts in Metabolic

Cellular Stress Assessed by Microscopy." *Cells* 8 (1): 1–9. https://doi.org/10.3390/cells8010005.

Stehbens, Samantha J., Elena Scarpa, and Melanie D. White. 2024. "Perspectives in Collective Cell Migration – Moving Forward." *Journal of Cell Science* 137 (12). https://doi.org/10.1242/jcs.261549.

Stehbens, Samantha J., and Torsten Wittmann. 2014. *Analysis of Focal Adhesion Turnover. A Quantitative Live-Cell Imaging Example*. *Methods in Cell Biology*. 1st ed. Vol. 123. Elsevier Inc. https://doi.org/10.1016/B978-0-12-420138-5.00018-5.

Stock, Christian, Florian T. Ludwig, Peter J. Hanley, and Albrecht Schwab. 2013. "Roles of Ion Transport in Control of Cell Motility." *Comprehensive Physiology* 3 (1): 59–119. https://doi.org/10.1002/j.2040-4603.2013.tb00481.x.

Strale, Pierre-Olivier, Ammar Azioune, Ghislain Bugnicourt, Yohan Lecomte, Makhlad Chahid, and Vincent Studer. 2016. "Multiprotein Printing by Light-Induced Molecular Adsorption." *Advanced Materials (Deerfield Beach, Fla.)* 28 (10): 2024–29. https://doi.org/10.1002/adma.201504154.

Tábara, Luis Carlos, Mayuko Segawa, and Julien Prudent. 2025. "Molecular Mechanisms of Mitochondrial Dynamics." *Nature Reviews Molecular Cell Biology* 26 (2): 123–46. https://doi.org/10.1038/s41580-024-00785-1.

Tait, Stephen W.G., and Douglas R. Green. 2012. "Mitochondria and Cell Signalling." *Journal of Cell Science* 125 (4): 807–15. https://doi.org/10.1242/jcs.099234.

Tang, Dale D., and Brennan D. Gerlach. 2017. "The Roles and Regulation of the Actin Cytoskeleton, Intermediate Filaments and Microtubules in Smooth Muscle Cell Migration." *Respiratory Research* 18 (1): 1–12. https://doi.org/10.1186/s12931-017-0544-7.

Thapa, Narendra, Tianmu Wen, Vincent L. Cryns, and Richard A. Anderson. 2023. "Regulation of Cell Adhesion and Migration via Microtubule Cytoskeleton Organization, Cell Polarity, and Phosphoinositide Signaling." *Biomolecules* 13 (10). https://doi.org/10.3390/biom13101430.

Theveneau, Eric, and Roberto Mayor. 2011. "Can Mesenchymal Cells Undergo Collective Cell Migration? The Case of the Neural Crest." *Cell Adhesion and Migration* 5 (6): 490–98. https://doi.org/10.4161/cam.5.6.18623.

Tikhomirova, Maria S., Avihay Kadosh, Aksel J. Saukko-Paavola, Tom Shemesh, and Robin W. Klemm. 2022. “A Role for Endoplasmic Reticulum Dynamics in the Cellular Distribution of Microtubules.” *Proceedings of the National Academy of Sciences of the United States of America* 119 (15): 1–12. https://doi.org/10.1073/pnas.2104309119.

Todd, Derrick J., Ann Hwee Lee, and Laurie H. Glimcher. 2008. “The Endoplasmic Reticulum Stress Response in Immunity and Autoimmunity.” *Nature Reviews Immunology* 8 (9): 663–74. https://doi.org/10.1038/nri2359.

Tower, Zach, and Hao Chang. 2025. “Technical Considerations for Detecting Protein-Protein Interactions Using Proximity Ligation Assay.” *Journal of Proteome Research* 24 (5): 2564–68. https://doi.org/10.1021/acs.jproteome.4c00855.

Trepat, Xavier, Zaozao Chen, and Ken Jacobson. 2012. “Cell Migration.” *Comprehensive Physiology* 2 (4): 2369–92. https://doi.org/10.1002/cphy.c110012.

Vaidžiulyt, Kotryna, Sophie Macé, and Aude Battistella. 2022. “Persistent Cell Migration Emerges from a Coupling between Protrusion Dynamics and Polarized Trafficking,” 1–30.

Vaidžiulyte, Kotryna, Mathieu Coppey, and Kristine Schauer. 2019. “Intracellular Organization in Cell Polarity – Placing Organelles into the Polarity Loop.” *Journal of Cell Science* 132 (24): 1–9. https://doi.org/10.1242/jcs.230995.

Vallenius, Tea. 2013. “Actin Stress Fibre Subtypes in Mesenchymal-Migrating Cells.” *Open Biology* 3 (JUN). https://doi.org/10.1098/rsob.130001.

Vannuvel, Kayleen, Patricia Renard, Martine Raes, and Thierry Arnould. 2013. “Functional and Morphological Impact of ER Stress on Mitochondria.” *Journal of Cellular Physiology* 228 (9): 1802–18. https://doi.org/10.1002/jcp.24360.

Villalobos-Labra, Roberto, Pablo J. Sáez, Mario Subiabre, Luis Silva, Fernando Toledo, Francisco Westermeier, Fabián Pardo, Marcelo Farías, and Luis Sobrevia. 2018. “Pre-Pregnancy Maternal Obesity Associates with Endoplasmic Reticulum Stress in Human Umbilical Vein Endothelium.” *Biochimica et Biophysica Acta - Molecular Basis of Disease* 1864 (10): 3195–3210. https://doi.org/10.1016/j.bbadis.2018.07.007.

Villalobos-Labra, Roberto, Francisco Westermeier, Carolina Pizarro, Pablo J. Sáez, Fernando Toledo, Fabián Pardo, Juan P. Kusanovic, et al. 2019. “Neonates from Women with Pregestational Maternal Obesity Show Reduced Umbilical Vein Endothelial Response to

Insulin.” *Placenta* 86 (April): 35–44. https://doi.org/10.1016/j.placenta.2019.07.007.

Vliet, Alexander R. van, and Patrizia Agostinis. 2017. “PERK and Filamin A in Actin Cytoskeleton Remodeling at ER-Plasma Membrane Contact Sites.” *Molecular and Cellular Oncology* 4 (5): 1–3. https://doi.org/10.1080/23723556.2017.1340105.

Vliet, Alexander R. van, Francesca Giordano, Sarah Gerlo, Inmaculada Segura, Sofie Van Eygen, Geert Molenberghs, Susana Rocha, et al. 2017. “The ER Stress Sensor PERK Coordinates ER-Plasma Membrane Contact Site Formation through Interaction with Filamin-A and F-Actin Remodeling.” *Molecular Cell* 65 (5): 885-899.e6. https://doi.org/10.1016/j.molcel.2017.01.020.

Walsh, Dietrich W.M., Christian Siebenwirth, Christoph Greubel, Katarina Ilicic, Judith Reindl, Stefanie Girst, Giovanna Muggiolu, et al. 2017. “Live Cell Imaging of Mitochondria Following Targeted Irradiation in Situ Reveals Rapid and Highly Localized Loss of Membrane Potential.” *Scientific Reports* 7 (March): 1–11. https://doi.org/10.1038/srep46684.

Wang, Min, Dakai Yang, Linli Li, Peipei Wu, Yaoxiang Sun, Xu Zhang, Cheng Ji, Wenrong Xu, Hui Qian, and Hui Shi. 2024. “A Dual Role of Mesenchymal Stem Cell Derived Small Extracellular Vesicles on TRPC6 Protein and Mitochondria to Promote Diabetic Wound Healing.” *ACS Nano* 18 (6): 4871–85. https://doi.org/10.1021/acsnano.3c09814.

Wang, Xia, and Ben He. 2024. “Endothelial Dysfunction: Molecular Mechanisms and Clinical Implications.” *MedComm* 5 (8): 1–27. https://doi.org/10.1002/mco2.651.

Wang, Yanhui, Xiaoyun Zhang, Xin Li, Min Cheng, and Xiaodong Cui. 2025. “The Vascular Microenvironment and Its Stem Cells Regulate Vascular Homeostasis.” *Frontiers in Cell and Developmental Biology* 13 (March): 1–14. https://doi.org/10.3389/fcell.2025.1544129.

Weber, Evan W., Fei Han, Mohammad Tauseef, Lutz Birnbaumer, Dolly Mehta, and William A. Muller. 2015. “TRPC6 Is the Endothelial Calcium Channel That Regulates Leukocyte Transendothelial Migration during the Inflammatory Response.” *Journal of Experimental Medicine* 212 (11): 1883–99. https://doi.org/10.1084/jem.20150353.

Wedlich, Doris. 2005. “Cell Migration in Development and Disease.” *Cell Migration in Development and Disease* 2: 1–349. https://doi.org/10.1002/3527604669.

Wehrle-Haller, Bernhard, and Beat A. Imhof. 2003. “Actin, Microtubules and Focal Adhesion

Dynamics during Cell Migration." *International Journal of Biochemistry and Cell Biology* 35 (1): 39–50. https://doi.org/10.1016/S1357-2725(02)00071-7.

Wolf, Dane M, Mayuko Segawa, Arun Kumar Kondadi, Ruchika Anand, Sean T Bailey, Andreas S Reichert, Alexander M van der Bliek, David B Shackelford, Marc Liesa, and Orian S Shirihai. 2019. "Individual Cristae within the Same Mitochondrion Display Different Membrane Potentials and Are Functionally Independent." *The EMBO Journal* 38 (22): 1–21. https://doi.org/10.15252/embj.2018101056.

Wortel, Inge M.N., Annie Y. Liu, Katharina Dannenberg, Jeffrey C. Berry, Mark J. Miller, and Johannes Textor. 2021. "CelltrackR: An R Package for Fast and Flexible Analysis of Immune Cell Migration Data." *ImmunoInformatics* 1–2 (July): 100003. https://doi.org/10.1016/j.immuno.2021.100003.

Wu, Pei-Hsun, Jude M Phillip, Wenxuan Du, Andre Forjaz, Praful R. Nair, and Denis Wirtz. 2025. "Methods to Analyze Cell Migration Data: Fundamentals and Practical Guidelines." *Nature Methods*. https://doi.org/10.1038/s41592-025-02935-5.

Xian, Hongxu, and Yih Cherng Liou. 2021. "Functions of Outer Mitochondrial Membrane Proteins: Mediating the Crosstalk between Mitochondrial Dynamics and Mitophagy." *Cell Death and Differentiation* 28 (3): 827–42. https://doi.org/10.1038/s41418-020-00657-z.

Xu, Haoxing, Enrico Martinoia, and Ildiko Szabo. 2015. "Organellar Channels and Transporters." *Cell Calcium* 58 (1): 1–10. https://doi.org/10.1016/j.ceca.2015.02.006.

Yamada, Kenneth M., and Michael Sixt. 2019. "Mechanisms of 3D Cell Migration." *Nature Reviews Molecular Cell Biology* 20 (12): 738–52. https://doi.org/10.1038/s41580-019-0172-9.

Zhang, Jian, and Yu Li Wang. 2017. "Centrosome Defines the Rear of Cells during Mesenchymal Migration." *Molecular Biology of the Cell* 28 (23): 3240–51. https://doi.org/10.1091/mbc.E17-06-0366.

Zhang, Kezhong, and Randal J. Kaufman. 2008. "From Endoplasmic-Reticulum Stress to the Inflammatory Response." *Nature* 454 (7203): 455–62. https://doi.org/10.1038/nature07203.

Zorova, Ljubava D., Vasily A. Popkov, Egor Y. Plotnikov, Denis N. Silachev, Irina B. Pevzner, Stanislovas S. Jankauskas, Valentina A. Babenko, et al. 2018. "Mitochondrial Membrane Potential." *Analytical Biochemistry* 552: 50–59. https://doi.org/10.1016/j.ab.2017.07.009.

Figure index

Table index

Acknowledgements

I would like to start by thanking the members of my Thesis Committee, **Pablo J. Sáez**, **Maike Frye** and **Thomas Oertner**. Thank you for agreeing to be a part of my thesis journey and for taking your role as a supervisor seriously. The discussions during the progress report session were very helpful in shaping the rest of the project and your offers to lend a helping hand were very much appreciated.

Next, I want to thank Pablo and all the past and present members of the CellComM Lab. **Pablo**, your passion for the topic and science in general were always inspiring and I will always be grateful that you gave me the chance to work on such a fascinating topic. Thank you for the trust that you put in me these past three years, I never took it for granted. It was always reassuring to know that you trusted us all to make the right decisions when it came to protocol planning and running experiments.

Most importantly, you managed to bring together a bunch of people from all over the world that I now get to call my friends. The hours spent in the lab and the fun we had during work, but especially outside of work made it possible to stay motivated and inspired during this PhD experience. This is why my most special thanks go out to: **Tamara** (Tami), **Johan** (JK), **Svitlana** (Svi), **Martina** (Marti), **David** (Dave), **Javier** (Javi) and **Magdalena** (Magda). I can't imagine how different my experiences would have been without you guys supporting me throughout. It's rare to share the same enthusiasm with a group of people as amazing as you.

Tami, you're a part of all my favourite memories during this experience. I love that I got to share my whole PhD with you and I learnt more from you than anyone else these past three years. Your quiet confidence and never-ending support gave me trust in myself and helped me more than you'll ever know.

JK, I don't know how to properly thank you for everything you do for all of us. You kept this lab running and made sure we were never missing anything. The calm and trust you put in all of us was very much appreciated. Thank you for never complaining when I asked you where stuff was and thank you for the never-ending reassurance that it will work out in the end. I wish I was even half as calm and chill as you.

Svi, your work ethic and support inspired me every day and I'm so grateful that I got to meet you. The circumstances that made you join the lab were and still are extremely difficult to comprehend, but the fact that you continue to show up every day and offer your support no matter what, makes you one of the strongest people I've ever met.

Marti, I'm so happy you came back to join the team as our post-doc. Your knowledge and support was very much appreciated and it was so great to have a discussion partner outside

of the core HFSP group. Thank you for always being encouraging and even though I sometimes complained, I will miss your constant humming/singing/talking.
Dave, even though you left a while ago, I'm so lucky to know you. The scientific discussions about mito dynamics, but more importantly the discussions outside the lab about anything and everything will remain one of my favourite moments. Meeting you also meant that I got to meet my favourite book partner for life, **Tanya**. I can't wait for the memories we still get to make.
Javi, you're still the most cheerful person I've ever met (even though Madga comes close) and I'm still hoping and praying for you to maybe come back to Hamburg. I missed you every day while being in the lab and I still can't get over your knowledge when it comes to bioinformatics and just general coding stuff. Thank you for the enthusiasm whenever I sent you my favourite pictures I took (you were always the first person I showed them to).
Magda, you made the last PhD year so great. Even though many things went wrong, you stayed consistently happy and infected us all with your good mood. I never thought I would meet someone who embodies "golden-retriever-energy" in real life, but there you are.

I also want to thank the incredible neighbouring lab that is the **Heeren** lab. We are so lucky to share a space with you and work closely with such kind and happy people. **Jörg**, thank you for the support and the feedback after every MAB presentation. To **Kim, Johanna, Karthik, Jenny** and **Janina**, thank you for the support and the friendship outside of the lab. I hope we get to make more memories together and I only wish you the best for all your future plans.

Als Letztes möchte ich den Menschen danken, ohne die ich diese Erfahrung nicht geschafft hätte bzw. gar nicht erst hätte starten können. Ich bin wahnsinnig dankbar für meine beste Freundin, **Birga**, die immer ein offenes Ohr für mich hatte und sich zusammen mit mir aufgeregt hat, wenn mal wieder gar nichts funktioniert hat. Ich bin dankbar für **Rita** und **Helene**, die immer im Hintergrund für mich gejubelt haben, wenn ich eine neue Erfahrung machen durfte. Eure Unterstützung bedeutet mir sehr viel. Meine Studiengeschichte startete vor 10 Jahren mit meinem Jurastudium, bei dem ich das große Glück hatte, **Svantje** – und dadurch auch **Malte** – kennenzulernen. Eure Freundschaft und Teilhabe bedeutet mir viel. **Raphaela**, du bist mit mir von Jura zu Pharmazie gewechselt und ich freue mich, dass wir uns immer noch bei unseren akademischen Abenteuern zur Seite stehen und anfeuern. Ein weiterer Dank geht an **Thomas** und **Martin**, danke für euren Input während dieser Zeit. Danke an **Matsi, Lola, Annika, Raphie** und **Miriam**, eure Freundschaft bedeutet mir viel.
An **Jan** und **Jannes**: Ich danke euch so sehr, dass ihr die letzten 1,5 Jahre mit mir zusammen durchlebt habt. Euer Vertrauen in mich und das, was ich mache, hat mir die Motivation gegeben, mein Bestes zu geben. Ich bin euretwegen so weit gekommen. Danke ☺

An honorable mention goes out to **George** who kept making me laugh during every zoom call we shared since meeting in March of 2025. Also thank you for never letting me panic about deadlines, failed experiments or writing the discussion.

During my master studies, Pablo made it possible for me to do an internship in Utrecht. I'm very thankful for the people of the **Klumperman lab** for helping me during my first time abroad and teaching me how to perform one of the coolest techniques, electron microscopy. I was very lucky to live with two amazing people that felt like a second family. So I want to say thank you to **Guus** and **Lianne** for making Utrecht feel like home and giving me a reason to always wanting to come back and visit.

My second internship abroad happened during my first PhD year. Thank you to **Yamuna** for welcoming me into the **Krishnan lab** and teaching me how to perform chemical imaging. I'm grateful for **Sangyoon, Avantika** and **Rui** for showing me around Chicago and the lab.

Bevor ich den wichtigsten Menschen in meinem Leben danke, ein kleiner persönlicher Gruß an die Dinge, die mir in den letzten Jahren sehr viel Freude bereitet haben. Danke an Felix und Tommi, die mich jeden Mittwoch konstant zum Lachen gebracht haben, **Gemischtes Hack**, bestes Hack. **Taylor Swift**, denn ohne ihre Musik wäre ich verloren gewesen. Rebecca, Ali, Emily, Stephanie, Jessa, Sarah (x2) und Liz, danke für die Charaktere, die mir alles bedeuten.

Mein größter Dank gehört wie immer meiner Familie, insbesondere meiner **Mama** und meinem **Papa**. Ich weiß wirklich nicht, was ich richtig gemacht habe, um eure bedingungslose Unterstützung zu verdienen. Die letzten Jahre wären ohne euch nicht möglich gewesen und ich werde immer dankbar für die Möglichkeiten sein, die ich euretwegen erleben darf. Ich liebe euch sehr. Ich möchte im Speziellen auch meiner **Tante** danken, die nie an mir gezweifelt hat, diese Arbeit ist daher auch für dich. Ich bin froh, dich immer an meiner Seite zu wissen und habe dich sehr lieb. Abschließend möchte ich noch meinen Großeltern danken. **Oma** und **Opa Jenny** und **Oma** und **Opa Samson**. Danke für euer Vertrauen und dafür, dass ihr mir immer gesagt habt, wie stolz ihr auf mich seid. Ich hab euch lieb. **Opa Jenny**, du konntest das Ende dieser Zeit leider nicht mehr persönlich erleben und das finde ich immer noch unfair, weil du von euch vieren immer das meiste Interesse an dieser Arbeit gezeigt hast. Ich danke dir dafür und ich vermisse dich. Das hier ist auch für dich.

Curriculum vitae

EDUCATION

April 2023 - present	**Universitätsklinikum Hamburg-Eppendorf (UKE),** **PhD student**
	Thesis title: Organelle ion channel control of directional mesenchymal cell migration **Supervisor:** Pablo J. Sáez, Universitätsklinikum Hamburg-Eppendorf
	Internship: Krishnan Laboratory, Department of Chemistry, University of Chicago, Illinois
October 2025 - present	**Universität Hamburg, UKE** **Staatsprüfung, Studium Medizin**
October 2021 - March 2023	**Universität Hamburg,** **Master of Science, Molecular Life Sciences**
	Thesis title: ER stress disruption of mitochondrial dynamics during cell migration **GPA:** 1.03, mit Auszeichnung bestanden (distinction)
	Internship: Klumperman Laboratory, Department of Cell Biology, University Medical Center (UMC), Utrecht, Netherlands
October 2017 - April 2021	**Universität Hamburg** **Bachelor of Science, Biologie**
	Thesis title: Influence of an Influenza A virus infection on the DNA damage response of MCF7 and T47D cell lines depending on hormone receptor expression **GPA:** 1.42

Eidesstattliche Versicherung

Ich versichere ausdrücklich, dass ich die Arbeit selbstständig und ohne fremde Hilfe, insbesondere ohne entgeltliche Hilfe von Vermittlungs- und Beratungsdiensten, verfasst, andere als die von mir angegebenen Quellen und Hilfsmittel nicht benutzt und die aus den benutzten Werken wörtlich oder inhaltlich entnommenen Stellen einzeln nach Ausgabe (Auflage und Jahr des Erscheinens), Band und Seite des benutzten Werkes kenntlich gemacht habe. Das gilt insbesondere auch für alle Informationen aus Internetquellen.
Soweit beim Verfassen der Dissertation KI-basierte Tools („Chatbots") verwendet wurden, versichere ich ausdrücklich, den daraus generierten Anteil deutlich kenntlich gemacht zu haben. Die „Stellungnahme des Präsidiums der Deutschen Forschungsgemeinschaft (DFG) zum Einfluss generativer Modelle für die Text- und Bilderstellung auf die Wissenschaften und das Förderhandeln der DFG" aus September 2023 wurde dabei beachtet.
Ferner versichere ich, dass ich die Dissertation bisher nicht einem Fachvertreter an einer anderen Hochschule zur Überprüfung vorgelegt oder mich anderweitig um Zulassung zur Promotion beworben habe.
Ich erkläre mich einverstanden, dass meine Dissertation vom Dekanat der Medizinischen Fakultät mit einer gängigen Software zur Erkennung von Plagiaten überprüft werden kann.

Unterschrift:

Hamburg, 12.01.2026